The Design of an Uninhabited Air Vehicle for Remote Sensing in the Cryosphere

By

William R. Donovan
Bachelors of Science, Aerospace Engineering
University of Kansas, 2007
Lawrence, Kansas

Submitted to the Department of Aerospace Engineering and the Faculty of the Graduate School of the University of Kansas in partial fulfillment of the requirements for the degree of Masters of Science.

_____
Dr. Richard Hale, Chairman

_____
Dr. Mark Ewing

_____
Dr. Ron Barrett

_____
Date Defended

The Thesis Committee for William R. Donovan certifies that this is the approved version of the following thesis:

The Design of an Uninhabited Air Vehicle for Remote Sensing in the Cryosphere

By

William R. Donovan
Bachelors of Science, Aerospace Engineering
University of Kansas, 2007
Lawrence, Kansas

Committee:

_____
Dr. Richard Hale, Chairman

_____
Dr. Mark Ewing

_____
Dr. Ron Barrett

_____
Date Approved

Abstract

This document summarizes the results of the preliminary design of an Uninhabited Air Vehicle (UAV) for use in Cryospheric research. This includes the development of a mission specification with all related performance requirements. In general, the design mission of this aircraft, named the Meridian, is to takeoff from a remote base camp in either Antarctica or Greenland, fly to some area of interest, acquire data such as ice thickness and surface elevation with ground penetrating radar, then return to base. These types of missions, which to date have been flown with inhabited aircraft, can be described as both dull and dangerous. These are characteristics that support the use of a UAV for this mission.

The design of the Meridian is performed in parallel to the development of the primary payload: a ground penetrating Synthetic Aperture Radar (SAR). This concurrent system development warranted a certain amount of flexibility in the aircraft design. This led to the development of three candidate configurations, from which the primary configuration was selected and carried through to the more detailed design phases. This process, commonly referred to as Class I and Class II design phases, was used to develop three Class I conceptual configurations, named the Red, White, and Blue designs. The three designs represent three methods of integrating the radar antennas into the aircraft structure. The Red design utilizes a structurally synergistic approach where the antennas are integrated directly into the wing structure. The White design is a more flexible approach in that the antennas are simply mounted on pylons hung below the wing. The Blue design is a hybrid of the

other configurations in that it integrates the antennas into a dielectric lower wing of a biplane configuration.

Weight is one of the most common performance metrics associated with the merit of a preliminary aircraft design. This is due to the fact that the acquisition and operational cost of an aircraft are directly related to the vehicle weight. In these terms, the Red concept proved to be the most weight efficient with a takeoff weight of 760 lbs, while the White was the least efficient with a takeoff weight of 1,270 lbs. However, the purpose of this design is to choose the best design with respect to the whole system. The White concept was selected as the primary configuration as it represents the most flexible in terms of antenna integration. This is vital to the risk mitigation of this aircraft development.

The White design was refined in the Class II design process resulting in the Meridian UAV. The Meridian has a takeoff weight of 1,080 lbs, an empty weight of 615 lbs, and a range of 950 nm (with reserves for an additional 160 nm). The Meridian is a turboprop powered aircraft with a design cruise speed of 120 kts and a takeoff and landing distance of 1,500 ft. The aircraft has ten hardpoints along the wing for antenna mounting, and is specifically designed for cold weather operations to include anti-icing provisions, system heating and cooling, and the ability to operate from snow/ice runways. The Meridian represents the application of conventional aircraft design methodologies to a UAV. This document discusses the viability of using these methods, which are typically used on inhabited aircraft, to design an uninhabited vehicle.

Acknowledgments

I would first like to thank my advisor, Dr. Richard Hale, for all of his support and guidance throughout my undergraduate and graduate years. I would also like to thank Dr. Barrett and Dr. Ewing for the long hours they spent answering my many questions regarding this vehicle design. Thanks also go to each member of the KU Aerospace Engineering faculty individually as they have each had a significant impact on my professional development.

I would like to thank my family and friends for their support and patience, especially my parents, Bill and Coleen. They have been a constant source of love and encouragement and have unconditionally supported me throughout my life.

Special thanks go to the entire CReSIS team for supporting me in this research as well as to the National Science Foundation for providing the funding that made this work possible.

This material is based upon work supported by the National Science Foundation under Grant No. AST-0424589. Any opinions, findings, and conclusions or recommendations expressed in this material are those of the author and do not necessarily reflect the views of the National Science Foundation.

Table of Contents

List of Figures

List of Tables

Nomenclature

Symbol	Description	Units (Metric)	Units (English)
AR	Aspect Ratio	~	~
b	Span	m	ft, in
c_a	Aileron Chord	m	ft
c_{bar}	Mean Geometric Chord	m	ft, in
C_D	Drag Coefficient	~	~
C_{D0}	Zero-Lift Drag Coefficient	~	~
C_{Da}	Variation of drag coefficient with angle of attack	rad^{-1}	rad^{-1}
C_{Divee}	Variation of airplane drag coefficient with V-tail incidence angle	rad^{-1}	rad^{-1}
C_{Dq}	Variation of drag coefficient with pitch rate	rad^{-1}	rad^{-1}
C_{Du}	Variation of Drag Coeff. With Speed	~	~
c_f	Flap Chord	m	ft
C_L	Lift Coefficient	~	~
C_{L1}	Steady State Lift Coefficient	~	~
C_{La}	Variation of lift coefficient with angle of attack	rad^{-1}	rad^{-1}
$C_{La,dot}$	Variation of lift coefficient with rate of change of angle of attack	rad^{-1}	rad^{-1}
C_{lb}	Variation of rolling moment coefficient with sideslip angle	rad^{-1}	rad^{-1}
C_{Livee}	Variation of airplane lift coefficient with V-tail incidence angle	rad^{-1}	rad^{-1}
C_{lp}	Variation of airplane rolling moment coefficient with roll rate	rad^{-1}	rad^{-1}
C_{Lq}	Variation of lift coefficient with pitch rate	rad^{-1}	rad^{-1}
C_{lr}	Variation of airplane rolling moment coefficient with yaw rate	rad^{-1}	rad^{-1}
C_{Lu}	Variation of Lift Coeff. With Speed	~	~
$C_{L\alpha}$	Lift-Curve Slope	rad^{-1}	rad^{-1}
$C_{l\beta dot}$	Variation of airplane rolling moment coefficient with rate of change of sideslip	rad^{-1}	rad^{-1}
C_{Ma}	Variation of pitching moment coefficient with angle of attack	rad^{-1}	rad^{-1}
$C_{Ma,\ dot}$	Variation of pitching moment coefficient with rate of change of angle of attack	rad^{-1}	rad^{-1}
C_{mivee}	Variation of airplane moment coefficient with V-tail incidence angle	rad^{-1}	rad^{-1}

Symbol	Description	Units (Metric)	Units (English)
	Variation of pitching moment coefficient	rad^{-1}	rad^{-1}
C_{Mq}	with pitch rate		
C_{MT}	Pitching Moment Coefficient Due to Thrust	~	~
	Variation of pitching moment coefficient	rad^{-1}	rad^{-1}
C_{MTa}	due to thrust with angle of attack		
	Variation of airplane pitching moment coefficient due to thrust with dimensionless	~	~
C_{MTu}	speed		
	Variation of Pitching Moment Coeff. w/	~	~
C_{Mu}	speed		
$C_{M\alpha}$	Pitching Moment Coefficient	rad^{-1}	rad^{-1}
	Variation of airplane yawing moment	rad^{-1}	rad^{-1}
C_{np}	coefficient with roll rate		
	Variation of airplane yawing moment	rad^{-1}	rad^{-1}
C_{nr}	coefficient with yaw rate		
	Variation of airplane yawing moment	rad^{-1}	rad^{-1}
$C_{nT\beta}$	coefficient due to thrust with sideslip		
	Variation of airplane yawing moment	rad^{-1}	rad^{-1}
$C_{n\beta}$	coefficient with sideslip angle		
	Variation of airplane yawing moment	rad^{-1}	rad^{-1}
$C_{n\beta dot}$	coefficient with rate of change of sideslip		
c_p	Specific Fuel Consumption	kg/kW-hr	lbm/hp-hr
C_{Tx}	Thrust Coefficient	~	~
C_{Txu}	Variation of Thrust Coeff. With speed	~	~
c_w	Wing Chord	m	ft
	Variation of side force coefficient with	rad^{-1}	rad^{-1}
C_{Yb}	sideslip angle		
	Variation of airplane sideforce coefficient	rad^{-1}	rad^{-1}
C_{Yp}	with roll rate		
	Variation of airplane sideforce coefficient	rad^{-1}	rad^{-1}
C_{Yr}	with yaw rate		
	Variation of sideforce coefficient with rate	rad^{-1}	rad^{-1}
$C_{Y\beta,dot}$	of change of sideslip		
D	Drag	N	lbf
D_p	Propeller Diameter	m	ft
e	Oswald's Efficiency	~	~
E_t	Touchdown Energy	J	ft-lbs/s
f	Equivalent Parasite Area	m^2	ft^2
F_F	Fuel Expansion Factor	%	%
L	Lift	N	lbf
L_M	Main Gear Length	in	m
L_m	Distance from Main Gear to c.g.	in	in

Symbol	Description	Units (Metric)	Units (English)
L_N	Nose Gear Length	in	m
L_n	Distance from Nose Gear to c.g.	in	in
M	Munk's Span Factor	~	~
n	Load Factor	g	g
N_g	Ratio of Maximum Gear Load to Static Load	~	~
n_p	Number of Propeller Blades	~	~
n_s	Number of Struts	~	~
P	Engine Power	kW	hp
P_{bl}	Blade Power Loading	kW/m^2	hp/ft^2
P_M	Main Gear Load	lbs-f	N
P_m	Main Gear Load	N	lbs
P_N	Nose Gear Load	lbs-f	N
P_n	Nose Gear Load	N	lbs
R	Range	km	nm
S	Wing Area	m^2	ft^2
S_s	Strut Stroke Length	m	in
s_t	Tire Deflection	m	in
S_{vee}	V-Tail Planform Area	m^2	ft^2
S_{Wet}	Wetted Area	m^2	ft^2
t/c	Thickness-to-Chord Ratio	~	~
V	Airspeed	km/hr	kts
W_E	Empty Weight	kg	lbm
W_F	Fuel Weight	kg	lbm
W_{PL}	Payload Weight	kg	lbm
W_{TO}	Takeoff Weight	kg	lbm
$X_{LE,vee}$	V-Tail Leading Edge Fuselage Station	m	in
$Z_{c/4,vee}$	Vertical Location of V-Tail Quarter-Chord	m	in

Greek Symbols

Symbol	Description	Units (Metric)	Units (English)
α	Angle of Attack	deg	deg
ε_w	Wing Twist	deg	deg
$\eta_{i,f}$	Inboard Flap Station	~	~
η_p	Propeller Efficiency	~	~
σ	Biplane Interference Factor	~	~
Γ	Dihedral Angle	deg	deg
$\eta_{o,f}$	Outboard Flap Station	~	~
$\eta_{i,a}$	Inboard Aileron Station	~	~

Symbol	Description	Units (Metric)	Units (English)
$\Lambda_{c/4,w}$	Wing Quarter-Chord Sweep	deg	deg
ε_w	Wing Geometric Twist	deg	deg
$\eta_{o,a}$	Outboard Aileron Station	~	~
η_s	Strut Absorption Efficiency	~	~
η_t	Tire Absorption Efficiency	~	~
λ_w	Wing Taper Ratio	~	~

Subscripts

Symbol	Description
a	Aileron
vee	V-Tail
w	Wing

Abbreviations

Abbreviation	Description
AAA	Advanced Aircraft Analysis
AML	Adaptive Modeling Language
AMRAVEN	Adaptive Modeling Rapid Vehicle ENgineering
CEF	Cost Escalation Factor
CER	Cost Estimation Relationship
CReSIS	Center for Remote Sensing of Ice Sheets
FAA	Federal Aviation Administration
FAR	Federal Aviation Regulations
FLIR	Forward Looking Infrared
LIDAR	Light Detection And Ranging
MALE	Medium Altitude Long Endurance
MDO	Multi-Disciplinary Optimization
mgc	Mean Geometric Chord
MOM	Measure of Merit
MOM	Measure of Merit
NAS	National Air Space
NASA	National Aeronautics and Space Administration
NSF	National Science Foundation
NSF	National Science Foundation
PC	Personal Computer
PWM	Pulse Width Modulation
RADAR	Radio Detection and Ranging
RATO	Rocket Assisted Takeoff
SAR	Synthetic Aperture Radar
UAS	Uninhabited Aircraft System
UAV	Uninhabited Air Vehicle
USAF	United States Air Force
WAIS	West Antarctic Ice Sheet

1 Introduction

The driving question behind the design mission of this aircraft is: “What changes are occurring in the mass of the Earth’s ice cover, and how will those changes affect the climate?”[1] To answer this question, four areas must be studied: Sea ice, terrestrial ice sheets, glaciers, and ice caps. Measuring the area, concentration, and thickness of sea ice is crucial to the understanding of how the mass balance of terrestrial ice sheets is changing. [1]

Advances in aircraft and satellite remote sensing have enabled progress in the study of the ice sheet mass balance. The most important parameters used to define large ice sheets are surface elevation and its change with time, ice velocity and grounding line locations, ice thickness, and surface melting. All of these parameters except for ice thickness can be measured with satellites. This is done, however, at low spatial and temporal resolutions. Efforts are currently underway at NASA to develop a means of measuring ice thickness from orbit in addition to using NASA’s Geoscience Laser Altimeter System to produce precise lidar measurement of ice surface elevation and its change over time. This technology has yet to be fully developed though. [1]

The use of sub-orbital platforms, especially high performance uninhabited air vehicles, can offer significant improvements in the spatial and temporal resolution of ice sheet measurements. [1]

This document describes the development of an Uninhabited Air Vehicle (UAV) for use in polar research in support of the Center for Remote Sensing of Ice Sheets at the University of Kansas. This includes the development of a set of requirements and

mission specification as well as the preliminary configuration design of a new UAV for remote sensing. The aircraft design is broken into two phases: Class I and Class II. The Class I design phase utilizes somewhat simplified analysis methods such that configuration can be developed with a limited amount of engineering work [2]. The Class II design phase consists of more detailed analyses, which result in more accurate results, but require more engineering time [2]. Three Class I concepts are presented. One of these concepts is selected as the primary configuration and is carried through the Class II design phase.

2 Related Work

The purpose of this section is to discuss the science rationale driving this aircraft design, the current state of Polar research using aircraft, and to describe the state-of-the-art design tools used in the design of new inhabited and uninhabited vehicles.

2.1 Aircraft Design Tools and Methodologies

This section discusses the design processes and tools currently used for preliminary aircraft design.

2.1.1 Knowledge Based Design and Analysis Tools

There are several design tools that can be used to automate the calculations and iterations required during the preliminary aircraft design phase. Programs such as the Advanced Aircraft Analysis software (AAA) [3] produced by DARcorporation and RDS-Professional [4] produced by Conceptual Research Corporation are some of the most widely used aircraft preliminary design tools. These programs utilize similar design methodologies to assist the designer in preliminary sizing, weight and balance, aerodynamics, stability and control, performance, and cost estimation.

The AAA program is currently being combined with an object-oriented language called Adaptive Modeling Language (AML [5]) [6]. This new design and analysis environment named AMRaven [6] offers knowledge based conceptual and preliminary design tools based on the AAA program, aircraft specific computer aided design (CAD) tools, aerodynamic analysis using panel based codes, structural analysis using automated meshing, and optimization algorithms [7].

2.1.2 Multidisciplinary Design Optimization

One of the primary focuses in the aircraft design community is the application of Multidisciplinary Design and Optimization (MDO) strategies to the aircraft preliminary design. MDO in its simplest form can be defined as:

> A methodology for design of complex engineering systems that are governed by mutually interacting physical phenomena and made up of distinct interacting subsytems (suitable for systems for which) in their design, everything influences everything else.
>
> Sobieski [8]

Aircraft preliminary design is an ideal candidate for MDO as it is a process where "everything influences everything else."

The implementation of MDO can take many forms. The very process of aircraft design is, by definition, a form of multidisciplinary optimization. For instance, many Class I aircraft design studies can be performed using classical methods, analyzed, and compared to determine the "optimal" design. This process has been used for several decades and it works extremely well, but requires a large amount of engineering time. In other words, the "optimization" process can be improved.

The current state of digital computing has made it possible to automate several of the aircraft design processes and to implement a variety of optimization algorithms. Essentially, this means a designer can perform design studies at a much higher rate resulting in more optimized solutions.

There are several MDO processes that have been developed for the preliminary design of both uninhabited and inhabited aircraft. These algorithms can be broken into the following types:

- Analysis Driven MDO
- Knowledge Based MDO

2.1.2.1 Analysis Driven MDO

There are several types of analysis driven MDO methods. Some algorithms use mathematically driven optimization strategies based on classical design formulas. These algorithms attempt to minimize (or maximize) the result of some governing objective function.

The derivative of the cost function with respect to the design variables is used as a means to determine the direction and size of the step in design variables. Most of the current aircraft design MDO algorithms, however, use some form of zeroth order optimization algorithm combined with Class I preliminary design calculations to determine the optimum configuration. A zeroth order optimization algorithm is one that does not use gradient or slope information to determine variable step direction [7]. Instead these programs calculate some measure of merit or MOM (Often W_{TO} or Cost) then change the design variables and recalculate the measure of merit. If the MOM improves with the new design then it is kept as the current design and the process is repeated until convergence. Essentially, this method is equivalent to performing many preliminary designs and comparing the results.

This type of optimization scheme has been shown to work very well for the preliminary design of several types of aircraft [7]. There is some debate among the design community as to which algorithms work best, as well as where and how these algorithms should be implemented. A large amount of research has been done by Raymer [7] to determine the optimization strategies that work best for different types of aircraft design. However, the proper implementation of an optimization strategy for aircraft design is often dependent on the design problem at hand, which makes it difficult to create one optimization code that works for all designs.

2.1.2.2 Knowledge Based MDO Tools

Another type of MDO uses tables of historical aircraft data to make design decisions automatically. This process, referred to as data mining [8], uses large UAV databases to determine possible design drivers for specific design decisions. One example of this process is to examine engine type used on several aircraft. A data mining algorithm could determine that cruise speed appears to be correlated to engine selection. Then the engine type for a new design would be based on the typical engine type used on other aircraft with similar cruise speed requirements.

The focus of this type of design strategy is to generate a method of automating design decisions related to the configuration selection process. This process can then be coupled with a typical analysis driven optimization strategy to create a more robust optimization package that minimizes the required user input. This process is not dissimilar from some of the classical design methods [2], in which design decisions are made based on current and historical aircraft with similar missions.

2.1.3 Summary of Aircraft Design Methods

One of the major problems with using optimization methods in preliminary aircraft design is the very idea that there is some "optimum" design for a given mission. There are often several designs that will satisfy a given mission. A good historical example of this can be seen in the comparison of the Boeing B-47 and AVRO Vulcan bombers as discussed in [2]. These aircraft were designed for very similar missions, but have very different configurations.

These aircraft are similar in almost all of the quantifiable, performance driven measures of merit such as range and cruise speed. However, they differ in other, qualitative areas, such as engine accessibility, maintainability, and radar cross-section.

This simple example shows how the interpretation of these qualitative requirements can lead to very different design solutions. One of the major drawbacks to current MDO processes is that they rely almost entirely on numerical requirements and measures of merit. Factors such as engine accessibility, future growth capabilities, modularity, and portability all affect the design of a vehicle, but are difficult to quantify. Furthermore, when these qualitative requirements are transformed into quantifiable parameters, the assumptions and interpretations required to do so will often affect the optimization. In fact, the "optimum" design is quite often driven by the designer's interpretations of vague requirements. Failure to realize this fact will lead to improperly conceived design decisions.

For this reason it is imperative that the design process be dissected into phases that can benefit from MDO and phases where designer intuition and interpretation are required. In addition to this, it is important to determine the design phases where knowledge-based design and analysis is useful as opposed to the phases that would benefit more from analysis driven optimization. The development of the AMRaven design tools exemplify this ideal in that they offer a combination of automated analysis and optimization with classical design approaches requiring designer input.

The design process used for the Meridian UAV utilizes primarily classical preliminary design methods, which are supported by the AAA software. Phases of the design process that can benefit from optimization codes such as preliminary sizing and weight and balance calculations are discussed, but no formal MDO methods are used. The Meridian UAV represents the design of an uninhabited aircraft utilizing methods typically used on inhabited aircraft.

2.2 Mission Concepts for Remote Sensing

This section discusses the current state of remote sensing in terms of previously conducted experiments as well as several proposed mission concepts utilizing both inhabited and uninhabited vehicles.

Remote sensing in Antarctica using aircraft dates back to the 1940's when US military pilots noticed that their radar altimeters malfunctioned while flying over the ice. The radar altimeters gave false readings because, as was theorized at the time, the radio waves penetrated the ice and reflected off of the bedrock instead of the

surface of the ice. This information spurred on the beginning of using airborne radar for ice thickness measurement [9].

During the 1960's the US National Science Foundation (NSF) funded a program for airborne remote sensing using the Scott Polar Research Institute Mark II radio echo sounding equipment. This program utilized C-121 and C-130 aircraft provided by the US Navy Special Development Squadron Six and the US Navy Support Force Antarctica. [9]

Several remote sensing campaigns have been performed in Greenland and Antarctica in the recent past using large inhabited aircraft such as the De Havilland Twin Otter and the Lockheed Martin P-3 Orion aircraft [11], [12]. These projects have provided extremely useful data that furthers the understanding of the current state of the ice sheet mass balance. However, the aircraft used for these missions are typically larger than needed in terms of today's science equipment and are costly to operate. In addition, performing remote sensing in areas such as Antarctica and Greenland is an extremely dull and dangerous mission. These are mission qualities that are considered to be ideal for uninhabited aircraft systems (UAS).

In addition to the Cryospheric research, there are a number of remote sensing applications currently being developed to utilize some form of Synthetic Aperture Radar (SAR) to perform a variety of observations [13], [14] and [15]. There are currently two directions of this type of research: mission concepts utilizing large High Altitude Long Endurance (HALE) UAVs such as a General Atomics Altair [16], or

mission concepts utilizing small aircraft such as the Aerosonde UAV [15]. There is very little research being done utilizing mid-sized platforms.

While there are few applications of mid-scale UAVs for science missions, NASA Langley has performed some investigation of new vehicle design for microwave remote sensing [13], which resulted in a vehicle concept with a gross weight of approximately 2,000 lbs, a wingspan of 28 ft, and a cruise speed of 100 kts. This vehicle falls in between the currently used platforms in terms of size, and is different from typical UAVs as it is designed for low altitude operations.

The current state of remote sensing using UAVs shows that there is both a lack of and need for the utilization of mid-size uninhabited aircraft.

3 Requirements Definition and Development

One of the first and most important steps in the aircraft design process is to fully define all of the requirements that will be imposed on the design. Typically, the majority of these requirements is directly requested by a customer or based on some sort of market analysis. Some of these parameters include a minimum range, cruise speed, or payload capacity. The specific combination of requirements depends on the design mission and therefore varies from project to project.

In addition to the requirements directly specified by the customer, aircraft must often meet a set of derived requirements determined by the designer. These requirements typically consist of parameters that are driven by the designer's interpretation of the customers requests. For example, a design request might call for

the ability to easily load payload into a cargo bay. The designer could then use this requirement to specify a minimum size for the payload door opening.

Another example of a derived requirement occurs in the instance when a customer has very specific needs in certain areas but is flexible in others. For the CReSIS project the payload integration is clearly stated in the requirements definition [17], but parameters such as aircraft range and general performance are not directly specified. Combinations of the following methods were used to develop derived requirements based on the qualitative requirements specified in [17]:

1. Use market research to determine the values of performance related parameters that would result in the most commercially competitive vehicle.
2. Use aircraft regulations such as FAR 23 to determine the requirements based on the aircraft class most similar to the design.
3. Use a combination of the given requirements and goals to determine the importance of the unspecified parameters, then assign a goal to the parameter rather than a specific number, such as “Increase range” or “Decrease takeoff distance.”
4. Use aircraft cost requirements to determine the ‘best’ design that is fiscally feasible.

The intent of this discussion is to show that it is imperative for a designer to transform as many of the qualitative requirements specified in a mission definition into quantifiable parameters as possible to more easily assess the merit of a given

design. However, this must be done with great care such that the derived requirements do not arbitrarily drive the design.

The development of the mission concept and requirements definition is discussed in the remainder of this section.

3.1 Areas of Interest

Two areas of interest have been identified for the design mission of this aircraft:

- Jakobshavn, Greenland
- Thwaites Glacier, Antarctica

3.1.1 Jakobshavn, Greenland

The Jakobshavn Glacier is located on the west coast of Greenland as shown in Figure 3.1. The survey areas are near "Swiss Camp" (69^{o}34'N, 49^{o}20'W) which is approximately 50 nm (~80 km) east of Ilulissat. The elevation of the area of interest is approximately 3,700 ft (~1,150 m). [18]

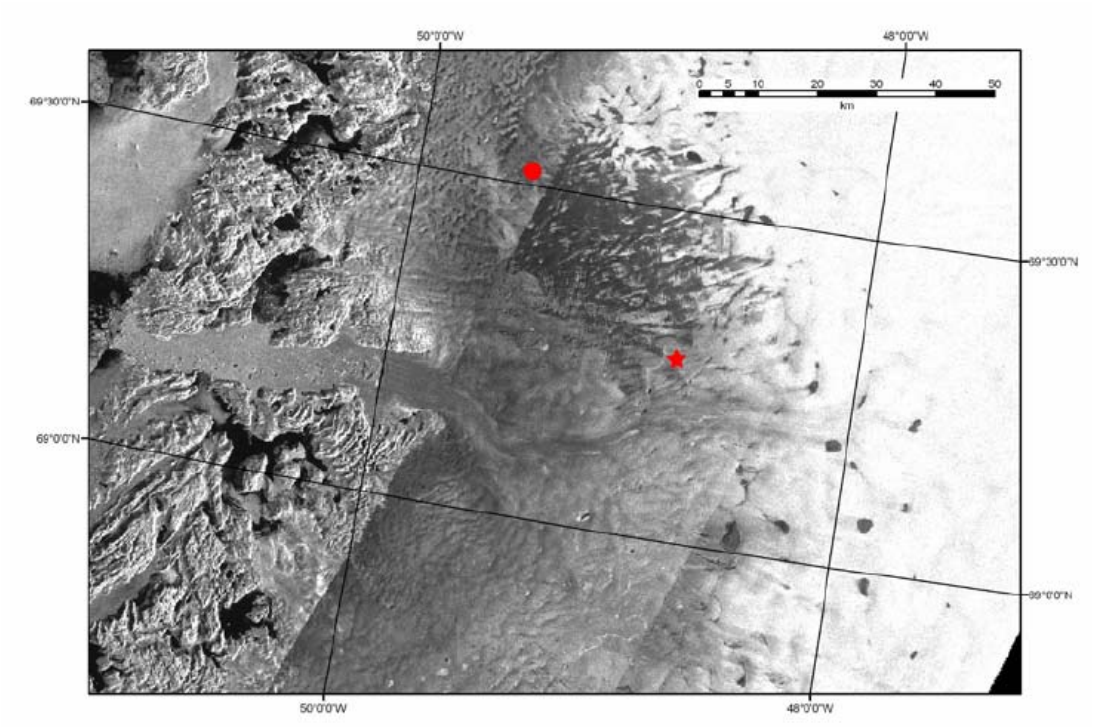

Figure 3.1: Jakobshavn Glacier [18]

3.1.2 Thwaites Glacier, Antarctica

The Thwaites Glacier shown in Figure 3.2 is located on the west coast of Antarctica, near the Wais Divide Camp [18]. The work proposed will augment the survey flown by the University of Texas-Austin and by BAS in 2004-2005 [18]. The three red stars indicate proposed locations of Fine scale surveys.

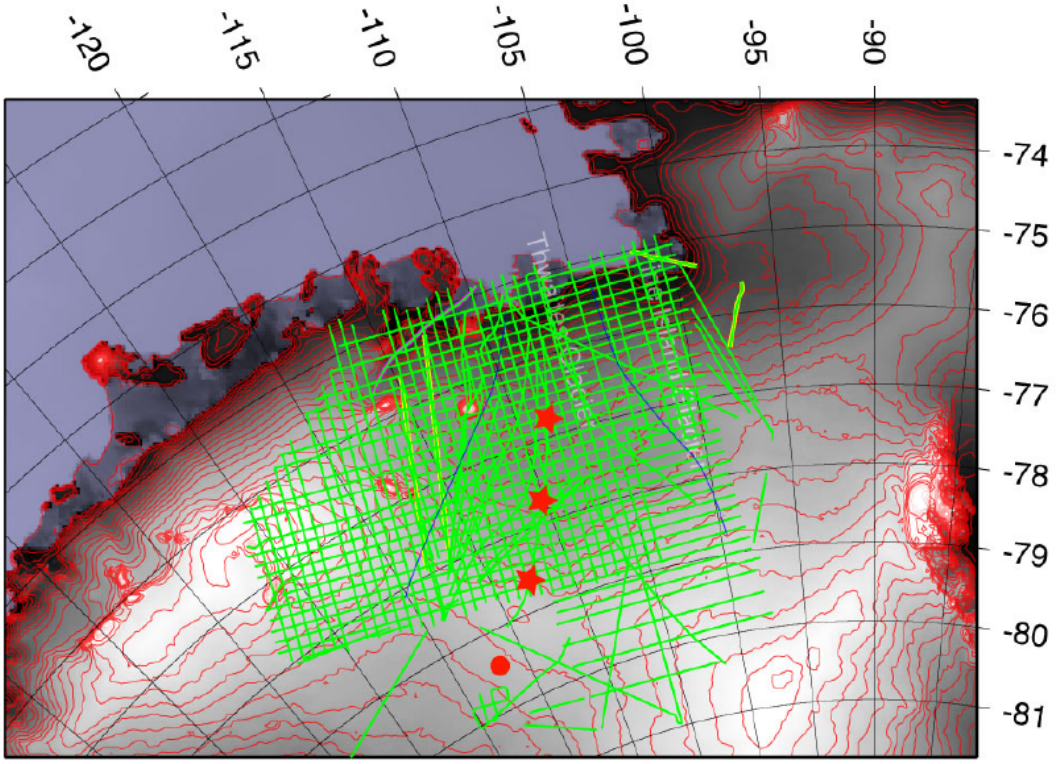

Figure 3.2: Thwaites Glacier [18]

3.2 Aircraft Range

One of the most important and most difficult requirements to specify for this mission was the aircraft range. During the early stages of the CReSIS UAV design, numerous trade studies were performed investigating the required aircraft range based on the location, size, and number of runways in Antarctica [1]. These studies showed that 75 percent of the continent could be reached from three bases with an aircraft with a range of 4,000 km as shown in Figure 3.3.

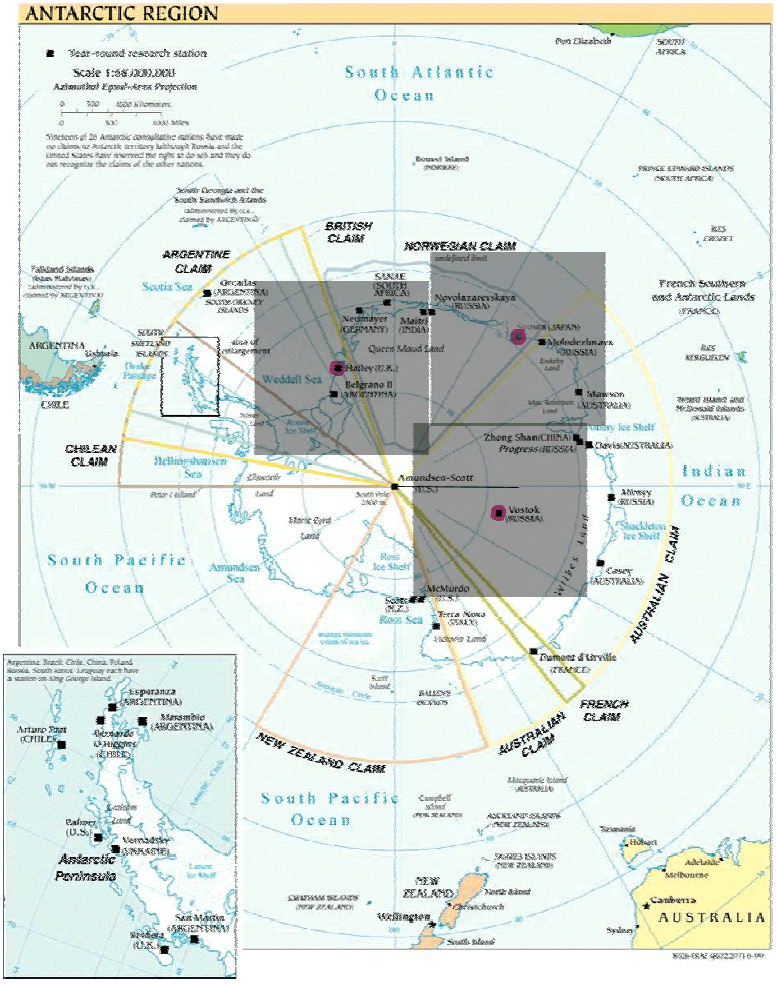

Figure 3.3: Map of Antarctica [1]

Similar studies were performed for vehicles operating from off continent as well as from the smaller, remote camps in Antarctica. These studies lead to the development of a three tiered mission specification. This description of this tiered mission specification as well as the refinement of the vehicle range requirements are discussed in this section.

3.2.1 Tiered Approach to the Mission Specification

In general terms, the concept for the science mission is to fly from some fixed base to an area of interest, perform a detailed survey of the ice then return to base. Several

of these missions will be conducted in a given season to complete a science campaign.

Past experiences have shown that significant science missions can be accomplished with aircraft ranging from a relatively short range vehicle such as a DeHavilland Twin Otter to much larger, longer range vehicles such as a Lockheed Martin P-3 or C130. [19]

Due to this large spectrum of possible missions, three mission concepts were developed [1]. These are referred to as the "Tier A," Tier B," and "Tier C" mission concepts and are described as:

Tier A

- Small, short-range (<1,000 km) vehicle capable of carrying either the scanning LIDAR topographic mapper OR the radar depth sounder (~50 kg).

Tier B

- Medium range (~5,000 km) vehicle capable of carrying the scanning lidar topographic mapper AND the radar depth sounder (~100 kg).

Tier C

- Long range (>10,000 km) vehicle capable of flying from off-continent any time of the year and capable of carrying the scanning lidar topographic mapper, the radar depth sounder, as well as other small payloads such as cameras or gravimeters (~150 kg).

Each of these concepts was investigated in terms of commercially available UAVs that meet the respective requirements, as well as new UAV designs. The results of this showed that the Tier C concept would be far too expensive for this science mission, while the Tier A concept may not be large enough to carry the required science payload.

3.2.2 Refinement of the Range Requirement

Further investigation of the mission concepts resulted in the development of more detailed science requirements. The science requirements [19] produced three survey definitions as follows:

Regional Survey:

- 500 km x 500 km with 10-15 km line spacing

Local Survey:

- 100 km x 100 km with 2.5 km line spacing
- 350 km Ingress/Egress Distance

Fine Survey:

- 20 km x 20 km with 1 km spacing
- 350 km Ingress/Egress Distance

The technology requirements specify that the UAV must be able to fly three fine scale missions in one four week period by July 2008. Upon success of this mission, at least one local scale survey and one fine scale survey should be flown in a 4 week

period. This would allow a science team to survey a large area, then return to survey a smaller area of high interest.

The proposed survey areas were converted into vehicle range requirements by first calculating the ground track distance that must be covered for each survey using Equation 3.1.

$$Ground\,Track\,Dist. = (W * L) / Line\,Spacing + W + L \qquad \text{Equation 3.1}$$

Equation 3.1 is used to calculate the ground track distance assuming a lawn-mower type pattern in one direction. The requirements call for dual coverage with perpendicular flight paths, which doubles the ground track distance for each survey area.

The ground track distances for each mission are shown in Table 3.1. The ingress/egress distances shown are for missions near Thwaites Glacier in Antarctica as these were determined to be the most critical [20].

Table 3.1: Mission Information for Fine, Local, and Regional Surveys

Parameter	SI Units	Fine	Local	Regional
Ground Speed:	km/hr	200	200	200
Grid Width:	km	20	100	500
Grid Length:	km	20	100	500
Line Spacing:	km	1	2.5	10
Distance from Base:	km	350	350	0
Ground Track Distance:	km	880	8,400	52,000
Total Time of Data Acquisition:	hrs	4.4	42	260

Parameter	English Units	Fine	Local	Regional
Ground Speed:	kts	108	108	108
Grid Width:	nm	10.8	54	270
Grid Length	nm	10.8	54	270
Line Spacing:	nm	0.54	1.35	5.4
Distance from Base:	nm	189	189	0
Ground Track Distance:	nm	475.2	4,536	28,080
Total Time of Data Acquisition:	hrs	4.4	42	260

The ground track distances shown in Table 3.1 were then used to determine the number of flights required to complete a Fine, Local, and Regional mission for aircraft with various ranges. This is shown in Table 3.2.

Table 3.2: Aircraft Range Trade Study Based on Number of Flights Required

		Fine Scale		Local		Regional	
		# of Flights Required	Length of Each Flight	# of Flights Required	Time for Each Flight	# of Flights Required	Time for Each Flight
		~	hrs	~	hrs	~	hrs
Vehicle Range (km)	1000	3	5	28	5	52	5
	1500	2	7.5	11	7.5	35	7.5
	2000	1	4.4	7	10	26	10
	2500	1	4.4	5	12.5	21	12.5
	3000	1	4.4	4	15	18	15
	3500	1	4.4	3	17.5	15	17.5
	4000	1	4.4	3	20	13	20
	4500	1	4.4	3	22.5	12	22.5
	5000	1	4.4	2	25	11	25

The Fine and Local scale missions are the only ones considered under these requirements. The Regional scale data is shown for comparison only.

The absolute minimum range requirement was determined using the detailed survey requirements. For an aircraft with a range greater than 1,580km (800nm) the

Fine Scale mission would only take one flight. However, an aircraft with a higher range would be able to complete more missions in a given time period. A trade study was performed examining the effect of aircraft range and the 4 week time period on the number of missions that could be flown.

The weather in Antarctica is such that flying every day of the 4 week period would be improbable. Therefore, it is assumed that 1 of every 3 days will be flyable. This leaves 9 flyable days in a 4 week period. For an aircraft with a range of at least 1,580km, the fine scale mission would take one day. This leaves 8 flyable days to complete the Local Scale mission. The required aircraft range was calculated to be 1,750 km (945 nm) using Equation 3.2.

$$Range = \frac{R_{Gr_{Fine}}}{N_{Fine}} + 2R_{ingress/egress_{Fine}} + \frac{R_{Gr_{Local}}}{N_{Local}} + 2R_{ingress/egress_{Local}} \qquad \text{Equation 3.2}$$

Where: R_{Gr} = Ground Track Distance
N = Number of Flights
$R_{ingress/egress}$ = Ingress/Egress Distance (350 km)

Typically, fuel reserves for 45 minutes of additional flight are added to the fuel requirements. Due to the extreme nature of the design mission of this aircraft, fuel reserves will be sized to allow for 1.5 hours of extended flight. At a nominal cruise speed of 200 km/hr, this essentially adds 300 km to the range requirement.

The Range requirements for this aircraft design are:

- Range: 1,750 km (945 nm) with full payload
- Fuel Reserves: 300 km @ 200 km/hr

3.3 Takeoff and Landing Distances

The takeoff and landing distances were originally determined by the size of the closest available runway [1]. The location of Thwaites Glacier in Antarctica, however, is 2,500 km from the closest usable runway, which is greater than the desired range of the aircraft. Fortunately, a local runway will be established at the WAIS Divide Camp by 2008 [18]. The length of this runway has yet to be specified, but members of NSF have indicated that any area where this aircraft will be used will require supplies to be flown in with a Lockheed C130 aircraft, which will require a 10,000 ft runway. Essentially, this means that the runway length in Antarctica will not be the limiting factor.

Table 3.3: Summary of Airports in Antarctica [1]

Airport	Elevation		Runway	Length (m)	
~	meters	feet	~	meters	feet
Marimbo	232	760	Graded Earth	1,260	4,134
McMurdo	21	68	Snow	3,048	10,000
Palmer Station	45	149	Snow	762	2,500
Petrel	5	15	Snow	1,067	3,500
South Pole Station	2,835	9,300	Snow	3,658	12,000
Teniente Rodolfo Marsh Martin	45	147	Graded Earth	1,292	4,238

The runways available in Greenland are shown in Table 3.4. The possibility of using one of these commercial runways is undetermined. There is a possibility that a groomed snow runway will be used instead. The exact dimensions of the runway that will be used are unknown. Therefore, the takeoff and landing distance requirements are specified in another manner. Members of the NSF have expressed the desire to be

able to operate from the same runway that a DeHavilland Twin Otter could operate [21].

Table 3.4: Runways in Greenland [1]

Town	Airport Name	ICAO	Usage	Runway	IFR	Runway Length	Runway Length
						ft	m
Aasiaat	Aasiaat	BGAA	Civ.	Paved	Yes	2600	792
Constable Pynt	Constable Pynt	BGCO	Civ.	Unpaved	Yes	3200	975
Godthab	Godthab	BGGH	Civ.	Paved	Yes	3100	945
Jakobshavn / Ilulissat	Jakobshavn / Ilulissat	BGJN	Civ.	Paved	Yes	2700	823
Kulusuk	Kulusuk	BGKK	Civ.	Unpaved	Yes	3900	1189
Maniitsoq	Maniitsoq	BGMQ	Civ.	Paved	Yes	2600	792
Narsarsuaq	Narsarsuaq	BGBW	Civ.	Paved	Yes	6000	1829
Sisimiut	Sisimiut	BGSS	Civ.	Paved	Yes	2600	792
Sondre Stromfjord	Sondre Stromfjord / Kangerlussuaq	BGSF	Civ.	Paved	Yes	9200	2804
Thule	Thule Ab	BGTL	Mil.	Paved	Yes	10000	3048
Uummannaq	Qaarsut	BGUQ	Civ.	Unpaved	Yes	2900	884

The Twin Otter has a takeoff and landing distance of approximately 1,500 ft (455m) using conventional landing gear on a conventional runway. The takeoff and landing distance requirement will be specified as follows:

The aircraft must be sized to have the same conventional takeoff and landing distance as the Twin Otter (1,500 ft).

The runway length for snow/ice operations will be determined based on the final design and may differ from this requirement. In other words, this requirement does not mean the aircraft will be able to operate from 1,500 ft snow runways, but rather it will simply have the same takeoff and landing performance as a Twin Otter.

3.4 Cruise Speed

The cruise speed requirement prescribed in the aircraft requirements [12] was initially 200 km/hr or 108 kts. This requirement is driven by the sampling rate of the sensors. The faster the aircraft flies, the faster the data must be recorded which increases the power consumption of the sensors. If this requirement is correctly

interpreted, then it is clear that the true desire is for the aircraft to maintain a *ground* speed of 108 kts, not a cruise speed. This is a more complicated requirement, due to the fact that the wind speeds in Antarctica can be as much as 30 kts. This means that the actual cruise speed of the aircraft could be anywhere from 78-138 kts.

The ground speed will be allowed to vary to:

- 110 kts in a 30 kts headwind
- 140 kts in a 30 kts tailwind.

In terms of the design cruise speed requirement, this implies that the critical case is:

- 140 kts at Max Continuous Power
    - (Flying into the wind at 110 kts ground speed)

3.5 Stall Speed and Climb Performance

Requirements for the aircraft stall speed and climb performance were not specified in the technological requirements [17]. These values were determined based on the performance of the DeHavilland Twin Otter as this aircraft is a short takeoff and landing (STOL) aircraft that is commonly used in Antarctica. This set the required stall speed to 58 kts and the maximum rate of climb at 1,600 ft/min.

3.6 Payload Requirements

The original payload requirements as specified in [19] for the CReSIS UAV are:

- On-board data storage of at least 1 Terrabyte
- Potential operating frequency of 100MHz-8 GHz
- Payload weight 35kg ideal, 55kg worst case*

- Payload power, 300W
- Payload Volume 0.05 cubic meters (1.8 cu ft)
- Minimum antenna area:
  - 75 cm x 10cm each, 7 on 50 cm spacing (75 cm x 370 cm area)*
- Operating altitude <1500m AGL, nominally 1000m AGL
- Payload Accommodations:
  - Nadir port for secondary payload
  - External antennas mounted parallel to track
- *NOTE: These requirements were used for the preliminary design of three concept vehicles and were changed for the final design as discussed in Section 6 of this document.

The primary payload requirements that will affect the vehicle design are the antenna array size, the payload volume and weight, and the payload power consumption.

The antennas must be mounted parallel to the ground track and spaced laterally. This essentially means that they will be mounted to the wing in some fashion. In addition, the antennas are sensitive to the type of structure around them, specifically any electrically reflective materials that are directly above the antennas, in other words, in the wing.

Materials such as aluminum, carbon fiber, or even fuel can reflect the signals the antennas are receiving thereby adding extraneous noise to the signal. Three solutions to this problem are examined:

1. Place the antennas one quarter wavelength below the wing (0.5m or 20")
2. Build a radar absorbing material above the antennas allowing them to be flush-mounted in the lower surface of the wing.
3. Design a dielectric wing that would not reflect the signals, thereby allowing them to be flush-mounted in the wing.

The first mounting option is the best choice in terms of the antennas due to two factors. First, this option has the highest probability of success as the second and third options have not been fully investigated. Secondly, if the antennas are mounted a quarter wavelength below a reflective surface, then the interference from this surface will actually add to the total signal, thereby reducing the power required by the antennas.

In terms of the aircraft design, namely aerodynamic efficiency, the second and third options are the most desirable. However, the third mounting option was deemed unacceptable by the antenna designers due to its low probability of success [22].

At the time of this design there was insufficient data to support or refute the possibility of the second mounting option. Therefore, several independent aircraft designs were performed using the first two mounting options. This helped give insight into how much the antenna requirements are driving the aircraft design.

3.7 Size Requirements

Several items were considered to limit the overall geometry of the vehicle. These included:

- Shipping Constraints
- Facility Constraints – Hangar Size
- Manufacturing Facilities
- Runway Width

Of these constraints, the most critical was determined to be the shipping constraints. This is also one of the most easily quantifiable. The aircraft will be shipped to Antarctica and Greenland using standard size shipping containers. The dimensions for a standard twenty foot container as shown in Table 3.5 were used to set the maximum dimensions of the aircraft. This requirement will take the following form:

The aircraft, ground station, and all ground equipment required for the aircraft operation must fit entirely in a standard twenty foot shipping container.

This is different than simply specifying the maximum fuselage length or wing span of the vehicle as the wing could be manufactured in two pieces meaning the maximum wing span is larger than twenty feet.

Table 3.5: Dimensions of Standard Shipping Containers [23]

20 ft Dry Container			
	ft	inches	cm
Length	19.4	233.0	591.8
Height	7.7	92.1	234.0
Width	7.8	93.6	237.8

40 ft Dry Container			
	ft	inches	cm
Length	39.0	468.4	1189.7
Height	7.7	92.4	234.6
Width	7.8	93.6	237.8

3.8 Logistical Requirements

There are several requirements for the UAV that do not directly relate to performance or geometric requirements. Some of these items are:

- Maintenance
- Communications
- Regulatory Issues
- Environmental Issues
- Special Operations

3.8.1 Maintenance Requirements

The aircraft must be designed such that it is easily maintainable in the extreme environments it will be operating in. This means that accessibility to the engine, payload area, flight control system, and fuel system must be heavily considered throughout the design process. Also, the aircraft must be designed for easy assembly in cold weather. This means that the number of parts the aircraft is broken into for shipping should be minimized. It also has implications on the type of connections

and fasteners used as the mechanics working on the vehicle will most likely be wearing gloves.

3.8.2 Communications

The aircraft must be able to communicate with the ground station in terms of vehicle health and control commands. The ground station operator must be able to identify the health state of the UAV in terms of position, attitude, fuel quantity, etc and must also be able to command changes in the aircrafts mission. The update rate for this type of control can be on the order of 0.25 to 1 Hz. The communication requirements will be summarized as follows:

The aircraft must be able to carry the necessary data acquisition and communications devices to allow monitoring and control of the vehicle at up to 600 km from base station.

3.8.3 Regulations

The UAV will be designed for operation in Antarctica, Greenland, and testing in the United States. The aircraft must comply with all necessary regulations related to uninhabited air operations in each of these areas.

3.8.4 Environmental Issues

The most important requirements with respect to environmental issues in Antarctica are related to the requirement that no materials can be left on the continent. This has implications in several areas: fuel dumping, vehicle recovery, and deicing.

The landing weight of a vehicle can often be considered to be less than the maximum takeoff weight. This allows the designer to size the aircraft to a smaller landing distance. However, doing so requires that the aircraft dump fuel in the case of an emergency landing immediately after takeoff. This is not possible with this aircraft, so this requirement will set the design landing weight equal to the takeoff weight.

The environmental concerns have implications on the procedures used in the case of loss of communication. The primary issue is to determine what the aircraft will do if communications with GPS satellites or the ground station are lost for a specified amount of time. One option would be to deploy a parachute recovery system and land the aircraft at the point of last communication with the ground station. A second option would be to specify a "home" waypoint that the aircraft will return to after some specified period of lost communications. At the time of this vehicle design this matter was not resolved.

The environmental protection regulations in Antarctica prohibit the use of chemical deicing. This means that the any deicing system used on the Meridian must use some method other than weeping wing type technology.

3.8.5 Cold Weather Operations Requirements

This aircraft is being designed for operation in extremely cold climates, which must be accounted for in the design process. The aircraft system must be capable of heating the engine and all necessary systems to reasonable operating temperatures prior to flight. This can be done with external heaters that remain on the ground;

however the temperature of these systems must be maintained throughout the flight, which could require onboard heaters.

In addition to temperature control in the fuselage, wing icing must be considered. While flights will only be conducted in "blue sky" conditions, icing can occur and must be manageable. Therefore, this aircraft must employ some form of anti-icing on all critical surfaces.

3.9 Requirements Summary

The aircraft design requirements are summarized in Table 3.6. This table shows the design requirements as well as their relative importance. This table will be used in making design decisions throughout this aircraft design process. A typical mission profile for this aircraft is shown in Figure 3.4.

Table 3.6: Summary of Design Requirements

Parameter	Value	Importance	Source
Range	950 nm (~1750 km) w/ 1.5 hr Reserve	High	Trade Studies[1]
Endurance	> 9 hrs	Medium	Trade Studies[1]
Cruise Speed	100-120 kts (~180-220 km/hr)	Medium	Technology Requirements[3]
Maximum Ceiling	15,000 ft (4,500 m)	Low	Technology Requirements[3]
Rate of Climb	1,600 ft/min (490 m/min)	Low	Twin Otter Performance[5]
Takeoff Distance	1,500 ft (~450 m)	High	Twin Otter Performance[5]
Landing Distance	1,500 ft (~450 m)	High	Twin Otter Performance[5]
Payload Volume	20" x 20" x 8" (~0.5 x 0.5 x 0.2 m)	High	Technology Requirements[3]
Payload Weight	120 lbs (~55 kg)	High	Technology Requirements[3]
Payload Integration	Wing Mounted Antennas	High	Technology Requirements[3]
Payload Power	300 W	Medium	Technology Requirements[3]
Stall Speed	58 kts (105 km/hr)	Medium	Technology Requirements[3]
Stability and Control	FAR 23, where applicable	Low	www.faa.gov
Maneuvering Requirements	FAR 23, where applicable	Low	www.faa.gov
Aircraft Wingspan	Must fit in 20 ft Container	High	20 ft. Container Dimensions[5]
Aircraft Length	Must fit in 20 ft Container	High	20 ft. Container Dimensions[5]

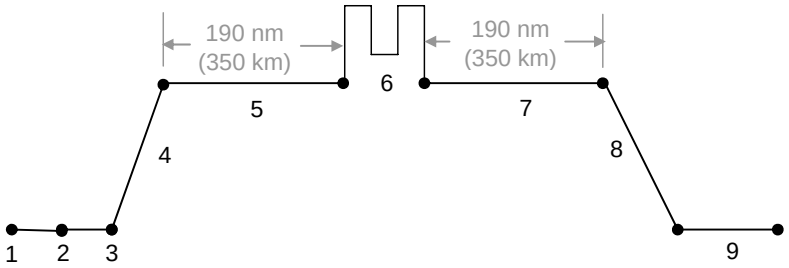

1. Warmup
2. Taxi
3. Takeoff
4. Climb (No Range Credit)
5. Cruise Out (Optimum Alt. and Speed)
6. Data Acquisition (120 kts @ 5,000 ft AGL)
7. Cruise Return (Optimum Alt. and Speed)
8. Descent (No Range Credit)
9. Land/Taxi

Figure 3.4: Design Mission Profile

4 Aircraft Market Survey

An aircraft market study was performed on both inhabited and uninhabited aircraft that could be used for this mission. The first step in this process was to investigate the aircraft that are currently used for this type of research in Antarctica and Greenland. This list of aircraft was then augmented by a variety of inhabited and uninhabited aircraft that have been investigated for use in this type of research.

4.1 Aircraft Currently Used in Cold-Weather Research

The first type of similar aircraft that are investigated for this mission are vehicles that are currently used in Antarctica and Greenland. Three of these vehicles are described here:

- Lockheed C130
- Lockheed P-3
- DeHavilland Twin Otter

4.1.1 Lockheed C130

The Lockheed C130 aircraft was originally procured in 1951. Since then over 70 variants have been designed and delivered. The model currently fielded in Antarctica is the C130H, which is what is described here. The geometry, weight, and performance data for the C130 are shown in Table 4.1. [24]

Figure 4.1: Lockheed C130 Operating from Snow Runway [24]

Table 4.1: Lockheed C130H Summary [24]

Lockheed C130H		
Parameter	**Units**	**Value**
Geometry		
Wing Span	ft	132.6
Wing Area	ft^2	1,745
Length	ft	97.75
Weights		
Takeoff Weight	lbs	155,000
Empty Weight	lbs	76,000
Performance		
Range	nm	4,250
Cruise Speed	kts	300
Stall Speed	kts	100
Takeoff Distance	ft	5,160
Landing Distance	ft	2,750

4.1.2 Lockheed P-3 Orion

The Lockheed P-3 Orion is a land-based maritime and anti-submarine warfare (ASW) aircraft. Development of the P-3 began in 1958 with the first flight in late 1959. As with the C130, there have been many variants and modifications of the original P-3 [24]. The data for the P-3C is shown in Table 4.2.

Figure 4.2: Lockheed P-3 Orion on Ice Runway in Antarctica [25]

Table 4.2: Lockheed P-3C Orion Summary [24]

Lockheed P-3 Orion		
Parameter	**Units**	**Value**
Geometry		
Wing Span	ft	99.7
Wing Area	ft^2	1,300
Length	ft	116.8
Weights		
Takeoff Weight	lbs	135,000
Empty Weight	lbs	61,490
Performance		
Range	nm	4,830
Cruise Speed	kts	328
Stall Speed	kts	112
Takeoff Distance	ft	5,490
Landing Distance	ft	2,770

4.1.3 DeHavilland DHC-6 Twin Otter

The Twin Otter – Canada's most successful commercial aircraft with over 800 built – was developed in early 1964. The aircraft's first flight of the 100 Series was in May of 1965. The -300 Series added an increased nose for more baggage storage as well as more powerful engines allowing for a higher takeoff weight. This vehicle is

heavily used in Antarctica as well due to its rugged design, short takeoff and landing capability, and proven performance in cold weather. The aircraft geometry, weight, and performance data are shown in Table 4.3. [24]

Figure 4.3: De Havilland Twin Otter Operating from Snow Runway [19]

Table 4.3: De Havilland Twin Otter-300 Summary [24]

DeHavilland Twin Otter		
Parameter	**Units**	**Value**
Geometry		
Wing Span	ft	65
Wing Area	ft^2	420
Length	ft	51.75
Weights		
Takeoff Weight	lbs	12,500
Empty Weight	lbs	7,400
Performance		
Range	nm	700
Cruise Speed	kts	182
Stall Speed	kts	58
Takeoff Distance	ft	1,500
Landing Distance	ft	1,940

4.2 Uninhabited Air Vehicles

A list of UAVs has been developed to help show the current state of the market with respect to the mission specification. This list includes geometry, weight, and performance data for over 200 UAVs. The data for this list was taken from a

combination of manufacturer's websites as well as a list of UAV resources (See References 26, 27, and 21).

The UAVs were organized in terms of range and payload capacity in Figure 4.4. Several inhabited platforms that are currently used in Cryospheric research are also shown in Figure 4.4.

There are several aircraft in that meet the Tier A requirements in terms of range and payload weight, but these aircraft do not meet the payload volume requirements. There are no aircraft that lie directly in the Tier B or Tier C design spaces. This is due to the fact that the requirements for these aircraft are skewed towards high range capability with low payload capacity.

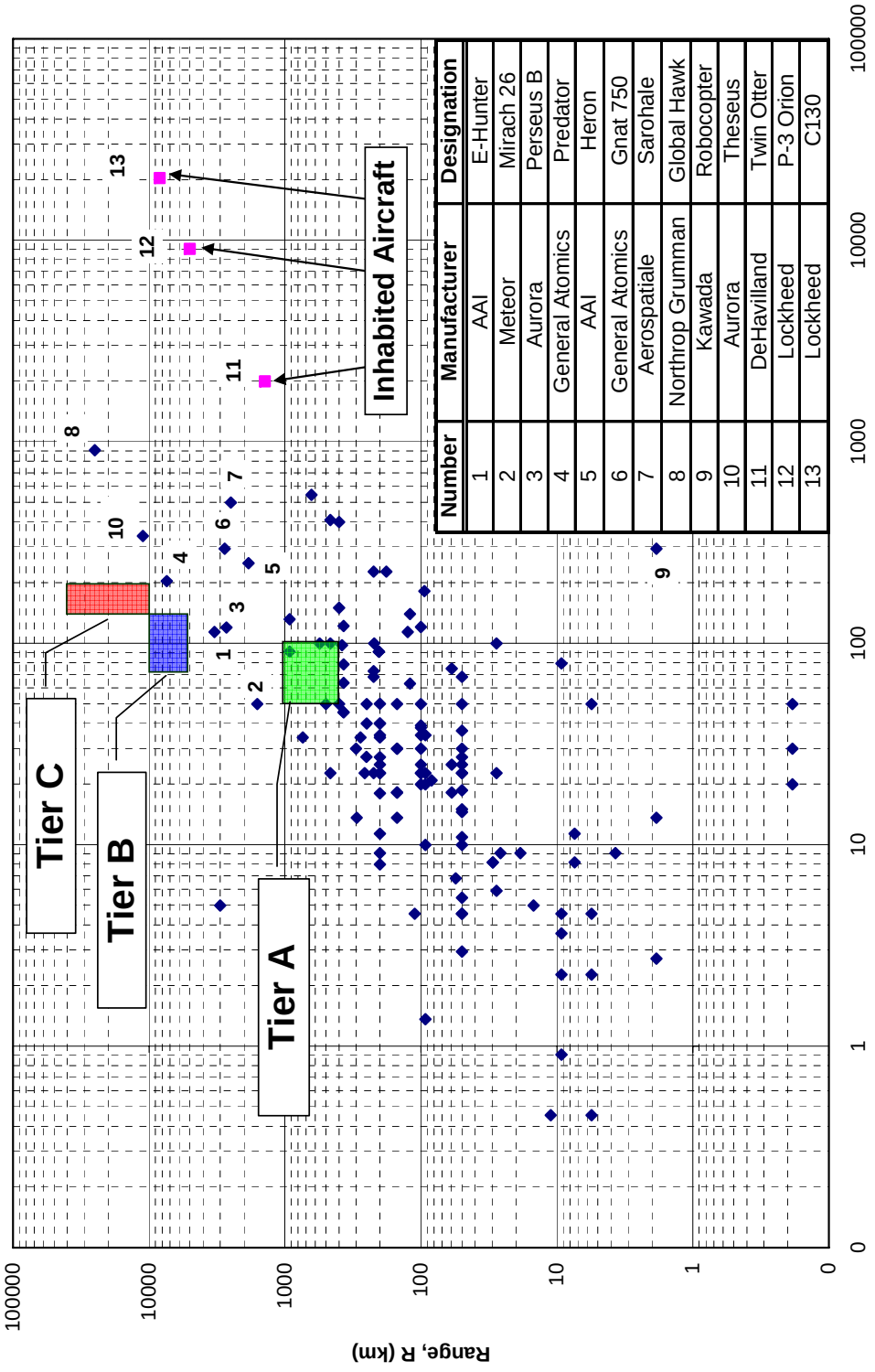

Number	Manufacturer	Designation
1	AAI	E-Hunter
2	Meteor	Mirach 26
3	Aurora	Perseus B
4	General Atomics	Predator
5	AAI	Heron
6	General Atomics	Gnat 750
7	Aerospatiale	Sarohale
8	Northrop Grumman	Global Hawk
9	Kawada	Robocopter
10	Aurora	Theseus
11	DeHavilland	Twin Otter
12	Lockheed	P-3 Orion
13	Lockheed	C130

Figure 4.4: Current Commercially Available UAVs [26, 27, 21]

4.2.1 Similar Uninhabited Air Vehicles

The list of UAVs was narrowed from those shown in Figure 4.4 to a list of aircraft that will be used for preliminary sizing. Generating a list of *similar* UAVs is difficult because, while the number of commercially available UAVs is growing, the market is relatively small considering the wide range of performance characteristics as shown in Figure 4.4. Therefore the *similar* aircraft must be selected using a slightly wide set of requirements. For this mission, high performance, long range, reconnaissance and tactical uninhabited aircraft will be considered. These aircraft are shown in Table 4.4. This list of aircraft was selected as they represent both high performance vehicles in the Predator and E-hunter as well as tactical, rugged vehicles such as the Shadow 200 and Geneva Aerospace Dakota. Note that the list of UAVs represents a wide range of size, which is useful for generating sizing trends.

Table 4.4: Summary of Similar Aircraft [26, 27, 21]

Country	Company	Designation	W_E lb	W_{TO} lb	W_{pay} lb	b_w ft	Length ft	End. hr	Range nm	Ceiling ft	Speed kts
U.S.	General Atomics	Predator B	2,800	6,500	3,800	66.0	36.0	30	OTH*	25,000	220
U.S.	General Atomics	Predator	1,200	2,350	450	48.7	27.0	40	7,400	25,000	220
U.S.	Northrop Grumman	E-Hunter	1,430	2,100	220	54.5	24.5	30	OTH*	25,000	120
U.S.	General Atomics	I-Gnat	850	1,650	650	42.2	20.8	48	1,500	30,000	160
U.S.	AAI	Shadow 600	327	585	85	22.4	15.6	14	-	17,000	108
U.S.	AAI	Shadow 200	200	316	50	12.8	11.2	8	-	15,000	115
U.S.	Geneva Aerospace	Dakota	160	240	80	15.6	9.5	4.5	575	20,000	100

Country	Company	Designation	W_E kg	W_{TO} kg	W_{pay} kg	b_w m	Length m	End. hr	Range km	Ceiling m	Speed km/hr
U.S.	General Atomics	Predator B	1,270	2,948	1,723	20.1	11.0	30	OTH*	7622.0	371
U.S.	General Atomics	Predator	544	1,066	204	14.8	8.2	40	13,705	7,622	371
U.S.	Northrop Grumman	E-Hunter	649	952	100	16.6	7.5	30	OTH*	7,622	203
U.S.	General Atomics	I-Gnat	385	748	295	12.9	6.3	48	2,778	9,146	270
U.S.	AAI	Shadow 600	148	265	39	6.8	4.8	14	-	5,183	182
U.S.	AAI	Shadow 200	91	143	23	3.9	3.4	8	-	4,573	194
U.S.	Geneva Aerospace	Dakota	73	109	36	4.8	2.9	4.5	1,065	6,098	169

* OTH - Over The Horizon

4.2.1.1 General Atomics Predator B

The General Atomics Predator B (Figure 4.5) was developed in 2000 as a high altitude, long endurance (HALE) uninhabited air vehicle for multiple missions and a variety of customers. The Predator B utilizes an internal payload bay as well as external payload mounting options [29].

Figure 4.5: General Atomics Predator B [29]

4.2.1.2 General Atomics Predator

The General Atomics Predator (Figure 4.6) was developed as an evolution of the Gnat system. The predator has been configured for air-to-air and air-to-ground weapons and has logged over 65,000 flight hours. The Predator went into full production in 1997 and is currently in production for the United States and Italian Air Force [29].

Figure 4.6: General Atomic Predator [29]

4.2.1.3 Northrop Grumman E-Hunter

The Northrop Grumman E-Hunter (Figure 4.7) is a medium altitude, medium endurance, tactical uninhabited air vehicle designed for reconnaissance and surveillance. The E-Hunter is based on the Northrop Grumman Hunter UAV [30]. It combines the fuselage of the original Hunter UAV with a new tail and longer wing.


Figure 4.7: Northrop Grumman E-Hunter [30]

4.2.1.4 General Atomics I-Gnat

The I-Gnat (Figure 4.8) is an improved version of the Gnat 750 [29], which was designed in 1988 and first flight tested in 1989. The I-Gnat was first introduced in 1999 and incorporated improved wing hardpoints, a new Synthetic Aperture Radar, glycol based de-icing, and a turbocharged heavy fuel engine. The I-Gnat is designated as an all-altitude, multi-mission, long-endurance aircraft. [21]

Figure 4.8: General Atomics I-Gnat [29]

4.2.1.5 AAI Shadow 200

The Shadow 200 (Figure 4.9) is a small, tactical UAV designed for surveillance and target acquisition. The vehicle is constructed of 90 percent composites and utilizes a detachable tricycle landing gear as well as options for catapult or rocket assisted takeoff (RATO). It is recovered using conventional wheeled landing or via a parachute. [21]


Figure 4.9: AAI Shadow 200 [31]

4.2.1.6 AAI Shadow 600

The Shadow 600 (Figure 4.10) is a larger, more capable version of the Shadow 200. This aircraft utilizes a pusher engine installation with a twin boom tail configuration. Over 95 percent of the aircraft is manufactured with composite materials. Like the Shadow 200, this aircraft can operate from conventional tricycle landing gear as well as a pneumatic catapult and rocket assisted takeoff. [21]

Figure 4.10: AAI Shadow 600 [31]

4.2.1.7 Geneva Aerospace Dakota

The Dakota UAV (Figure 4.11) is a small, low-cost, tactical UAV designed to carry a variety of payload packages. This aircraft has been used for surveillance as well as testing and research oriented missions. The Dakota utilizes conventional tricycle landing gear for takeoff and landing and is manufactured from a combination of composite materials and aluminum. [32]

Figure 4.11: Geneva Aerospace Dakota UAV [32]

4.3 Optionally Piloted Vehicle Concepts

Several inhabited aircraft were investigated for use in the CReSIS missions as optionally piloted aircraft. This was done for several reasons. First, an optionally piloted vehicle would mitigate the risk of system development as the aircraft could be operated by a pilot that can turn an autopilot system on and off. This helps to circumvent several of the regulatory barriers surrounding UAV testing in the United States National Airspace (NAS). Another reason is that crewed aircraft are more readily accessible in terms of acquisition cost than UAVs. Purchasing an inhabited aircraft and converting it for autonomous operation could be more cost-effective than purchasing a full UAV system that has more capabilities than what is needed for this mission. These advantages are currently being explored by Diamond Aircraft [33].

Table 4.5 shows the piloted vehicles chosen for comparison. These vehicles were chosen as they are representative of a wide variety of aircraft: small, single and twin

piston engine aircraft; medium sized turboprop aircraft; as well as much larger aircraft.

Table 4.5: Optionally Piloted Vehicle Performance Summary [24]

Company	Designation	Empty Weight	Gross Weight	Payload	Range	Cruise Speed	Takeoff Dist.
SI Units							
~	~	kg	kg	kg	km	km/hr	m
Lockheed Martin	C130	34,504	70,370	20,400	8,334	602	1,433
Lockheed Martin	P-3 Orion	27,916	63,451	9,075	5,000	611	1,673
DeHavilland	Twin Otter	3,677	5,675	1,990	1,400	241	457
Cessna	182	736	1,158	544	1,500	259	461
Cessna	208 (Caravan)	1,725	3,973	907	2,000	333	626
Beech	1900D	4,331	7,772	4,375	2,900	533	994
Diamond	Twin Star	1,260	1,700	440	2,360	250	350
English Units							
~	~	lbs	lbs	lbs	nm	kts	ft
Lockheed Martin	C130	76,000	155,000	44,974	4,500	325	4,700
Lockheed Martin	P-3 Orion	61,490	139,760	20,007	2,700	330	5,490
DeHavilland	Twin Otter	8,100	12,500	4,387	780	130	1,500
Cessna	182	1,621	2,550	1,200	820	140	1,514
Cessna	208 (Caravan)	3,800	8,750	2,000	1,100	180	2,053
Beech	1900D	9,540	17,120	9,645	1,589	288	3,260
Diamond	Twin Star	2,780	3,750	970	1,275	135	1,150

Table 4.5 shows that all of the aircraft investigated have much higher payload capacity than is needed for this mission. This excess weight can be converted into extra fuel by installing additional fuel tanks in the aircraft. The possible increases in aircraft range were investigated, the results of which are shown in Table 4.6.

Table 4.6: Additional Range Estimates for Crewed Aircraft

Company	Designation	Stock Range	Estimated Fuel Consumption	Additional Fuel Capacity	Range Adjusted for Extra Fuel	Total Fuel Used**
SI Units						
~	~	km	kg/hr	kg	km	Liters
Lockheed Martin	C130	8,334	3,900	10,173	8,856	71,504
Lockheed Martin	P-3 Orion	5,000	1,814	4,510	5,498	33,258
DeHavilland	Twin Otter	1,400	262	968	2,138	4,806
Cessna	182	1,500	52	245	2,820	956
Cessna	208 (Caravan)	2,000	136	426	2,626	2,494
Beech	1900D	2,900	249	2,160	4,632	4,573
Diamond	Twin Star	2,360	18	193	4,499	330
English Units						
~	~	nm	lbs/hr	lbs	nm	gallons
Lockheed Martin	C130	4,500	8,580	22,380	4,782	18,877
Lockheed Martin	P-3 Orion	2,700	3,991	9,922	2,969	8,780
DeHavilland	Twin Otter	756	577	2,129	1,155	1,269
Cessna	182	810	115	757*	1,523	252
Cessna	208 (Caravan)	1,080	299	937	1,418	658
Beech	1900D	1,566	549	4,752	2,501	1,207
Diamond	Twin Star	1,274	40	424	2,429	87

* Extra fuel may be limited by available volume.
** Fuel volume required to complete 3 Fine Scale Surveys.
- Currently used in polar research

The fuel consumption numbers were taken from manufacturer specifications. The additional range was simply determined by multiplying the estimated fuel consumption by the estimated additional fuel capacity. The additional fuel capacity was estimated as half of the vehicle payload capacity less the 55 kg (121 lb) science payload requirement. The fuel densities were assumed to be 6.0 lbs/gal for aviation gasoline and 6.8 lbs/gal for Jet-A.

The numbers for the Diamond Twin Star shown in Table 4.6 were verified against an experimental flight test performed by Diamond Aircraft [34]. This test showed the vehicle range was increased from 1,275 nm to 1,900 nm after installing an additional 26 gallon ferry fuel tank to the existing 78 gallon fuel tank. Only 72 gallons of fuel were used for the flight. The company estimates that the vehicle with the ferry tanks could achieve a 2,500 nm range, which is very close to the estimate shown in Table 4.6.

The value of total fuel used represents the amount of fuel that would be used to complete 3 Fine Scale surveys. The highlighted aircraft in Table 4.6 represent the aircraft that are currently used for polar research. The column indicating the amount of fuel required to complete 3 Fine Scale missions is representative of the possible savings in operational costs that can be achieved by transitioning to smaller, more efficient platforms.

From an operational cost standpoint, the Diamond Twin Star is the best candidate for this mission based on the aircraft listed in Table 4.5. The Twin Star is a high performance aircraft that fits nearly all of the proposed requirements. However,

integrating the antenna array into the Twin Star would be difficult. Also, this aircraft is much larger than a UAV of similar performance. These facts do not eliminate the Twin Star as a viable candidate for this mission. They do, however, support the argument that a new aircraft design should be performed to determine if a better solution can be achieved.

5 Preliminary UAV Designs

The following aircraft configurations were considered for this design:

1. Conventional Tail-Aft
2. Twin Fuselage
3. Canard
4. Three-Surface
5. Joined Wing
6. Tandem Wing
7. Flying Wing

The preliminary aircraft design concepts and trade studies performed prior to this design helped in the selection of the candidate configurations [1]. The canard and three-surface configurations were not chosen for direct investigation based preliminary sizing studies that indicated that a single, fuselage mounted engine will be used [20]. The use of a canard is incompatible with a fuselage-mounted, tractor engine. However, the implementation of a canard will be considered if the engine is mounted in a pusher configuration. The tandem wing design is fundamentally incompatible with the antenna integration requirement [20]. The flying wing configuration was eliminated based on poor cross-wind capability [20]. The conventional and joined wing (biplane) configurations were selected as the options for further study.

In the payload requirements definition, two antenna mounting options were developed. One assuming flush-mounted antennas and one assuming the antennas would hang below the wing. In addition, at the time of this design the type and frequency range of the antennas had not been finalized.

Typically, in aircraft configuration design it is desirable to perform independent design studies of different configurations. These concepts can then be evaluated to determine the best configuration that will be selected for further optimization in the detail design process. Also, the uncertainty in the antenna integration and type calls for some amount of flexibility in the configurations. Three preliminary aircraft configuration design studies are performed, each with a different antenna mounting solution. Ideally, these configuration designs would be performed by separate, completely isolated teams. However, time and funding did not allow for this approach so there is some amount of similarity between the three designs as this prevented the need to duplicate work. The fuselage layout, engine selection and placement, empennage design, and landing gear layout are examples of areas containing a great deal of commonality for the three configurations. The main difference in the configurations pertains to the wing design as follows:

Aircraft Configurations:

1. Red Design: Conventional Monoplane w/ Flush-Mounted Antennas
2. White Design: Conventional Monoplane w/ Hanging Antennas
3. Blue Design: Biplane with Antennas Mounted in Lower Wing

The purpose of the remainder of this chapter is to describe the Class I preliminary design of these three configurations. The preliminary design of the Red, White, and Blue concepts was performed using the process described in *Airplane Design Part I: Preliminary Sizing of Airplanes* by Dr. Roskam [2]. The preliminary configuration design sequence can been divided into Class I and Class II segments as described by Dr. Roskam [2]. The Class I design sequence includes:

- Preliminary Aircraft Sizing
- Fuselage Layout
- Propulsion Selection
- Wing Planform and Lateral Controls Design
- High-Lift Device Sizing
- Empennage Sizing
- Landing Gear Selection and Sizing
- Class I Weight and Balance
- Class I Stability and Control Analysis
- Class I Aerodynamic Analysis

5.1 Description of Preliminary Concepts

The three concepts are described in detail. The White and Blue design utilize hanging antennas. The separation distance of 0.5 m (19.7 in) corresponds to one quarter wavelength at 150 MHz, which is the lowest expected operating frequency of the antennas.

Red Design

The Red Design will be a conventional tail aft aircraft with the following requirement imposed:

Figure 5.1: Red Concept

The antennas will utilize a special material backing such that the antennas can be mounted flush with the wing skin and the electrical interference properties of the wing do not need to be limited.

White Design

The White Design will be a conventional tail aft aircraft with the following requirement imposed:

Figure 5.2: White Concept

The antennas will be mounted 0.50 meters beneath the bottom surface of the wing, which will be made of some electrically reflective material such as aluminum or carbon fiber.

Blue Design

The Blue Design will be a biplane aircraft with the following requirement imposed:

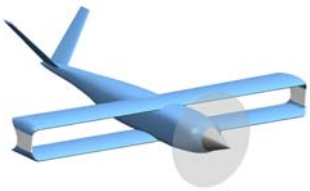

Figure 5.3: Blue Concept

The antennas will be mounted in a dielectric lower wing 0.50 meters beneath the bottom surface of the upper wing, which is made of some electrically reflective material.

5.2 Preliminary Aircraft Sizing

The purpose of this section is to determine an estimation of the aircraft takeoff, empty, and fuel weights. This is accomplished using data from similar aircraft as well as estimates for the amount of fuel used during a mission.

5.2.1 Takeoff Weight Regression

A takeoff weight regression plot was created using the aircraft listed in Table 4.4 as shown in Figure 5.4. This is used to generate a relationship between takeoff and

empty weights of current aircraft. The level of confidence in a regression plot is related to the number of data points as well as the scatter about the trended line. Adding more aircraft to the list will decrease the technical risk of reaching the assumed takeoff-to-empty weight ratio. However, adding inefficiently designed aircraft to the list may result in an overly conservative design. The aircraft shown in Figure 5.4 were chosen after several iterations with different combinations of aircraft. These aircraft are some of the more efficient designs in terms of the takeoff-to-empty weight ratio and therefore represent a moderately aggressive design strategy.

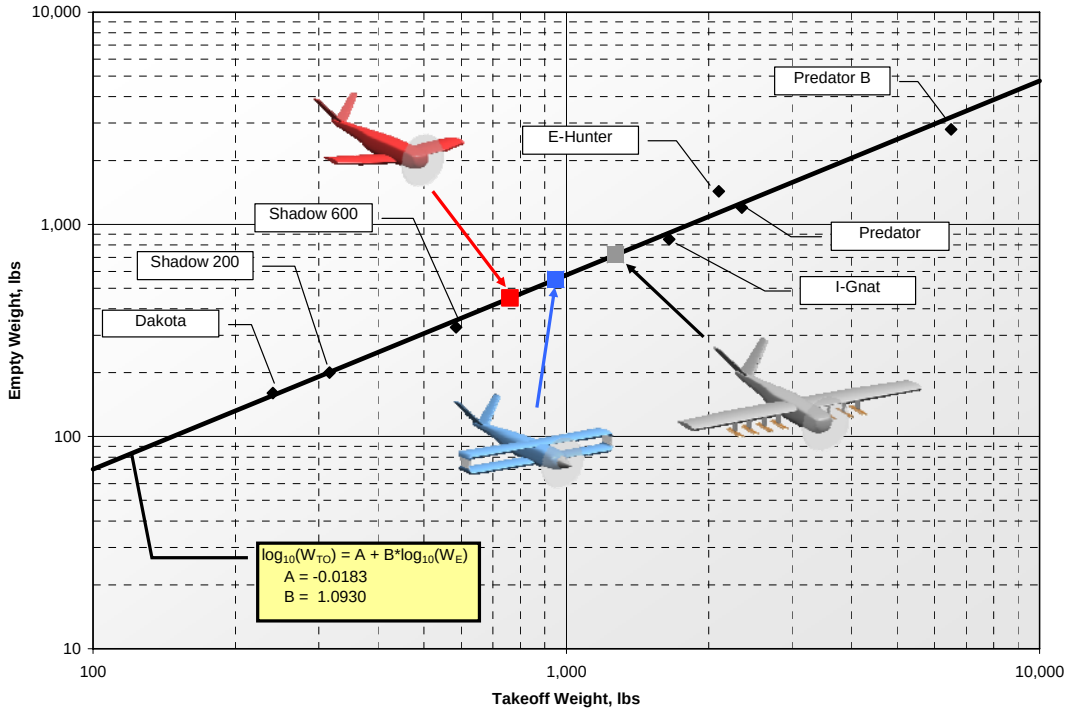

Figure 5.4: Takeoff Weight Regression Plot for Similar Aircraft

5.2.2 Mission Fuel Fractions

Fuel fractions were determined for each segment of the design mission profile as specified in Section 3.9 on page 30. A fuel fraction is defined as the ratio of end

weight to initial weight for a given segment. For simplicity, the cruise out, data acquisition, and cruise return segments of the mission profile were converted to one cruise segment. This implies the cruise speed is the same for the ingress, egress, and data acquisition segments.

The fuel fractions for the warm-up, taxi, takeoff, descent, and land/taxi segments were estimated using historical data. The warm-up fuel fraction was modified to account for the cold weather operations by doubling the warm-up time. This was implemented via Equation 5.1.

$$M_{ff_{warm-up}} = M^{2}_{ff_{Typ\ warm-up}} \qquad \text{Equation 5.1}$$

The fuel fractions for the climb and cruise segments were calculated using the Breguet endurance (Equation 5.2) and range (Equation 5.3) equations respectively [2].

$$M_{ff} = e^{\left(-\frac{(1.68\,\text{fps/kts})E_{Cl}}{(550\,\text{ft-lb/hp-s})(60\,\text{min/sec})}\frac{c_{PCl}}{\eta_{PCl}}\frac{V_{Cl}}{\left(L/D\right)_{Cl}}\right)} \qquad \text{Equation 5.2}$$

$$M_{ff} = e^{\left(-\frac{(1.68\,\text{fps/kts})R_{Cr}}{550\,\text{ft-lbs/hp-s}}\frac{c_{PCr}}{\eta_{PCr}}\frac{1}{\left(L/D\right)_{Cr}}\right)} \qquad \text{Equation 5.3}$$

The following assumptions were used for the climb segment:

- Climb Height: 5,000 ft
- Rate of Climb: 500 ft/min
- L/D: (Based on class I drag polar)
  - Red: 11.5

    - White: 9.5
    - Blue: 11.0
- Specific Fuel Consumption: 0.56 lbs/hp-hr
    - (Based on manufacturer's data for the Rotax 912-A [35])
- Propulsive Efficiency: 0.80 (Conservative Assumption)
- Speed: 80 kts

The following assumptions were used for the cruise segment:

- Range: 950 nm (1,750 km)
- Speed: 120 kts
- Propulsive Efficiency: 0.75 (Conservative Assumption)
- Specific Fuel Consumption: 0.47 lbs/hp-hr
    - (Based on manufacturer's data for the Rotax 912-A [35])
- L/D: (Based on class I drag polar)
    - Red: 10.5
    - White: 8.0
    - Blue: 10.0

The mission fuel fractions for the three preliminary designs are shown in Table 5.1. The most critical fuel fraction for all of the designs is for the cruise segment as would be expected.

Table 5.1: Mission Fuel Fractions

	Fuel Fractions		
Mission Segment	**Red**	**White**	**Blue**
Warm-Up	0.980	0.98	0.98
Taxi	0.996	0.996	0.996
Takeoff	0.996	0.996	0.996
Climb	0.996	0.996	0.997
Cruise	0.841	0.763	0.804
Descent	0.992	0.992	0.992
Land/Taxi	0.992	0.992	0.992
Total Mission	0.801	0.727	0.767

5.2.3 Takeoff Weight Estimation

The takeoff weight was then estimated using the method described in [2]. The following parameters were used in the takeoff weight estimation:

- Payload Weight: 120 lbs (55 kg)
- Trapped Fuel and Oil: 0.5% of W_{TO} (Assumed)
- Fuel Reserves: 160nm (300km)

The value of the trapped fuel and oil weight fraction was taken from [2]. The fuel reserve requirement is specified such that the aircraft can fly for an additional 160nm. [The preliminary sizing resulted in the weights shown in Table 5.2:

Table 5.2: Preliminary Sizing Results

	Red		White		Blue	
Parameter	lbs	kg	lbs	kg	lbs	kg
Takeoff Weight	760	345	1,270	577	950	431
Empty Weight	450	205	720	327	550	250
Fuel Weight	185	84	425	193	270	123

The preliminary sizing data shown here are the results of several iterations. This preliminary sizing process produces an estimation of the takeoff weight based on the mission specification and several assumptions including aerodynamic efficiency, engine performance, and selection of similar platforms. The aerodynamic and

propulsion performances can and have been verified using class I methods and will be discussed. However, the ratio of takeoff to empty weight is also driven by the selection of similar aircraft. Therefore, several iterations were performed using different combinations of aircraft in the regression plot to determine how this would affect the W_{TO} estimation. The final list was selected as the most reasonable based on the designer's judgment.

5.3 Sensitivity Analysis

The sensitivity of takeoff weight to the specific fuel consumption, lift-to-drag ratio, propeller efficiency, payload weight, and empty weight were calculated using methods described in [2]. These values are shown in Table 5.3 for the cruise and climb segments.

Table 5.3: Takeoff Weight Sensitivity Summary

			Red		White		Blue	
Sensitivity	**-**	**Units**	**Cruise**	**Climb**	**Cruise**	**Climb**	**Cruise**	**Climb**
Payload	$\delta W_{to}/\delta W_{pl}$	~	**4.8**	**4.8**	**6.97**	**6.97**	**5.65**	**5.65**
Empty Weight	$\delta W_{to}/\delta W_{e}$	~	**1.9**	**1.9**	**1.9**	**1.9**	**1.88**	**1.88**
Fuel Consumption	$\delta W_{to}/\delta c_{p}$	hp-hr	**1,100**	**31**	**3,820**	**48**	**1,950**	**29**
Range	$\delta W_{to}/\delta R$	lb/nm	**0.7**	**-**	**2.3**	**-**	**1.2**	**-**
Lift-to-Drag	$\delta W_{to}/\delta (L/D)$	lb	**-50**	**-1.5**	**-267**	**-3**	**-110**	**-1.5**
Propeller Efficiency	$\delta W_{to}/\delta (\eta_{p})$	lb	**-828**	**-19.2**	**-2,850**	**-36**	**-1470**	**-23**

The sensitivity analysis results must be examined carefully as a reasonable change in specific fuel consumption (s.f.c.) is much larger than that of payload or empty weight. To compare the results one must consider reasonable changes in the parameters. These are:

- Payload Weight: +/-10 lbs
- Empty Weight: +/-10 lbs
- Specific Fuel Consumption: +/-0.05 lbs/hp-hr
- Range: +/-50 nm
- Lift-to-Drag: +/-1.0
- Propeller Efficiency: +/-0.05

The results of the analysis show that a change of 10 lbs in the payload weight of the Red design would have about the same effect on the takeoff weight as a change in lift-to-drag of -1.0, or a change in specific fuel consumption of 0.05lbs/hp-hr. The results for the White and Blue Designs show that these configurations are more sensitive to the cruise s.f.c. and lift-to-drag ratio than the other parameters. This information is used throughout the configuration decision making process.

5.4 Performance Matching

The purpose of the performance matching is to select the appropriate wing loading (W/S), power loading (W/P), and maximum lift Coefficient, $C_{L,max}$ based on the performance requirements specified in Section 3.9. The performance requirements imposed on these designs are:

- Stall Speed: 58 kts
- Takeoff Distance: 1,500 ft
- Landing Distance: 1,500 ft
- Max Cruise Speed: 140 kts @ 100% Power
- Climb Requirements: 1,600 ft/min

The performance matching plot shown in Figure 5.5 was generated using the above requirements. The wing loading, power loading, and maximum lift coefficients chosen for the three preliminary designs are shown in Table 5.4.

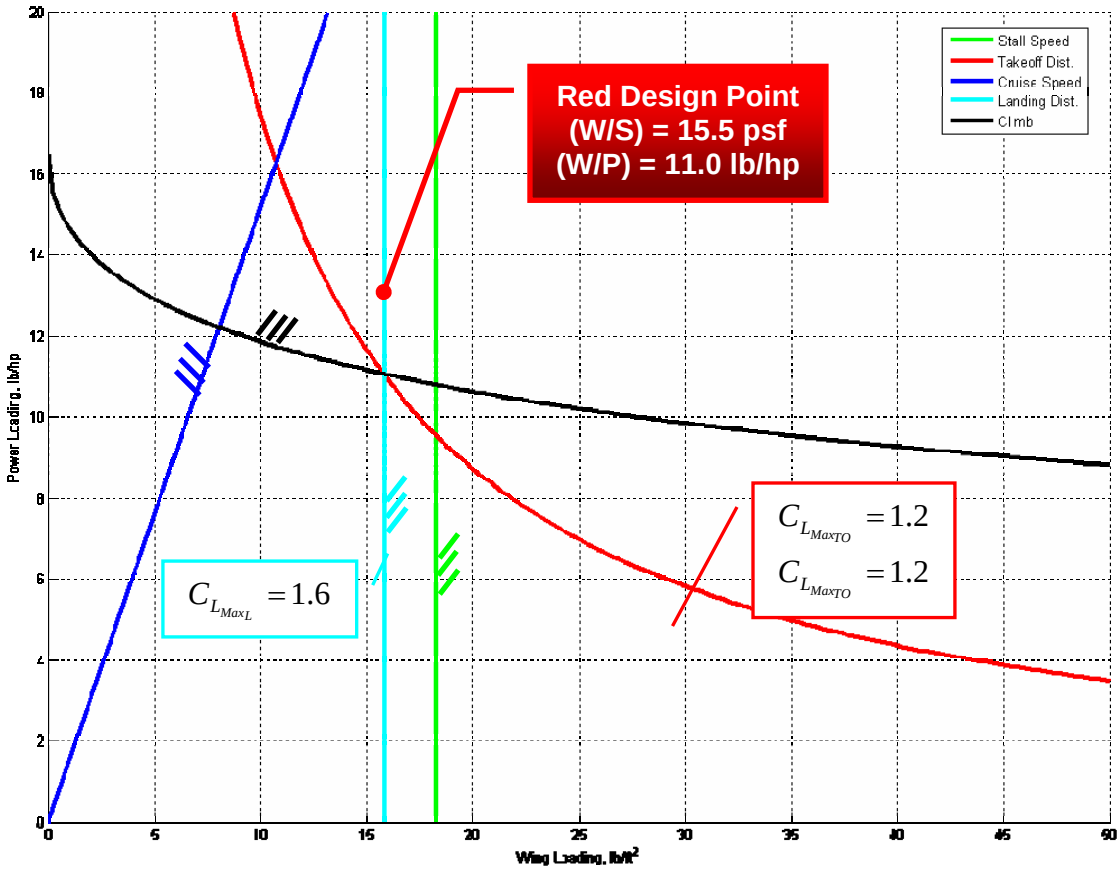

Figure 5.5: Performance Matching for Red Design

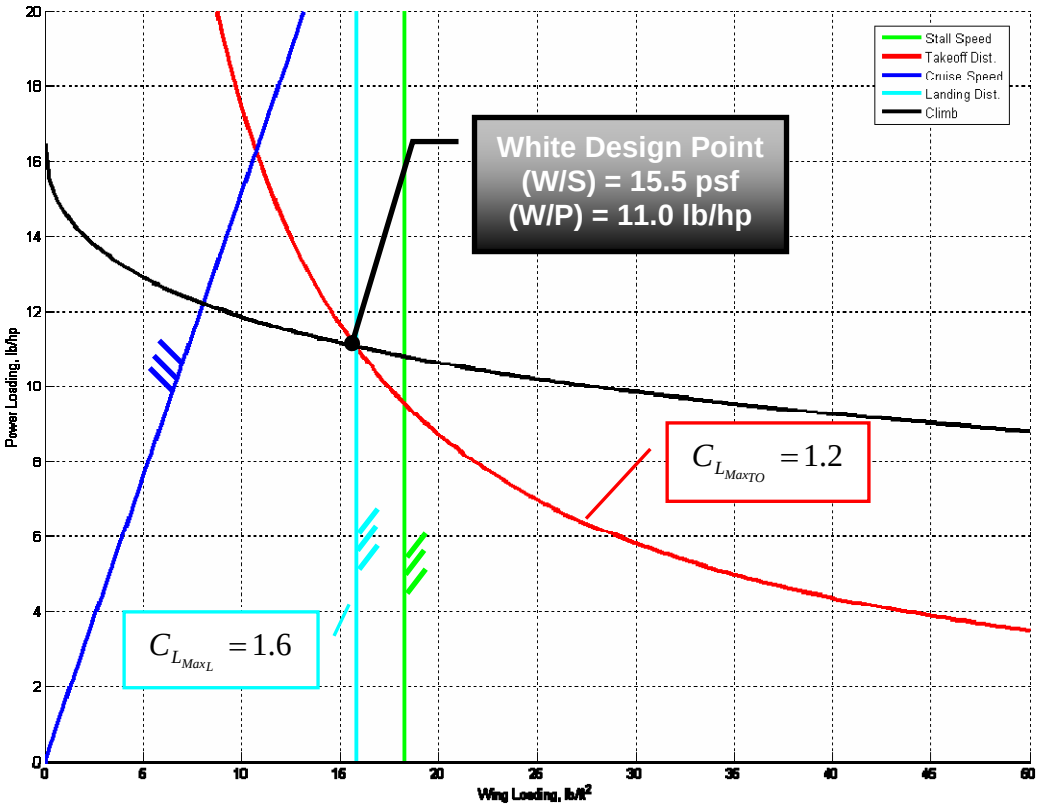

Figure 5.6: Performance Matching for White Design

The wing loading, power loading, and maximum lift coefficients were chosen as the result of several iterations trading airfoil selection, flap sizing, and performance requirements. In all cases the landing distance requirement sized the wing loading. The takeoff distance sized the power loading for the Red and White designs, while the cruise speed requirement was the limiting factor for the Blue design.

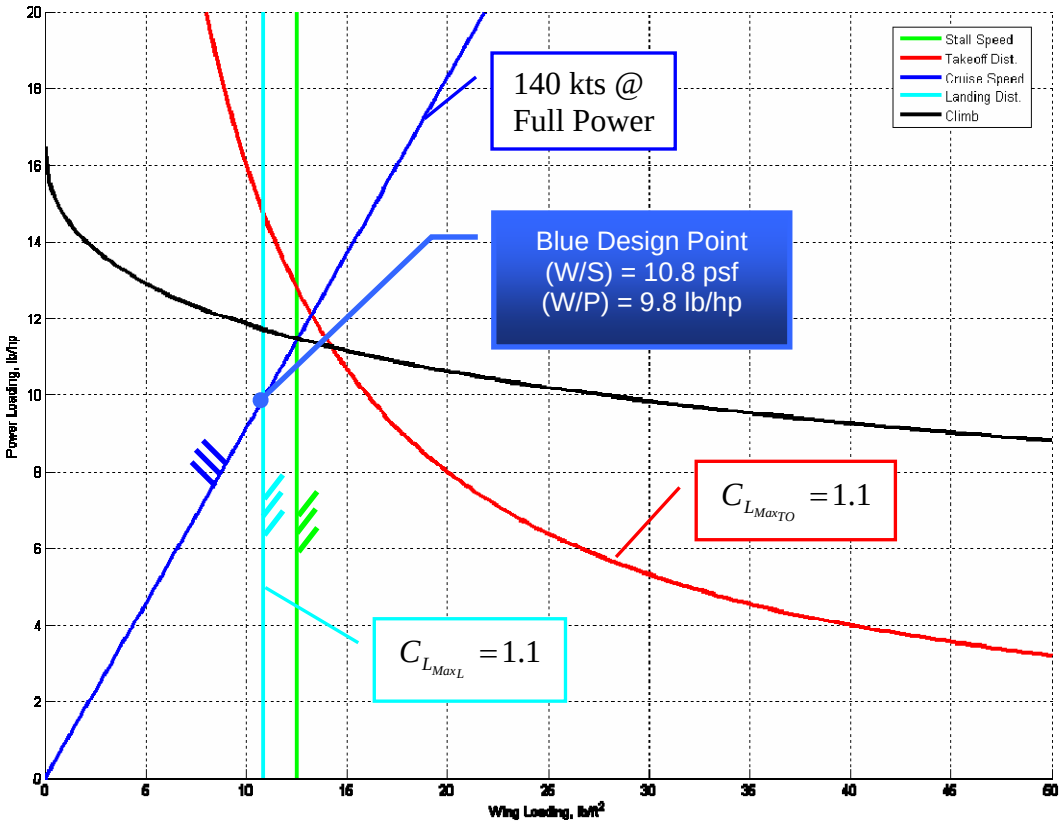

Figure 5.7: Performance Matching for the Blue Design

Table 5.4: Summary of Performance Matching for Preliminary Designs

Parameter	Units	Red	White	Blue
$(W/S)_{TO}$	lb/ft^2	15.5	15.5	10.8
$(W/P)_{TO}$	lb/hp	11.6	11.6	9.8
W_{TO}	lbs	760	1,270	950
W_E	lbs	450	720	550
W_{Fuel}	lbs	185	425	220
W_{Fuel_Res}	lbs	34	78	50
Wing AR	~	4.6	8	3.43
Wing Area	ft^2	49	82	88
P_{req}	hp	66	109	97

5.5 Configuration Design

The purpose of this section is to describe the configuration design in terms of fuselage layout, selection of the propulsion system, wing layout, empennage layout, and landing gear disposition.

5.5.1 Preliminary Fuselage Layout

The fuselage layouts of the three configurations are very similar as they are all designed to carry the same equipment. Only the fuselage layout for the Blue Design is discussed for brevity. The following items will be installed in the fuselage:

- Rotax 912-A Engine
- Science Payload (20” x 20” x 8”)
- Avionics (Approximately 6” x 6” x 6”)
- Data Acquisition/Health Management (Approximately 15” x 8” x 8”)
- Nose Gear
- Main Gear
- Fuel Tank and Systems
- GPS Antenna (Assumed 3” x 3” x 3”)
- Communications Antenna (Assumed 12” x 6” x 6”)

This list of equipment merely lists the high-level equipment that will be carried in the fuselage. The sub-system components such as actuators and fuel pumps will be discussed in the Class II design.

The fuselage layout can be seen in Figure 5.8. The engine and science payload widths are fairly similar and drive the fuselage width. The height of the fuselage is

driven by the engine size. The science payload and fuel volume were both located close to the estimated center of gravity to minimize c.g. travel.

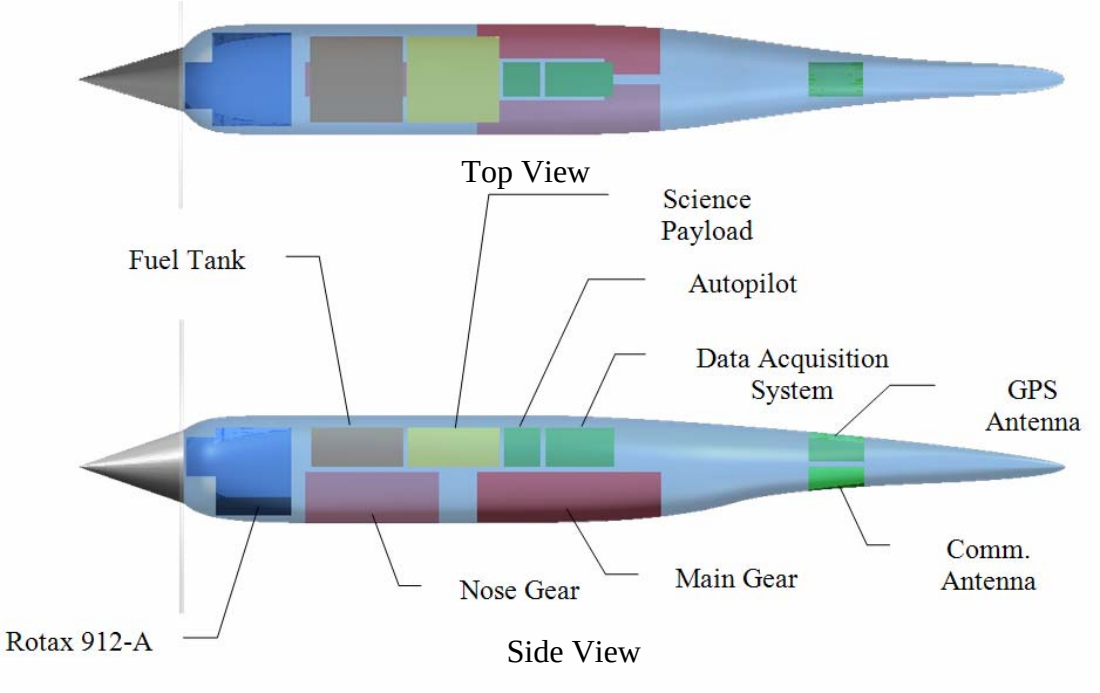

Figure 5.8: Preliminary Fuselage Layout (Applies to all designs)

5.5.2 Propulsion System Selection and Disposition

The aircraft will be powered by an existing piston/propeller or turboprop engine. The decisions regarding the propulsion system are discussed in this section.

5.5.2.1 Number of Engines

Originally, a requirement for two engines was derived from the CReSIS mission specification for redundancy purposes [1]. This requirement was created when the aircraft range was expected to be >10,000 km. The reasoning behind it was that the aircraft should be able to return to base upon losing an engine as it would be very difficult to recover the equipment. Now that the range requirement has been

decreased, the aircraft will be operating much closer to base. This greatly increases the probability of being able to retrieve the aircraft in the case of a crash. Also, the amount of data that would be lost in the event of a crash would be much less than previously thought.

The sensitivity analysis shown in Section 5.3 on page 56 of this report indicates that the engine specific fuel consumption is one of the most critical parameters for this design.

Table 5.5 shows that the engines that could be used in a twin-engine configuration (< 60 hp) have much higher s.f.c. values than the larger engines.

A single engine configuration was chosen for the purposes of simplifying the aircraft systems and maximizing efficiency in terms of fuel consumption.

Table 5.5: List of Viable Engines

Manufacturer	Country	Model	Cooling	Power	SFC	Weight	P/W
~	~	~	~	hp	lbs/hr-hp	lbs	hp/lb
Diesel Engines							
TAE[36]	Germany	Centurion 1.7	Liquid	135	0.36	295	0.46
DeltaHawk[37]	US	DH160V4	Liquid	160	0.40	327	0.49
DieselAir[38]	UK	DAIR-100	Liquid	100	0.53	205	0.49
SMA[41]	France	SR 305	Air	227	0.32	423	0.54
Zoche Aerodiesels[40]	Germany	ZO03A	Air	70	0.36	121	0.58
Avgas Engines							
UAV Ltd[39]	UK	AR801	Liquid	50	0.50	43	1.16
UAV Ltd[39]	UK	AR682	Liquid	95	0.52	112	0.85
Limbach[21]	Germany	L550 E	Air	50	0.70	35	1.41
Limbach[21]	Germany	L2000 EO/EC	Air	68	0.54	163	0.42
Limbach[21]	Germany	L2400 EB	Air	86	0.62	181	0.48
Rotax[35]	Austria	447-UL	Fan	42	0.70	59	0.71
Rotax[35]	Austria	582-UL	Liquid	65	0.59	64	1.02
Rotax[35]	Austria	912-A	Liquid	81	0.47	122	0.66
Rotax[35]	Austria	912-ULS	Liquid	100	0.47	125	0.80
Rotax[35]	Austria	914-UL	Liquid	115	0.47	141	0.82
Turboprop Engines							
Innodyn[41]	US	165TE	Air	165	0.70	188	0.88

5.5.2.2 Engine Selection

The selection of the engine depends on several factors:

- Power
- Weight
- Power-to-Weight Ratio
- Specific Fuel Consumption
- Cold Weather Operations
- Cost

The most important of these factors for these designs are fuel consumption, power, and cold weather operations. The engine power-to-weight ratio is important, but the sensitivity analysis showed that an increase in specific fuel consumption would have

a bigger effect on the overall design than an increase in empty weight. Therefore, the engine with the lowest s.f.c. that meets the power requirement is selected as the primary engine choice.

Figure 5.9 through Figure 5.11 show the power, weight, and power-to-weight ratios respectively for the selected engines, plotted against specific fuel consumption. As can be seen from the three plots, the Zoche ZO03A and Rotax 912-A are the most appealing engines in terms of power-to-weight ratio and s.f.c. However, the Zoche ZO03A engine has not been manufactured or tested. Using this engine as the primary choice for the CReSIS UAV would be extremely risky. Therefore, the Rotax 912-A was chosen as the primary engine for the Red and Blue Designs. The Rotax 914-F was chosen for the White Design.

A typical ratio of the engine weight fraction for single engine, general aviation aircraft is 0.15-0.20. While the CReSIS aircraft is not in the general aviation class, this weight ratio can still be used as a general guideline. The engine-to-takeoff weight ratios for the current designs are 0.16, 0.11, and 0.13 for the Red, White, and Blue designs respectively.

Heavy fuels are more accessible in the areas of operation. The heavy fuel engines shown in Figure 5.9 are appealing for this reason as well as for cold weather operations. However, the heavy fuel engines investigated are much heavier than the Rotax engines and have much higher specific fuel consumption in the case of the Innodyn. The Innodyn 165TE and Thielert Centurion 1.7 will be considered alternatives in the Class II design.

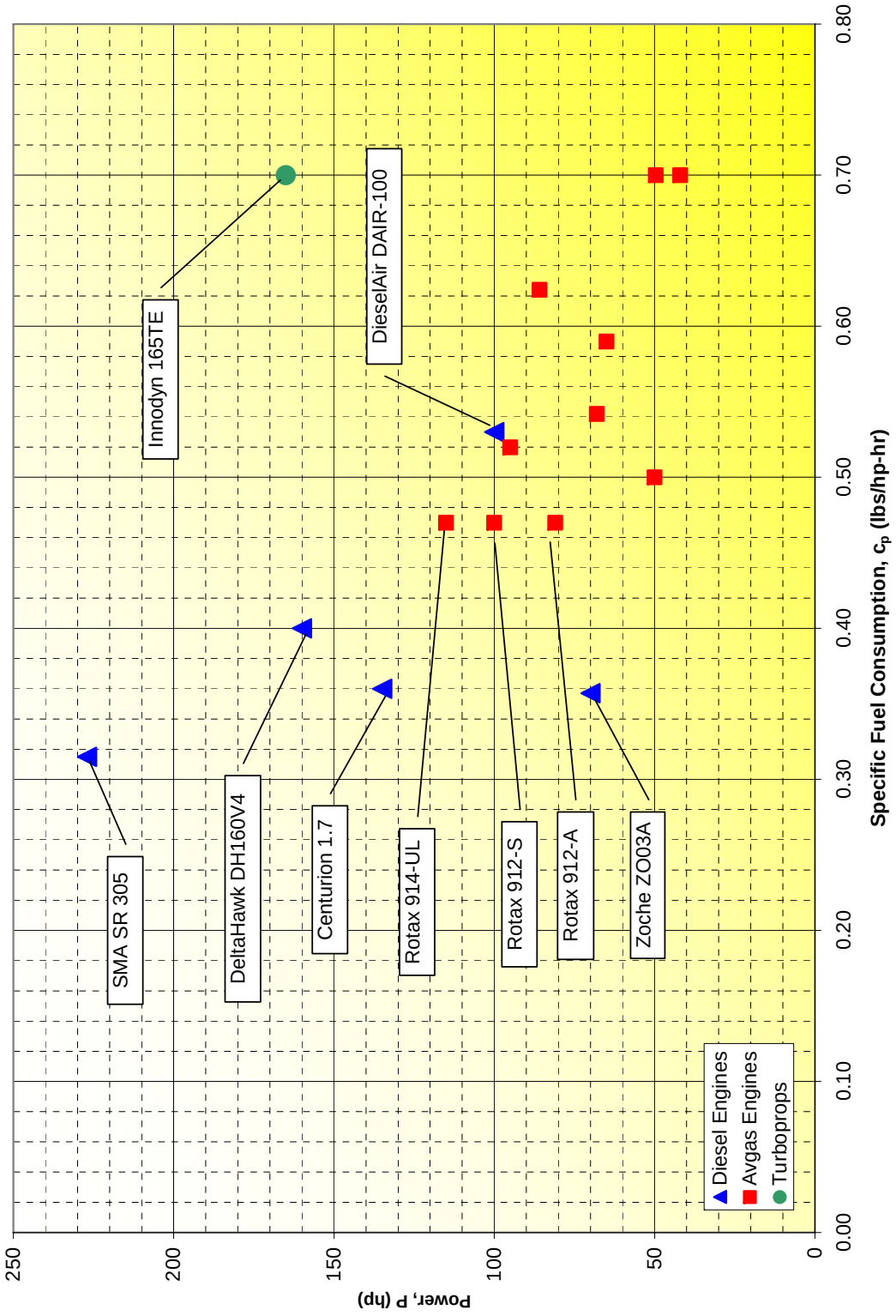

Figure 5.9: Engine Power

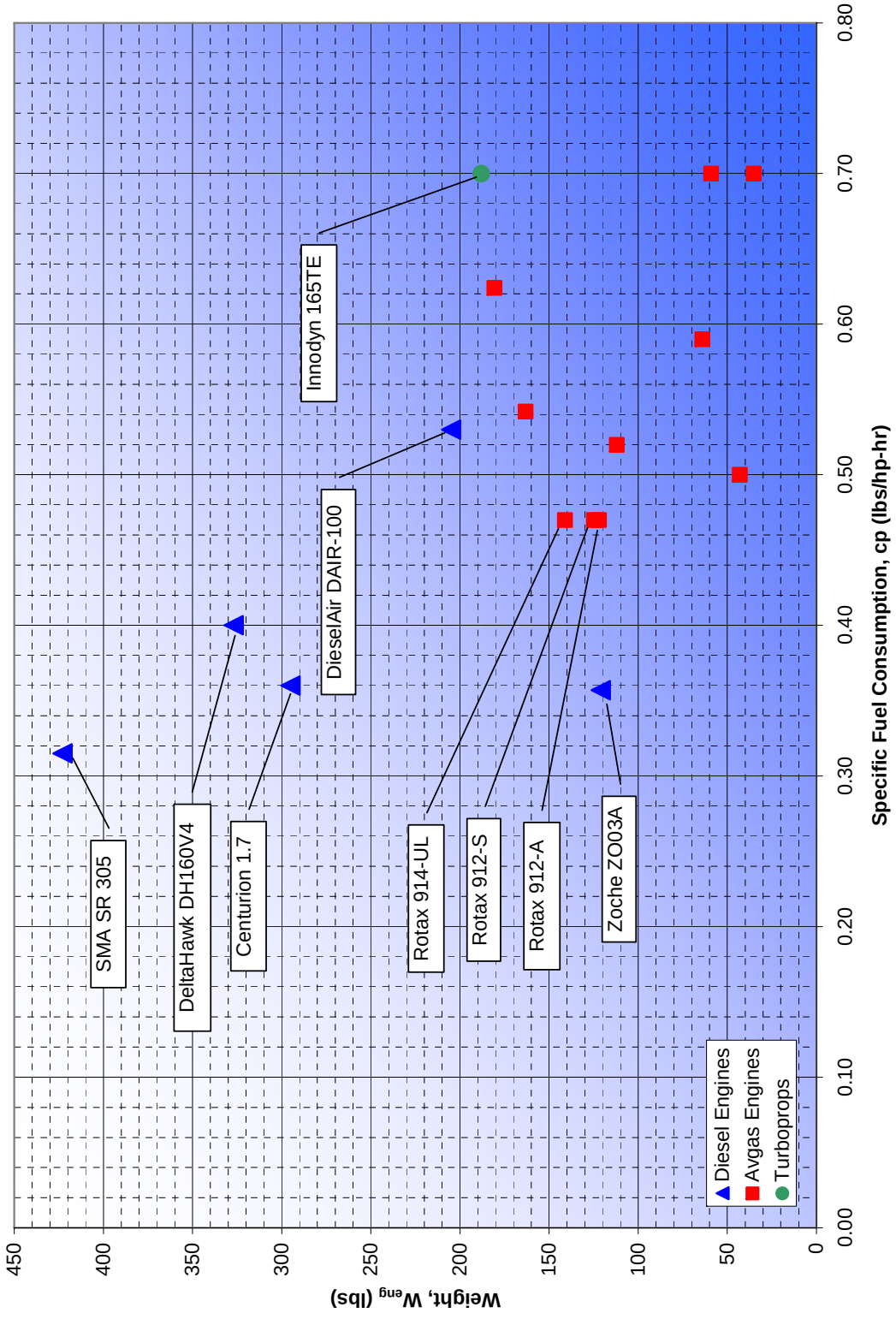

Figure 5.10: Engine Weight

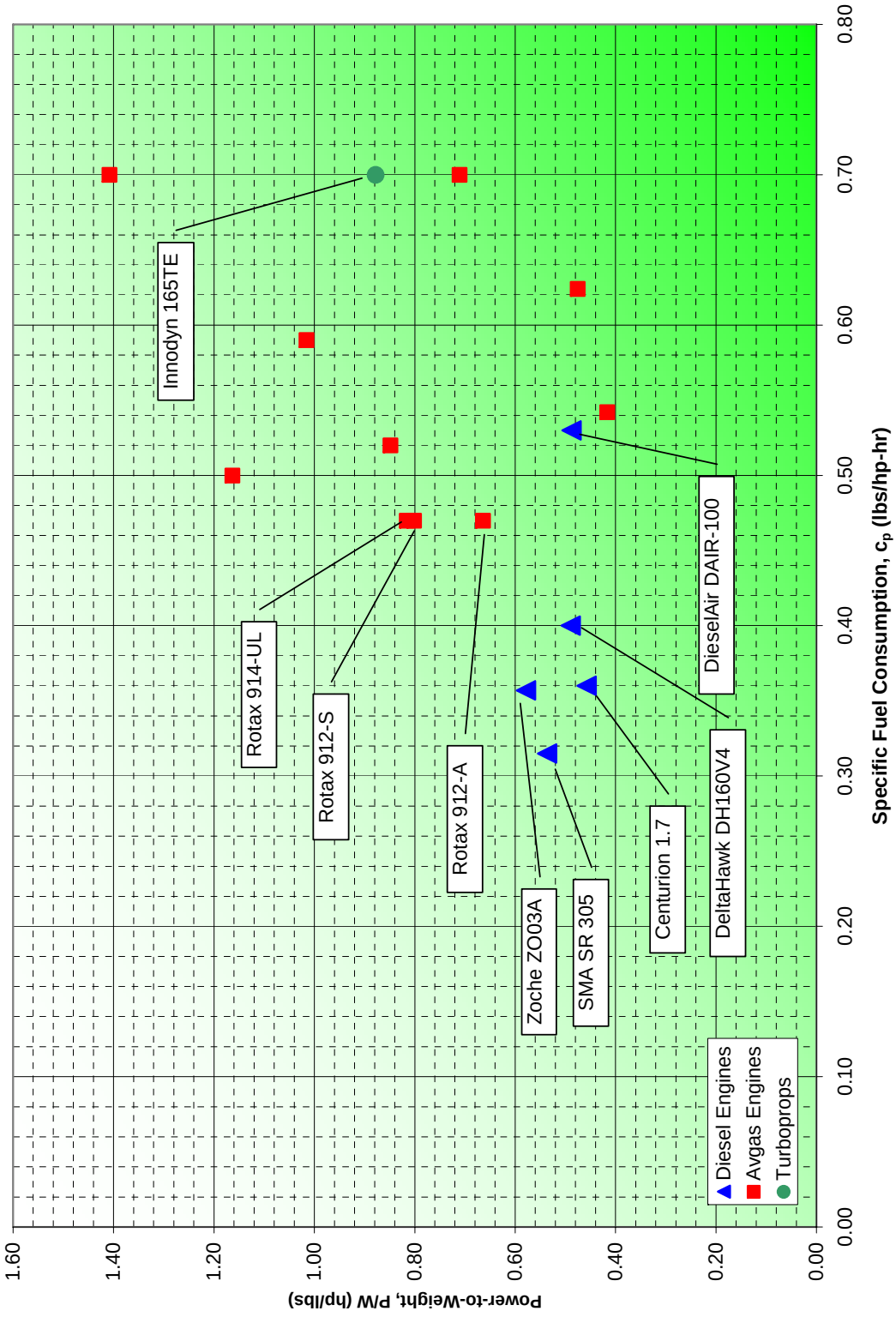

Figure 5.11: Engine Power-to-Weight Ratio

5.5.2.3 Propeller Diameter

The propeller diameter was determined using Equation 5.1.

$$D_P = \sqrt{\frac{4P_{Max}}{\pi n_p P_{bl}}} \tag{5.2}$$

Where: D_p = Propeller Diameter
n_P = Number of Blades
P_{max} = Maximum Power
P_{bl} = Blade Power Loading

The blade power loading was selected based on an average number for single engine aircraft from [2]. The power loading selected is 3 hp/ft^2, which resulted in propeller diameters of:

- Red: 50” (127 cm)
- White: 60” (152.4 cm)
- Blue: 50” (127 cm)

These diameters are comparable to typical propeller diameters for the Rotax 912 and 914 engines, so they are reasonable.

5.5.2.4 Engine Disposition

The decision between a tractor or pusher engine installation depends on several factors including:

- Aerodynamics around fuselage and wing
- Forward-looking visibility for cameras
- Empennage layout
    - The empennage for a pusher may require use of tail boom extensions from the wing.
- Stability considerations
    - Pusher engines are stabilizing.
- Buffeting
    - A pusher propeller will be closer to the horizontal tail, causing more possibilities for buffeting.
- Center of Gravity
- Systems layout
- Takeoff Rotation

Many currently available UAVs utilize a pusher engine configuration due to forward looking visibility for an infrared camera. There are no forward looking infrared (FLIR) requirements for this aircraft. The engine will be installed in a tractor configuration to simplify the takeoff rotation.

5.5.3 Wing Layout and Lateral Controls

The purpose of this section is to describe the design of the wing planform for the three preliminary concepts. This includes the wing layout, high-lift device sizing, and preliminary sizing of the lateral controls.

5.5.3.1 Wing Planform

As was discussed at the beginning of the preliminary design section, the primary difference between the Red, White, and Blue designs is in the wing design. This is due to the different antenna integration approaches. For all three designs, the antenna integration had a major effect on the wing planform as will be discussed.

Red Design

The wing planform geometry for the Red design is shown in Figure 5.12. The root chord was sized such that there is a 15% chord margin in front of and behind the antennas. The span and taper were then traded in an attempt to achieve the highest aspect ratio possible, while meeting the wing area requirement.

In general, for high aerodynamic efficiency, the wingspan should be maximized while minimizing the wetted area. In the case of this design increasing the wingspan is not possible without also increasing the wing area thereby increasing the wetted area.

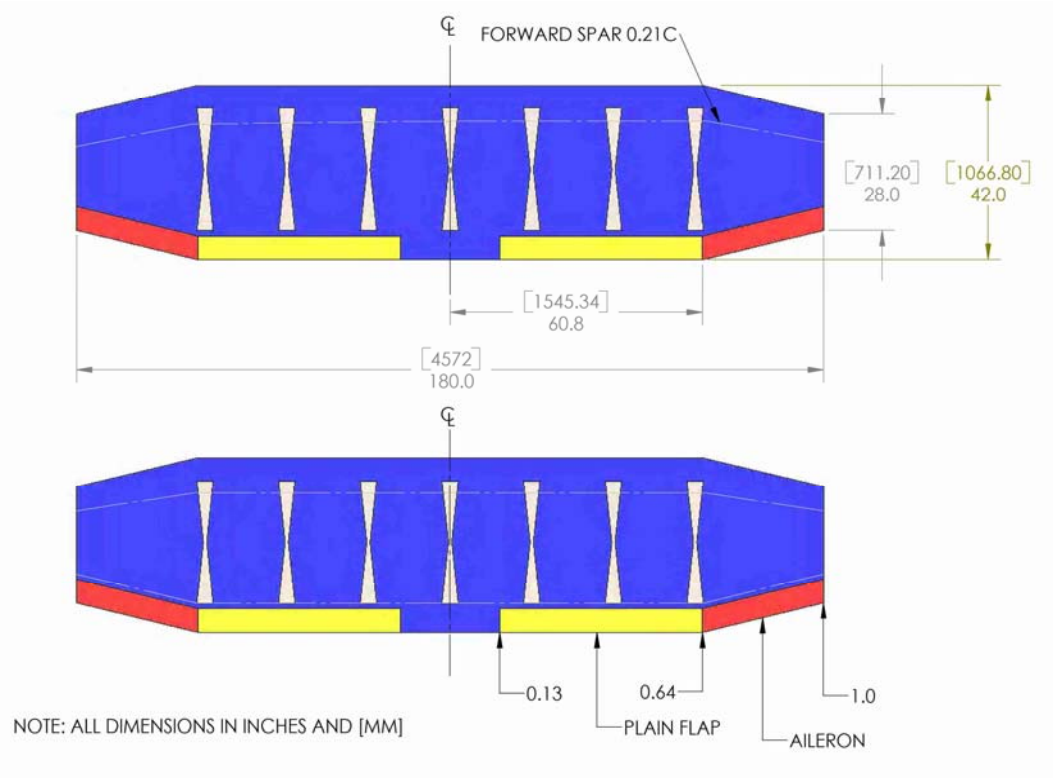

Figure 5.12: Red Design Wing Planform

White Design

The wing planform for the White design was driven by the antenna integration as is the case with the Red design. The White design utilizes eight antennas that hang approximately 20 inches (50 cm) below the lower surface of the wing. This distance corresponds to one quarter wavelength at 150 MHz. With this spacing, the lower surface of the wing is being used as a ground plane, which reflects energy to and from the antennas. For the wing to act as a ground plane, the wing planform must be slightly bigger than the antennas. The wing layout was iterated until reasonable values of aspect ratio, flap size, and taper ratio were achieved. This preliminary planform design will be iterated further in Class II design.

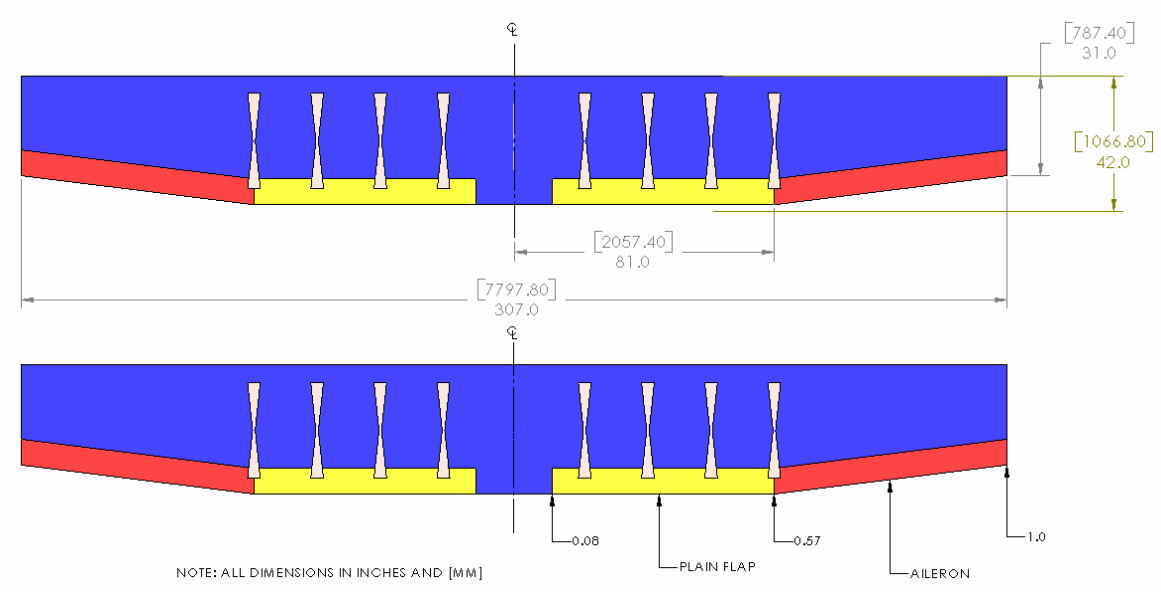

Figure 5.13: White Design Wing Planform

Blue Design

The wing planform of the Blue design is inherently different from typical wing design in that it is a biplane or box-wing. The biplane configuration was used for several decades, but faded away with the advent and improvement of the monoplane. Aerodynamic efficiency is primarily driven by wingspan and wetted area. The wingspan should be maximized while minimizing the wetted area. A biplane will typically have a lower wingspan than a monoplane of equivalent wetted area. Therefore, monoplanes are almost always superior to biplanes. Due to this, little work has been done to improve the performance of biplanes. One of the most notable areas of improvement lies in the endplate design.

Traditionally biplanes did not utilize endplates, but rather struts and wires. Properly designed endplates can produce decreases in the large induced drag

associated with low aspect ratio wings. This type of configuration – a biplane with endplates – is typically referred to as a box wing.

The endplate effects will not be heavily considered in Class I design. Traditional biplane design and analysis tools will be used to estimate the vehicle performance.

Biplane design and analysis is described in several NACA reports [43] as well as in Richard Von Mises *Theory of Flight* [44]. A problem of conventions presents itself with biplane design due to the fact that there are two wings instead of one. The convention used in [44] and in this document are:

- S – Sum of both wing planform areas
- AR – Average aspect ratio of the two wings
- mgc – Average mgc of the two wings

Biplane design also introduces several new design parameters:

- Decalage – The angle between the two wing chord lines
- Stagger – The distance from the leading edge of the lower wing to the leading edge of the upper wing measured in the direction of flight
- Gap – Vertical separation of the wings

Many biplanes have been flown with various combinations of these parameters. Positive stagger (meaning the top wing is forward of the lower wing) has shown to be aerodynamically beneficial. However, negative stagger has been shown to delay and smooth out wing stall.

Decalage can be used to distribute the load between the two wings in the desired manner. These effects will be ignored in Class I design.

The gap between the two wings has a large effect on the aerodynamics of the aircraft. Typically, the gap is set to be larger than the wing chord. This is not possible for this design however due to the antenna requirements – The lower wing must be ¼ wavelength (~20") below the upper wing.

The wing planform is shown in Figure 5.14. The lower wing is used to house the antenna and therefore must be completely dielectric. This means that all of the control surfaces and fuel must be in the upper wing. The Blue aircraft will not utilize flaps. The ailerons span the entire upper wing and have a chord ratio of $c_a/c_w = 0.30$.

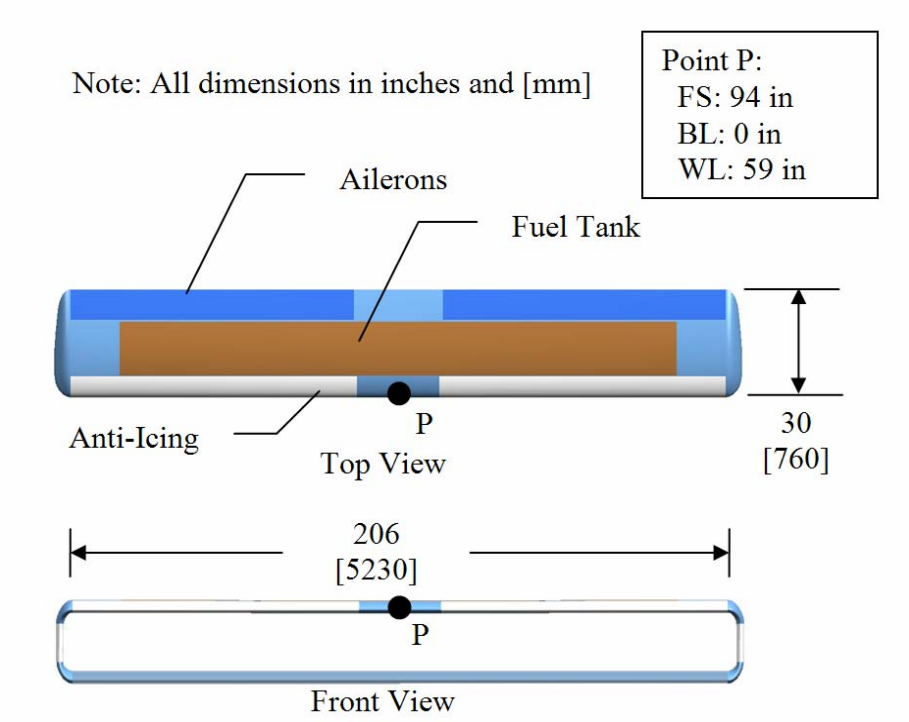

Figure 5.14: Blue Design Wing Planform

The wing planform is summarized in Table 5.6. Please note the upper and lower wings have the same chord, span, taper ratio, and quarter-chord sweep angle.

Wing Planform Summary

The wing planform geometry for the three concepts is summarized in Table 5.6.

Table 5.6: Preliminary Wing Planform Summary

Parameter	Units	Red	White	Blue
Area	ft^2	57.1	82	88
AR	~	6.15	8.3	3.43
Taper Ratio	~	0.49	0.59	1
$\Lambda_{c/4}$	deg	-3.2	1.7	0
Mean Chord	ft	3.17	3.2	2.5
Span	ft	18.75	26	17.17
Γ_W	deg	5	5	0
ε_w	deg	-2	-2	0
$\eta_{i,f}$	% b/2	17	8	-
$\eta_{o,f}$	% b/2	54	57	-
c_f/c_w	~	0.15	0.25	-
$\eta_{i,a}$	% b/2	54	57	13.5
$\eta_{o,a}$	% b/2	100	100	100
c_a/c_w	~	0.15	0.25	0.3
Gap	in	-	-	19.69
Stagger	in	-	-	0
Decalage	deg	-	-	0

5.5.3.2 Wing Disposition

The three designs represent three different wing dispositions in terms of placement on the fuselage: a low wing, a high wing, and a biplane. A low wing placement was chosen for the Red design to keep the wing antennas in the same plane (or close to it) as the antenna in the fuselage. A high wing was used in the White design to add as much clearance as possible between the antennas and the ground. This reduces the possibility of striking one of the antennas on landing. The biplane wing placement was driven by the antenna spacing requirement. The wings are spaced at approximately 20 inches (50 cm), which matches the height of the fuselage fairly closely.

5.5.3.3 Airfoil Selection

The Clark Y [45] airfoil (Figure 5.15) will be used for the wing in all three designs. This airfoil was chosen primarily for its flat bottom design as this will help with antenna integration. The flat bottom works well as a grounding plane for the hanging antennas in the White and Blue designs. This airfoil has a moderately high maximum lift coefficient, as well as a moderate pitching moment coefficient. The thickness of the Clark Y is approximately 12% of the mgc. This airfoil was thickened proportionately to be 18% thick to increase fuel capacity. The lift curve slope of the Clark Y airfoil was difficult to find as most of the data on this airfoil is represented in terms of 3-D data. The lift curve slope for the NACA 4418 was used as this airfoil matches the Clark Y geometry fairly well when the Clark Y thickness is increased to 18%. The lift-curve-slope of the NACA 4418 airfoil is shown in Figure 5.16.

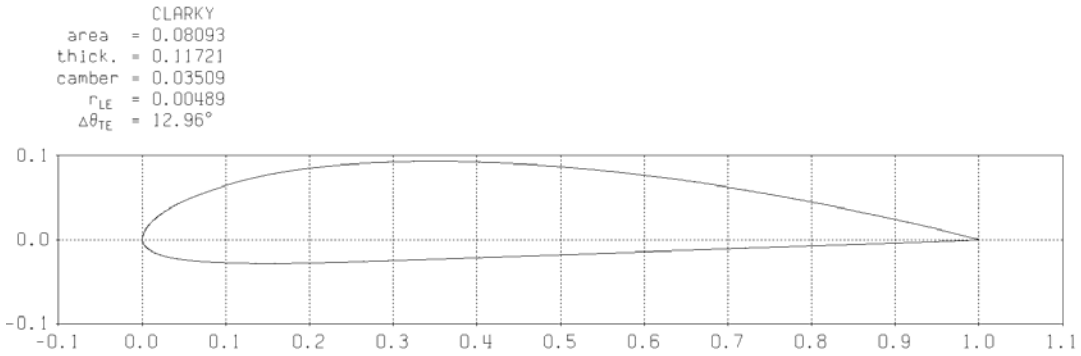

Figure 5.15: Clark Y Airfoil Plotted with XFOIL [45]

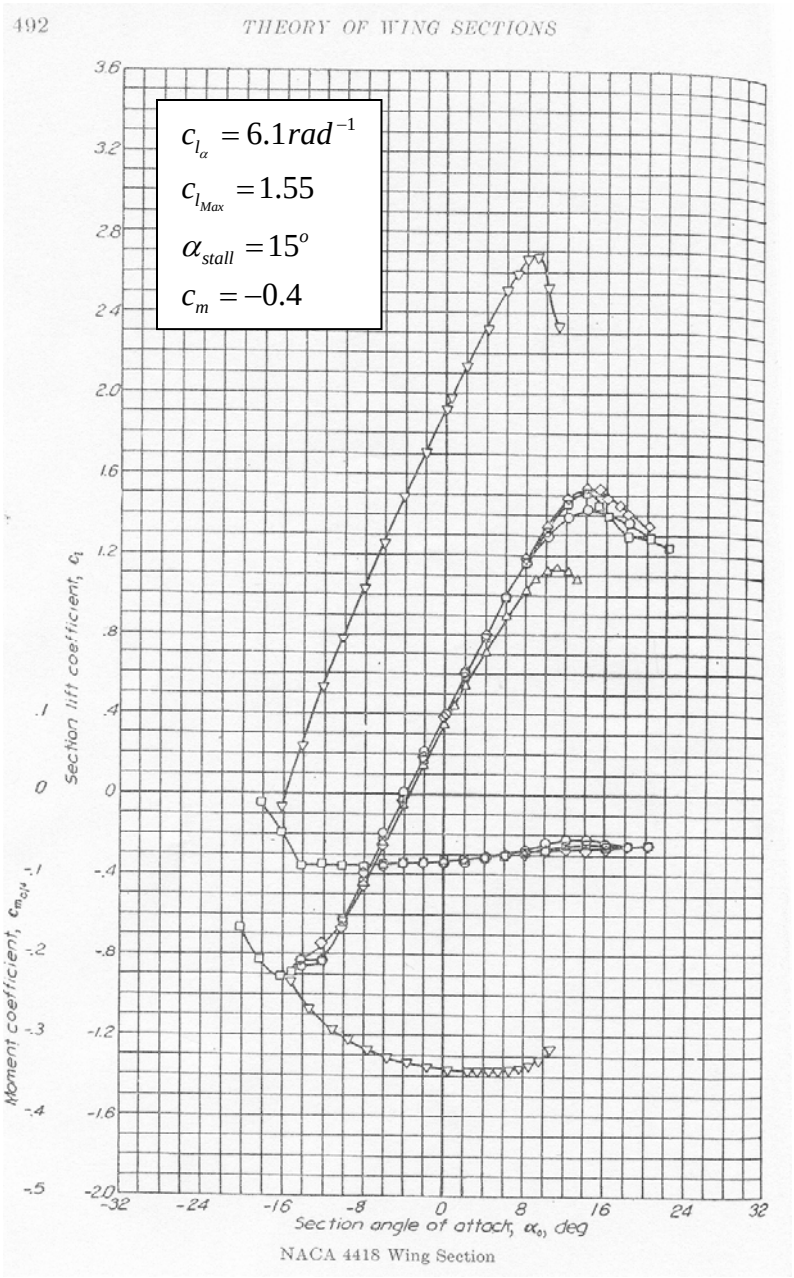

Figure 5.16: Lift-Curve-Slope for NACA 4418 [45]

5.5.3.4 High-Lift Device Sizing

The flap sizing was performed for each of the wing layouts using Advanced Aircraft Analysis [2]. Plain flaps were used on the Red and White designs. Flaps were not used on the Blue design as integrating flaps into the lower wing would be

difficult as the lower wing must be dielectric and using flaps on the upper wing of a biplane has negative effects due to the downwash created on the lower wing.

The first step in the flap sizing is to determine the maximum lift coefficient of the wing. This is done by determining the lift-curve-slope of the clean wing using Equation 5.4 from [2].

$$C_{L_{w\alpha_{clean}}} = \frac{2\pi AR_{l.s.} f_{gap_w}}{2 + \left\{ \frac{AR_w^2 \beta^2}{k^2} \left(1 + \frac{\tan^2 \Lambda_{c/2_w}}{\beta^2} \right) + 4 \right\}^{\frac{1}{2}}}$$

Equation 5.4

Where: f_{gap} = f(AR,gap location, gap size)

$$\beta = \sqrt{1 - M^2}$$

$$k = \frac{c_{l_\alpha}}{2\pi}$$

This is then combined with the stall angle of attack of the wing to determine the maximum clean lift coefficient for the wing. At this stage of the design it is safe to assume that the wing lift coefficient relates to the aircraft lift coefficient as follows:

$$C_{L_{Max_W}} = 1.05 C_{L_{Max}}$$

Equation 5.5

The maximum clean lift coefficient and the assumed lift coefficients for takeoff and landing are shown in Table 5.7 for the three designs. Note that flaps are not used on the Blue concept.

Table 5.7: Lift Coefficients Used for Flap Sizing

Parameter	Units	Red	White	Blue
$C_{Lmax,clean}$	~	1.0	1.0	1.1
C_{LTO}	~	1.1	1.0	1.2
C_{LL}	~	1.6	1.0	1.6

The flap sizing has shown that the wing designs are feasible with respect to flap integration.

5.5.3.5 Fuel Volume

There are a number of design options for places to store the fuel:

1. Store all fuel in wing
2. Store all fuel in fuselage
3. Store all fuel in tanks mounted at wing tip
4. Store fuel in fuselage and wing
5. Store fuel in fuselage and tip tanks
6. Store fuel in fuselage, wing, and tip tanks

The best option is to store all of the fuel in the wings due to root bending moment relief, center of gravity effects, payload integration, and wetted area. Therefore, the available storage of the wings was calculated first. This was done using Equation 5.6 from Ref [2] and verified using CAD.

$$V_{F_w} = 10 F_F b_w F_a c_{r_w}^2 \left[\left(\frac{t}{c}\right)_{rw} \eta - \left(\frac{\left(\frac{t}{c}\right)_{rw} - \left(\frac{t}{c}\right)_{tw} \lambda_w}{2} + \frac{(1-\lambda_w)\left(\frac{t}{c}\right)_{rw}}{2} \right) \eta^2 + \frac{(1-\lambda_w)}{3} \left[\left(\frac{t}{c}\right)_{rw} - \left(\frac{t}{c}\right)_{tw} \lambda_w \right] \right]_{\eta_{i_F}}^{\eta_{o_F}}$$

Equation 5.6

where:

$$F_F = F_{F_{structure}} F_{F_{expansion}}$$

Equation 5.6 is based on the following assumptions:

- Fuel is stored in wet wing.
- Density of fuel = 6.0 lbs/gal
- Fuel expansion = 4.0%

The assumption that the wing will be a wet wing, meaning the structure of the wing is sealed to form the fuel tank instead of using separate bladders, is not necessarily correct. There is a possibility that fuel bladders will be used.

The fuel volume calculations resulted in the numbers shown in Table 5.8. The Red and White designs have sufficient volume in the wings to store all of the fuel. The Blue design however can not store all of the fuel in the wings. This is due to the fact that the fuel volume is only calculated for the upper wing. The lower wing cannot contain any reflective materials, which includes fuel. This may drive the size of the Blue fuselage up.

Table 5.8: Fuel Volume Summary

	Red	White	Blue
Fuel Required			
lbs	184	425	270
gallons	30.7	70.8	45.0
ft^3	4.1	9.4	6.0
Available Fuel			
lbs	215	580.6	190
gallons	35.8	96.8	31.7
ft^3	4.8	12.9	4.2

5.5.3.6 Wing Dihedral Angle, Incidence Angle, and Twist

The wing dihedral angle was selected by examining similar single engine propeller driven configurations. A dihedral angle of 5^o was selected preliminarily for the Red Design. The dihedral angle for the White design was set to zero as the high wing placement creates some amount of dihedral effect without any geometric dihedral.

The dihedral angle of the Blue design was set at zero due to the biplane configuration. These values will be iterated in the detailed stability and control analysis.

A twist of -2^0 was selected for the Red and White designs due to the tapered wings. This value was chosen based on experience and will be investigated further in Class II design with the use of a spanwise lift distribution.

The wing incidence angles were chosen based on the mid-cruise lift coefficients of the three aircraft. The mid-cruise wing lift coefficients are both very close to 0.3, which is the zero angle of attack lift coefficient for the Clark Y. The wing incidence angles were therefore set to zero for these designs. The incidence of the Blue design was also set to zero and will be investigated further in Class II design.

5.5.4 Empennage Layout

The purpose of this section is to discuss the selection of the empennage size, location and disposition, as well as the size and disposition of the longitudinal and directional control surfaces.

5.5.4.1 Empennage Configuration

The following empennage configurations were considered for this design:

- Fuselage Mounted Vertical and Horizontal Tails
- Boom Mounted Tails
- T-Tail or Cruciform Tail
- Butterfly/V Tail

The V-tail design is appealing due to the decreased wetted area and decreased interference drag over the other designs. The V tail also decreases the number of actuators required for the longitudinal and directional control surfaces. Historically, these advantages came at the cost of complicated control mixers, but this is not the case in a UAV due to the digital flight control system. The V-tail design was selected for all three designs.

The volume coefficient method is used for the V-tail preliminary sizing. This process uses Equation 5.7 to calculate a V-tail area and moment arm based on current aircraft shown in Table 5.9 from [2]. The V-tail planform area is defined in Figure 5.17 from [2].

$$V_{vee} = \frac{S_{vee}\left(X_{ac_{vee}} - X_{cg}\right)}{S_w \bar{c}_w}$$ Equation 5.7

Table 5.9: Volume Coefficient Values for Existing Aircraft [2]

Aircraft	V_{vee}
V-35 Bonanza	0.512
Global Hawk	0.581
Predator	0.78
YF-23	0.194
Fouga	0.596
HKS III	0.597
SHK	0.586
Std. Austria SH 1	0.352
SB 5B	0.338
PIK 16 Vasama	0.426
HP-8	0.779
Moneral	0.34
HP-18	0.486
fs 23 "Hidalgo"	0.279

The surface area of the V tail is defined in Figure 5.17.

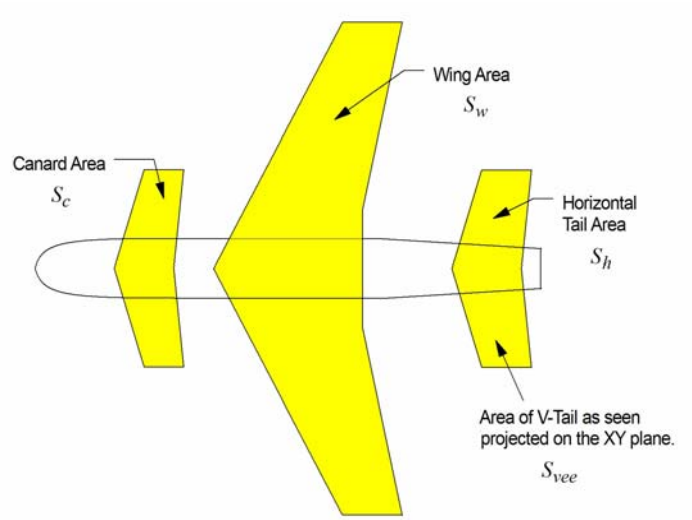

Figure 5.17: Definition of V-Tail Planform Area [2]

The volume coefficient chosen for this design is V_{vee} = 0.6 based on the data in Table 5.9. The empennage moment arm and V-tail area were then traded in an attempt to minimize wetted area for each of the designs. The Red design iterations resulted in the empennage design is shown in Figure 5.18. As a first estimate, the V-Tail dihedral angle was set at 45^o for all of the designs, which indicates that it is equally effective in the lateral and longitudinal modes. This will be optimized in the stability and control analysis.

The control surface, known as a ruddervator, was sized based on typical values for longitudinal control surfaces. The ruddervator will be a full-span control surface with a chord ratio of 0.30. The V-tail planforms for the three designs were very similar, so only the Red design planform is shown in Figure 5.18. The geometry data for the V-Tails are shown in Table 5.10.

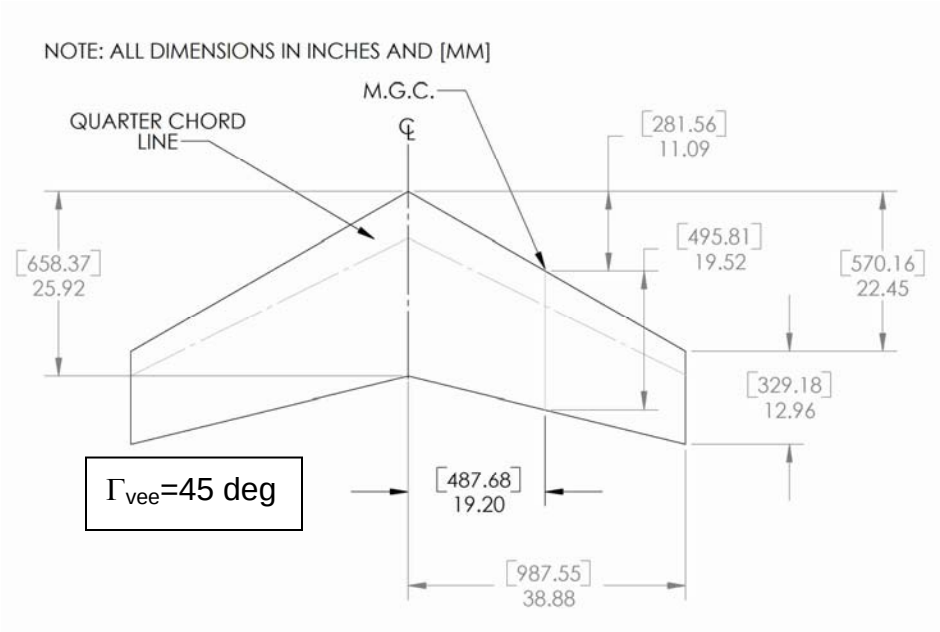

Figure 5.18: V-Tail Planform Drawing for the Red Design

Table 5.10: V-Tail Geometry Summary

Parameter	Units	Red	White	Blue
$X_{LE,\ Vee}$	in	205	205	207
$Z_{c/4,\ Vee}$	in	59.9	60.2	60
S_{vee}	ft^2	10.5	14	15.5
AR_{Vee}	~	4	4	4
λ_{vee}	~	0.5	0.5	0.5
$\Lambda_{c/4,vee}$	deg	26.3	26.3	26.3
c_{vee}	ft	1.68	1.94	2.04
b_{vee}	ft	6.475	7.48	7.87
Γ_{vee}	deg	45	45	45
$\eta_{i,e}$	% b/2	5	5	5
$\eta_{o,e}$	% b/2	100	100	100
c_e/c_{vee}	~	0.3	0.3	0.3

5.5.5 Landing Gear Disposition

The purpose of this section is to describe the preliminary sizing and disposition of the landing gear. The following parameters are determined in this section:

1. Number, type, and size of tires and skis

2. Length and diameter of struts
3. Preliminary disposition
4. Retraction feasibility

The landing gear integration is one of the most crucial parts of any airplane design. This seemingly simple step has been a show-stopper for many preliminary designs and therefore must be handled with great care. The unique payload requirements of this design are such that the landing gear integration will be difficult.

5.5.5.1 Landing Gear Type and Configuration

The first step in the landing gear design is to decide between retractable and fixed landing gear. Retractable landing gear will be used for the following reasons:

- To provide an unobstructed view for the antennas
- Increased aerodynamic efficiency

There are three possibilities that will be considered for the landing gear configuration:

1. Tailwheel
2. Conventional or Tricycle
3. Tandem with Outriggers

There are arguments that could support using any of the three types of landing gear. Table 5.11 shows a comparison of the three types of landing gear with relative pros and cons that pertain to this design.

Table 5.11: Landing Gear Disposition Comparison

Landing Gear Type	Pros	Cons
Taildragger	Good for rough field conditions. Provides weight savings over tricycle and tandem.	Propensity to ground loop. Complicates autopilot control for takeoff and landing.
Tricycle	Good handling qualities on the ground. No ground looping characteristics.	Nose gear integration is difficult with antenna in fuselage.
Tandem w/ Outriggers	Good for integration with complicated structure (Antenna in center of fuselage.)	Takeoff rotation is difficult if not impossible. Heavy.

The landing gear disposition choice was made based primarily on integration issues. The antenna integration requirements are such that placing the landing gear on the wing is unesirable. Also, the antenna located in the fuselage causes problems with integrating the landing gear into the fuselage (see Figure 5.20). A tandem landing gear does not necessarily agree well with the short field requirements due to takeoff rotation limitations of tandem gear configurations. The tandem gear configuration was then removed from consideration.

The tail-dragger configuration was considered due to the integration with the center antenna. The tail dragger was not chosen however as it would cause problems in the design of an auto-land/auto-takeoff system. The tricycle gear design is shown in Figure 5.20. The main gear cannot be mounted in the wing due to the antennas, so it will be mounted in the fuselage. The main gear retracts rearward utilizing a tilted pivot retraction scheme. The nose gear retracts straight back into the fuselage.

The landing gear width was sized to satisfy lateral tip-over constraints as specified in [2]. This is shown in Figure 5.19 for the Blue design. The fuselage station of the main gear was located to satisfy longitudinal tip-over. This can be seen in Figure 5.21.

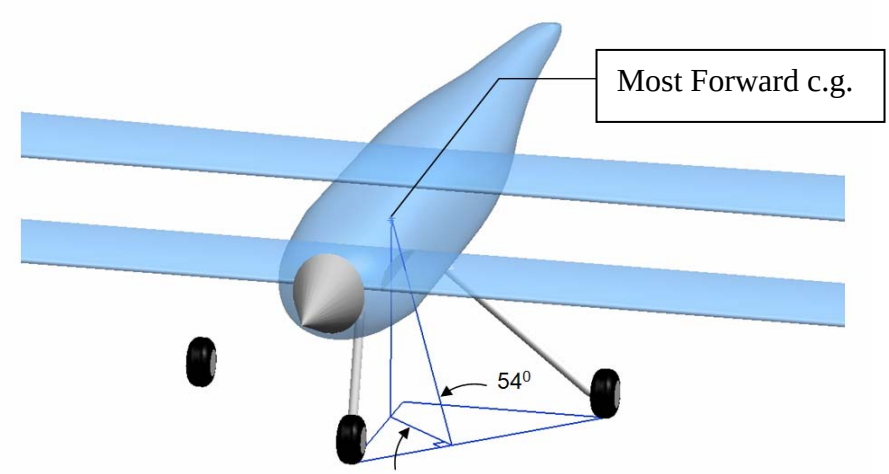

Figure 5.19: Landing Gear Placement for Lateral Tip-Over Requirements

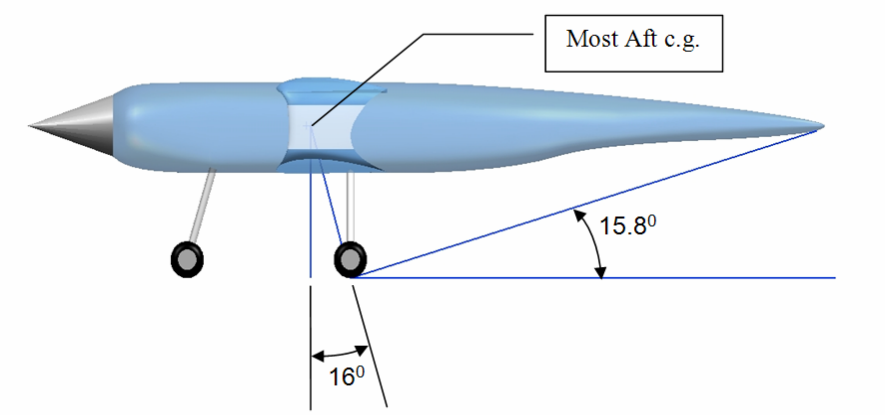

Figure 5.20: Landing Gear Layout and Retraction Scheme for Blue Design

The maximum static loads for each strut were calculated and tabulated in Table 5.12 for the Red Design. These values were used along with data from [2] to select reasonable tire sizes. These are also shown in Table 5.12. The tires selected for the Red design will also be suitable for the White and Blue designs.

Table 5.12: Tire Sizing Summary for the Blue Design

Parameter	Units	Value
Nose Gear F.S.	in	70.0
Main Gear F.S	in	115.0
L_n	in	30.8
L_m	in	14.2
P_n	lbs	299.1
P_m	lbs	324.5
P_n/W_{TO}	~	0.32
$2P_m/W_{TO}$	~	0.68
Tire Diameter	in	9
Tire Width	in	3.4

The design mission calls for the ability to use skis or tires as this aircraft will operate from a wide variety of surfaces. The ski design/selection will be performed in Class II design.

5.6 Class I Weight and Balance

The purpose of this section is to describe the preliminary aircraft component weight breakdown as well as the center of gravity calculations for the three concepts. The weight and balance analysis is one that is continually iterated throughout the design process with increasing levels of fidelity as the design progresses. The first level of this analysis is to use general weight ratios based on known aircraft to calculate weight budgets for the different weight groups such as the wing and fuselage. There is a limited amount of data on UAVs in terms of component weights, so weight ratios from inhabited aircraft are used. Essentially, this method just splits the estimated takeoff weight into the specified groups. Therefore, while using weight ratios based on inhabited aircraft is questionable, the results should be reasonable as the takeoff and empty weights were calculated based on UAV data.

5.6.1 Initial Component Weight Breakdown

The aircraft components were broken down into the following list for the weight fraction calculations.

1. Fuselage Group
2. Wing Group
3. Empennage Group
4. Engine Group
5. Landing Gear Group
6. Nacelle Group (Engine Cowling)
7. Fixed Equipment Group
8. Trapped Fuel and Oil
9. Fuel
10. Payload

The aircraft empty weight is the sum of items 1 through 7. The aircraft operating empty weight is defined as the sum of items 1 through 8. The aircraft gross takeoff weight is the sum of items 1 through 10. The “Nacelle group” refers to the engine cowl weight.

The weight of each of these components was calculated using the weight fraction method described in [2]. The weight fractions for several single engine aircraft are shown in Table 5.13. This data was taken from [2].

The weight fractions in Table 5.13 were averaged then multiplied by the gross takeoff weight of each design. This resulted in the data shown in Table 5.14. When the weights of the *initial estimate* column are added, they yield different values than the actual empty weights due to roundoff errors. The weights of the component are then adjusted in proportion to their component weight until the summation equals the empty weight..

Table 5.13: Group Weight Data for Single Engine Propeller Driven Aircraft [2]

Weight Item, lbs	C-150	C-172	C-175	C-180	C-182	L-19A	Beech J-35
Gross Takeoff Weight, GW	1500	2200	2350	2650	2650	2100	2900
Empty Weight, lbs	946	1243	1319	1526	1545	1527	1821
Structure/GW	0.406	0.352	0.330	0.319	0.326	0.327	0.312
Powerplant/GW	0.177	0.157	0.177	0.206	0.206	0.262	0.201
Fixed Equipment/GW	0.068	0.072	0.068	0.065	0.065	0.136	0.115
Empty Weight/GW	0.631	0.565	0.561	0.576	0.583	0.727	0.628
Wing Group/GW	0.144	0.103	0.097	0.089	0.089	0.113	0.131
Empennage Group/GW	0.024	0.026	0.024	0.023	0.023	0.030	0.020
Fuselage Group/GW	0.154	0.160	0.149	0.152	0.151	0.103	0.069
Nacelle Group/GW	0.015	0.012	0.013	0.012	0.013	0.016	0.021
Landing Gear Group/GW	0.069	0.050	0.047	0.042	0.050	0.064	0.071
Wing Group/S, psf	1.35	1.29	1.30	1.34	1.34	1.37	2.13
Empennage Group/S_{emp},psf	0.85	1.08	1.08	1.17	1.18	1.19	1.62
Ultimate Load Factor, g's	5.7	5.7	5.7	5.7	5.7	5.7	5.7
Wing Area, ft^2	160	175	175	175	175	174	178
Horizontal Tail Area, ft^2	28.5	34.6	34.6	34.6	34.1	35.2	0
Vertical Tail Area, ft^2	14.1	18.4	18.4	18.4	18.4	18.4	0
Empennage Area, ft^2	42.6	53	53	53	52.5	53.6	35.8

Table 5.14: Component Weight Breakdown Summary

	Initial Estimate	Adjustment	Class I Weight	Initial Estimate	Adjustment	Class I Weight	Initial Estimate	Adjustment	Class I Weight
Weight Group	lbs	lbs	lbs	lbs	lbs	lbs	lbs	lbs	lbs
Wing	83	-4	79	139	-12	127	104	-7	97
Empennage	19	-1	18	31	-3	28	23	-2	22
Fuselage	102	-5	97	170	-15	156	127	-9	119
Nacelles	11	0	11	18	-2	17	14	-1	13
Landing Gear	43	-2	41	71	-6	65	53	-4	50
Power Plant	150	-7	143	251	-22	230	188	-13	175
Fixed Equipment	64	-3	61	107	-9	98	80	-5	75
Empty Weight	471	-21	450	788	-68	720	590	-40	550
Payload			122			122			122
Fuel			184			423			270
Trapped Fuel and Oil			4.4			7.4			6.1
Takeoff Gross Weight			760			1270			948

5.6.2 Preliminary Aircraft Arrangement

The fuselage, wing, and empennage designs developed were combined to create preliminary arrangements of each aircraft. The arrangement of the Blue design is shown in Figure 5.21 as an example. These arrangements were then used to locate

each of the weight components listed in Table 5.14. The centers of gravity for the fuselage, wing, engine cowl, and empennage were then estimated using methods from Roskam [2]. These values were used to determine the center of gravity for the vehicles as shown in Table 5.15.

Table 5.15: Class I Weight and Balance Summary

Component	Red			White			Blue		
	Weight lbs	X_cg in	Z_cg in	Weight lbs	X_cg in	Z_cg in	Weight lbs	X_cg in	Z_cg in
Wing	79	106.3	45.0	127	106.0	45.0	97	104.0	50.0
Empennage	18	221.0	50.0	28	222.0	50.0	22	221.0	50.0
Fuselage	97	120.0	50.0	156	120.0	50.0	119	120.0	50.0
Cowling	11	60.0	50.0	17	60.0	50.0	13	60.0	50.0
Landing Gear - Extended	41	102.0	32.0	65	102.0	32.0	50	102.0	32.0
Landing Gear - Retracted	41	111.0	40.0	65	111.0	40.0	50	111.0	40.0
Power Plant	143	66.0	45.0	230	66.0	45.0	175	66.0	45.0
Fixed Equipment	61	110.0	45.0	98	110.0	45.0	75	110.0	45.0
Empty Weight - Gear Ext	450	100.0	45.2	720	99.9	45.2	551	99.4	46.1
Empty Weight - Gear Ret	450	100.8	45.9	720	100.8	45.9	551	100.4	46.8
Payload	121.2	100.0	50.0	121.2	100.0	50.0	121.2	100.0	50.0
Fuel	184	101.0	50.0	184	101.0	50.0	184	101.0	50.0
Trapped Fuel and Oil	4.4	101.0	50.0	4.4	101.0	50.0	4.4	101.0	50.0
TOTAL - Gear Extended	760	100.2	47.2	760	100.1	47.2	760	99.8	47.5
TOTAL - Gear Retracted	760	100.7	47.6	760	100.7	47.6	760	100.5	48.0

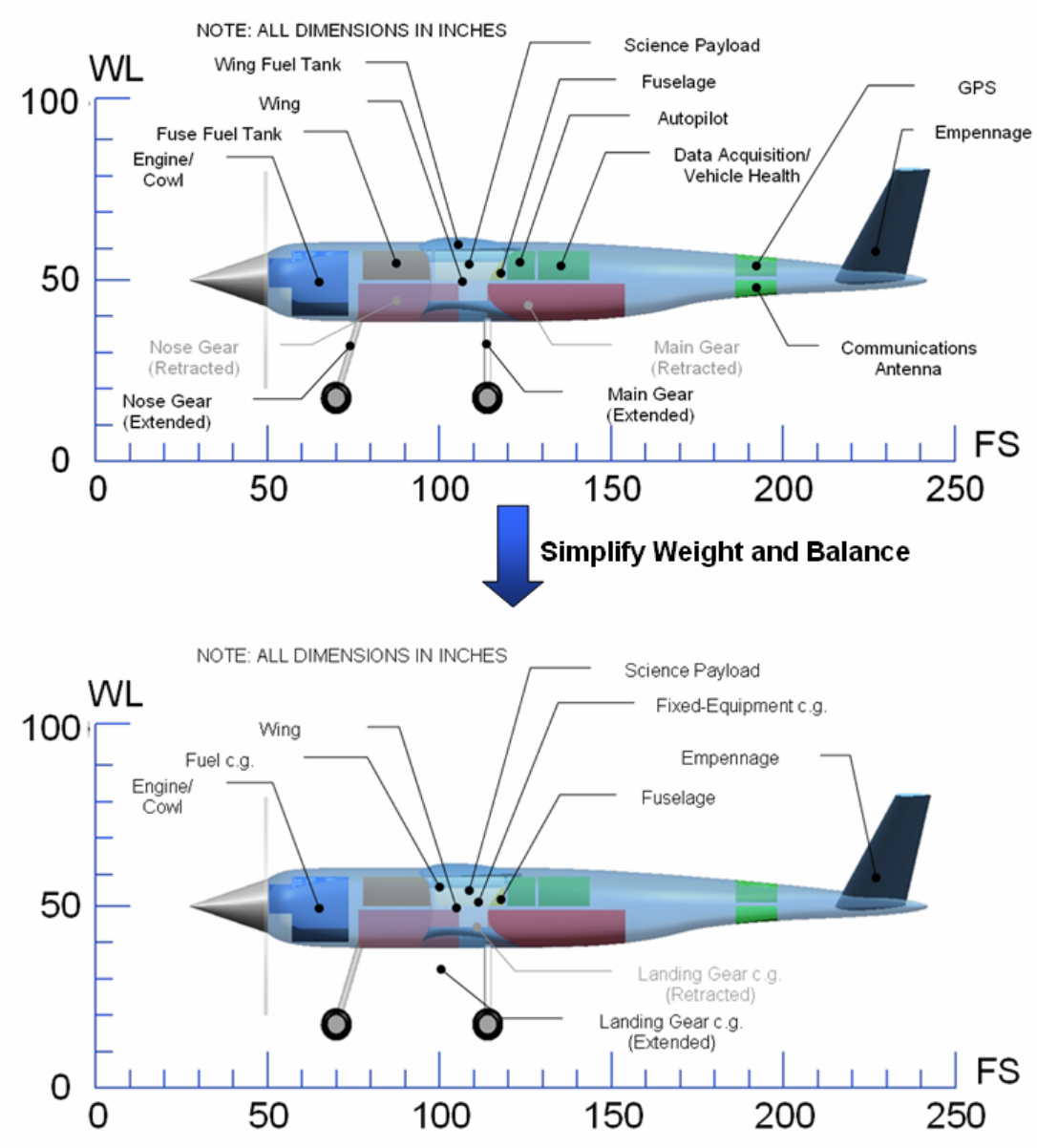

Figure 5.21: Preliminary Arrangement of Blue Design

Figure 5.21 shows the aircraft arrangement for a detailed arrangement as well as the simplified layout. A detailed CAD model is used to aid in the estimation of the centers of gravity for each component. This was then used to estimate the center of gravity for each group listed in Table 5.15. The simplified model is used because the exact weight and location of every component in the aircraft is not known at this

stage of the design. For Class I analysis using simplified weight groups provides the best weight and balance estimate.

C.G. excursion diagrams were created for each aircraft. The excursion for the Blue design is shown as in Figure 5.22. There are two feasible loading scenarios for this aircraft:

- Load Payload then Add Fuel
- Add Fuel then Load Payload

The total c.g. travel is the same for both scenarios, but the latter also shows the c.g. range for the aircraft with no payload (+Fuel leg). This is important as some of the initial flight tests may be performed without any payload.

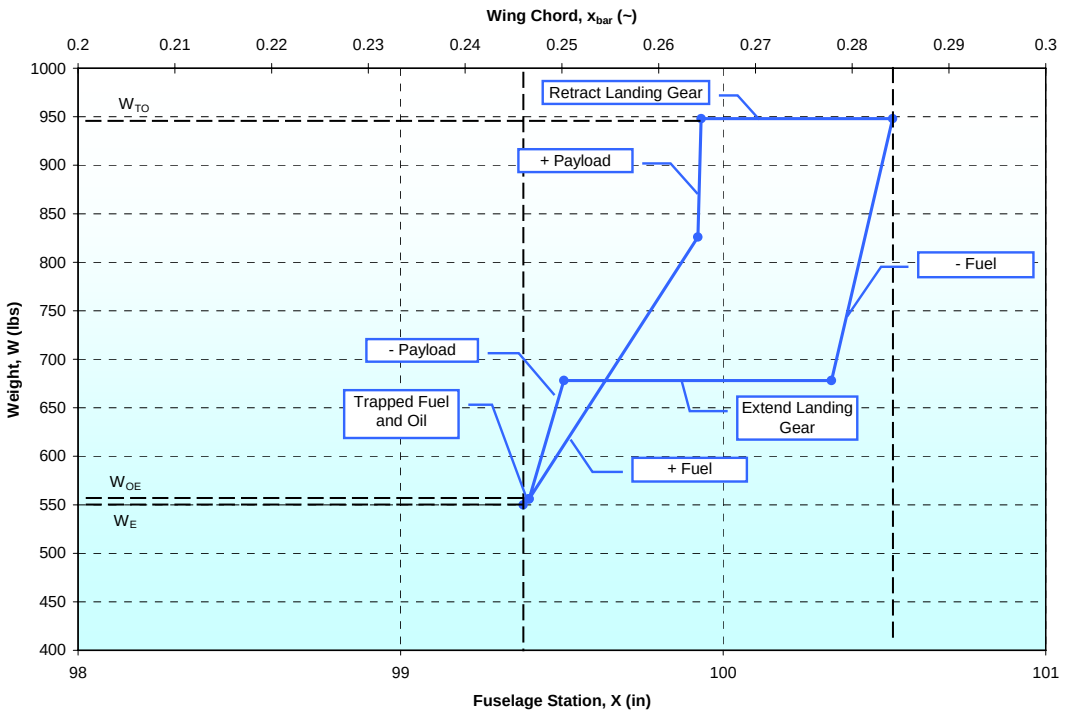

Figure 5.22: Center of Gravity Excursion for the Blue Design

The c.g. excursion shows that the landing gear has a significant effect on the center of gravity. The most forward and most aft center of gravity locations are shown in Table 5.16. The results are acceptable; however, the c.g. travel could be less if not for the landing gear contribution.

Table 5.16: Weight and Balance Summary

	Red		White		Blue	
Parameter	**Inches**	**% mgc**	**Inches**	**% mgc**	**Inches**	**% mgc**
Most Forward c.g.	100.0	0.23	99.9	0.25	99.7	0.19
Most Aft c.g.	101.6	0.27	101.5	0.29	101.4	0.25
c.g. Range	1.6	0.04	1.6	0.04	1.7	0.06

5.7 Class I Stability and Control

The purpose of this section is to describe the Class I stability and control analysis performed. This includes determining the static longitudinal stability and static directional stability. This is accomplished with the use of X-plots. These plots are used to determine minimum tail size and are very helpful in iterating the wing placement. Consideration was given to takeoff rotation and aircraft trim capability, but these factors were not included in these calculations as they are part of the Class II design.

The first step in the stability analysis process is to decide whether the aircraft will be designed for inherent or de-facto stability:

- Inherent Stability – Required of all aircraft that do NOT rely on a stability augmentation system.
- De-facto Stability – Required of all aircraft that are stable ONLY with a stability augmentation system.

The latter method provides improved aerodynamic efficiency due to decreased trim drag in cruise. However, this typically requires a certain amount of redundancy in the flight control system such that a failure in the autopilot would not cause a crash. For this design the aircraft will be designed for inherent stability with a static margin of at least 10 percent.

5.7.1 Longitudinal Stability

The static longitudinal stability of the aircraft was verified using a longitudinal X-plot. This plot shows how the aircraft center of gravity and aerodynamic center vary with V-tail size. This method was used to resize the V-tail as it is more precise than the volume coefficient method.

The longitudinal X-plot for the Red Design is shown in Figure 5.23. The minimum V-tail size is shown as 5.5 ft^2. This is the V-tail size shown in Figure 5.21. Similar plots were created for the White and Blue designs.

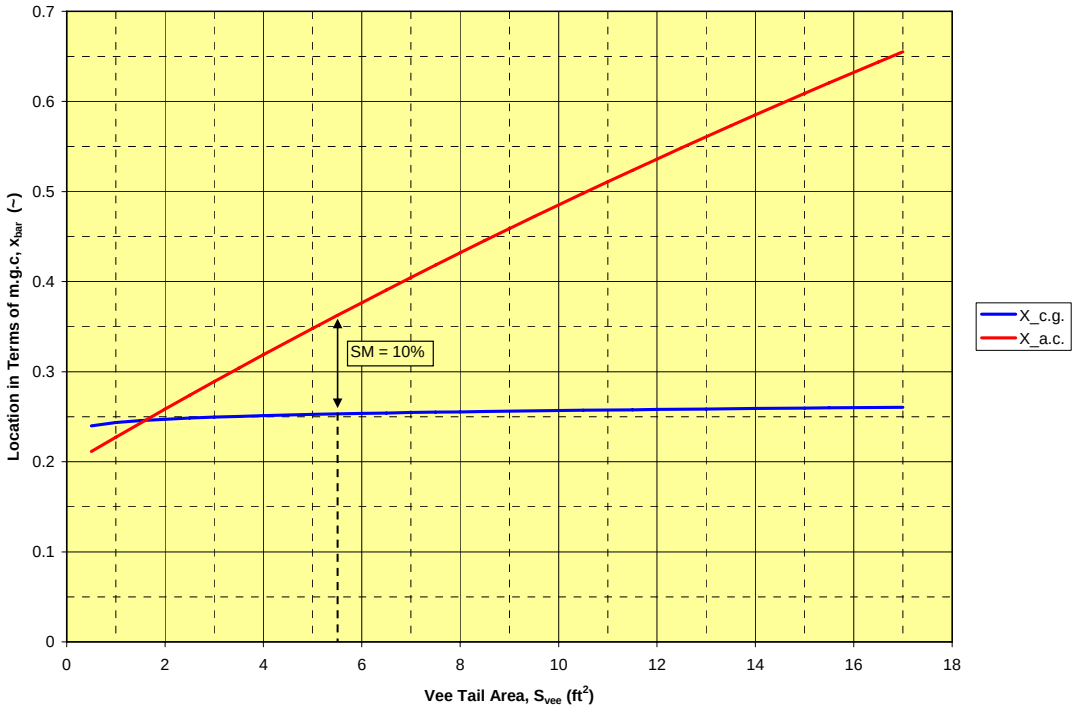

Figure 5.23: Longitudinal X-Plot for the Red Design

5.7.2 Directional Stability

The static directional stability of the aircraft was verified with a directional x-plot as shown in Figure 5.24. The target value for the overall directional stability is:

- $C_{n_\beta} = 0.001 \text{deg}^{-1}$

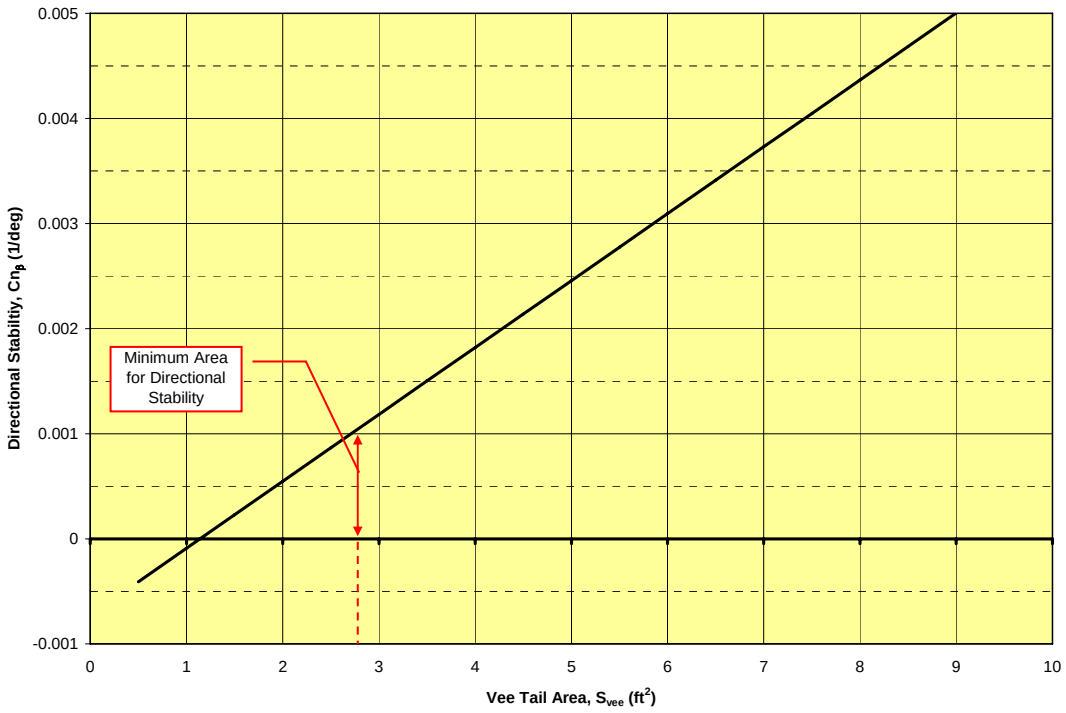

Figure 5.24: Directional X-Plot for the Red Design

Figure 5.24 shows that the directional stability requirements would drive the vertical component of the V-tail projected area to be approximately 2.8 ft^2 for the Red Design. This means that the V-tail dihedral angle should be changed using Equation 5.8 from [2], where S_v and S_h represent the projected tail areas based on the directional and longitudinal X-plots respectively.

$$\Gamma_{Vee} = Tan^{-1}\left(S_v / S_h\right) \qquad \text{Equation 5.8}$$

This results in a V-tail dihedral angle of 27^o for the Red Design. This is a fairly small dihedral angle for a V-tail. Experience has shown that the vertical tail size is usually driven by crosswind capability, not the directional X-Plot. Therefore, at this

time the V-tail dihedral angle will not be changed for any of the designs. This parameter will be investigated further in Class II design.

The stability and control analysis resulted in new tail geometry. The V-tail sizes were reduced in all cases. The results are:

- Red – $S_{vee} = 5.5\ ft^2$
- White – $S_{vee} = 7.0\ ft^2$
- Blue – $S_{vee} = 6.0\ ft^2$

These results will need to be iterated in Class II stability and control to ensure sufficient control power is achievable.

5.8 Class I Drag Analysis

The purpose of this section is to describe the development of the Class I drag polars for the three Designs. Drag polars were generated for the following flight conditions:

1. Cruise (Clean)
2. Takeoff – Gear Down
3. Takeoff – Gear Up
4. Landing – Gear Down
5. Landing – Gear Up
6. Power off

The first step in the Class I drag polar estimation process is to determine the aircraft wetted area. This was done using a 3-D solid model, and is therefore very accurate. The wetted areas for the three Designs are:

- Red – S_{Wet} = 200 ft^2
- White – S_{Wet} = 275 ft^2
- Blue – S_{Wet} = 247 ft^2

The Class I drag analysis assumes the aircraft drag follows the relationship shown in Equation 5.9. The Oswald's efficiency factors were assumed to be 0.80 for all of the designs. This assumption is verified in Class II design. The zero-lift drag coefficient is found using Equation 5.10 from [2].

$$C_D = C_{D_0} + \frac{1}{\pi A e} C_L^2 \qquad \text{Equation 5.9}$$

$$C_{D_0} = \frac{f}{S_w} \qquad \text{Equation 5.10}$$

The aerodynamic analysis for the Blue design is performed using methods described in [44]. This method utilizes the traditional drag polar equation, but with an equivalent aspect ratio based on the Munk span factor M as shown in Equation 5.11.

$$C_D = C_{D_0} + \frac{C_L^2}{\pi e M^2 A} \qquad \text{Equation 5.11}$$

$$M = \frac{(1+\nu)\mu}{\sqrt{\mu^2 + 2\mu\nu\sigma + \nu^2}} \qquad \text{Equation 5.12}$$

Where: $\mu = \frac{b_2}{b_1}$ $\qquad\qquad$ $\nu = \frac{L_2}{L_1}$

The biplane interference factor, σ, is shown in Figure 5.25 for various values of spans and gap-to-span ratios. The interference factor used for the Blue design is 0.65.

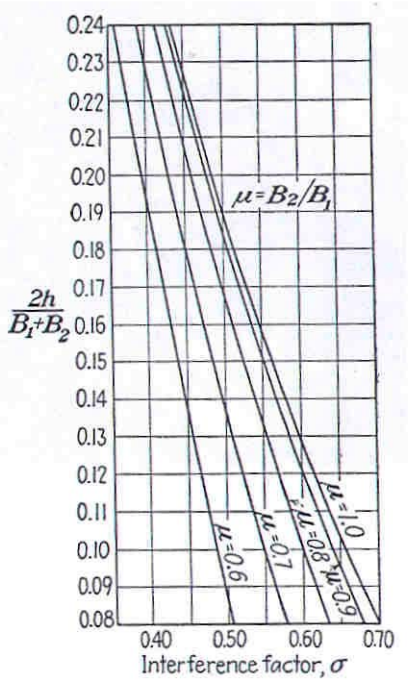

Figure 5.25: Biplane Interference Factor [44]

The drag polars for the Red, White, and Blue designs are shown in Figure 5.26, Figure 5.28, and Figure 5.30 respectively. The L/D ratios for the Red, White, and Blue designs are shown in Figure 5.27, Figure 5.29, and Figure 5.31 respectively. The cruise drag polars and lift-to-drag ratios for the three designs are shown together in Figure 5.32 and Figure 5.33 respectively.

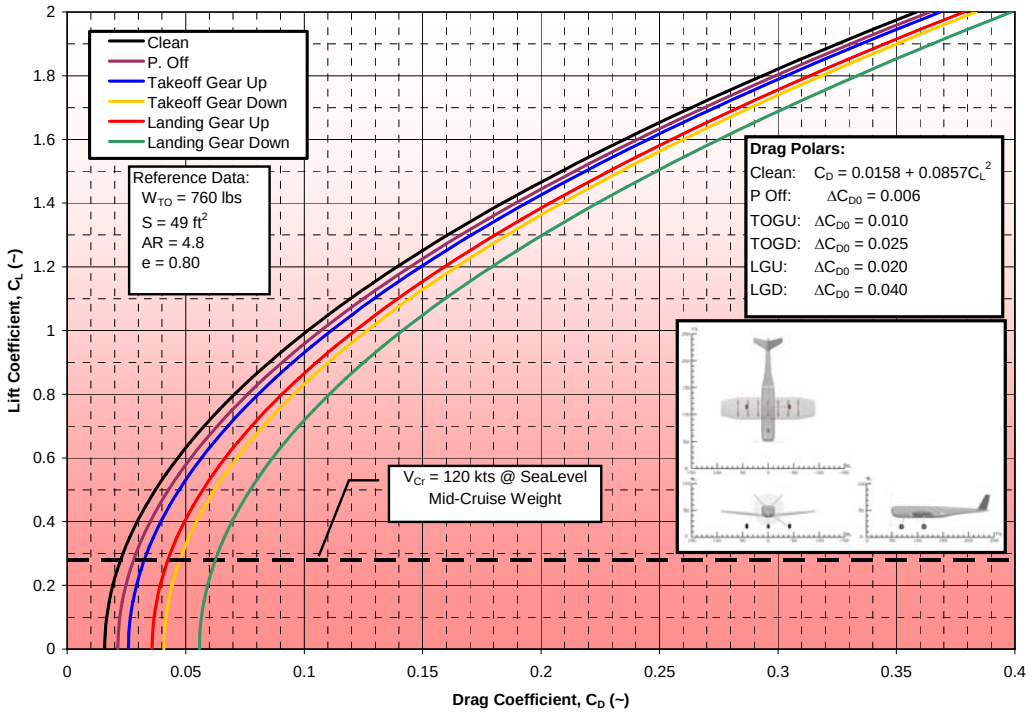

Figure 5.26: Drag Polars for the Red Design

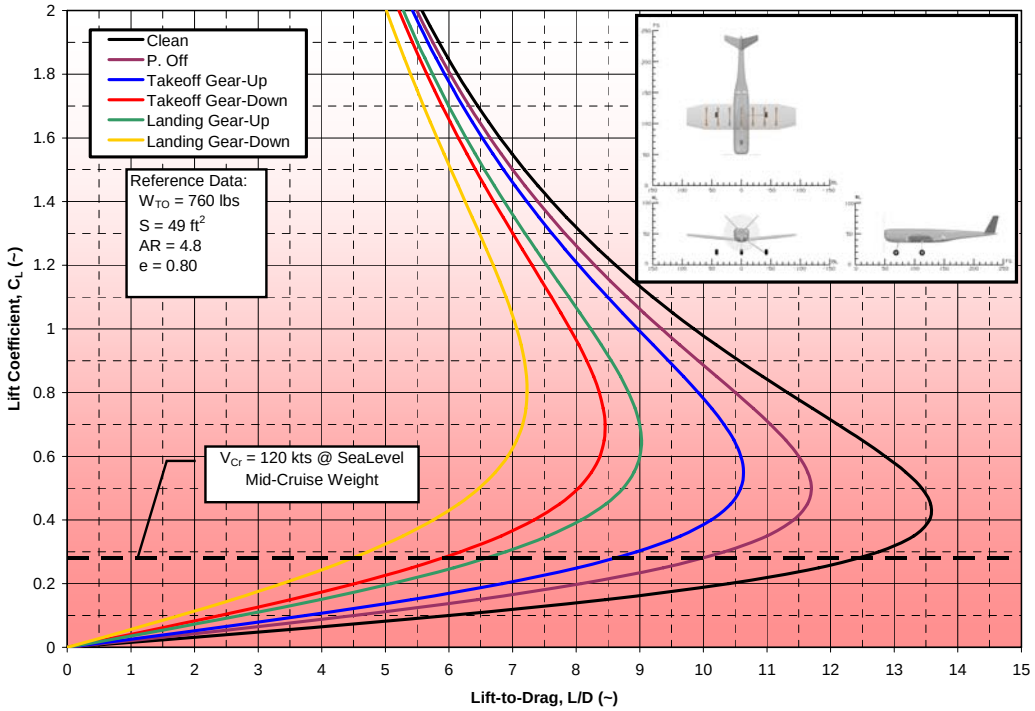

Figure 5.27: Lift-to-Drag for the Red Design

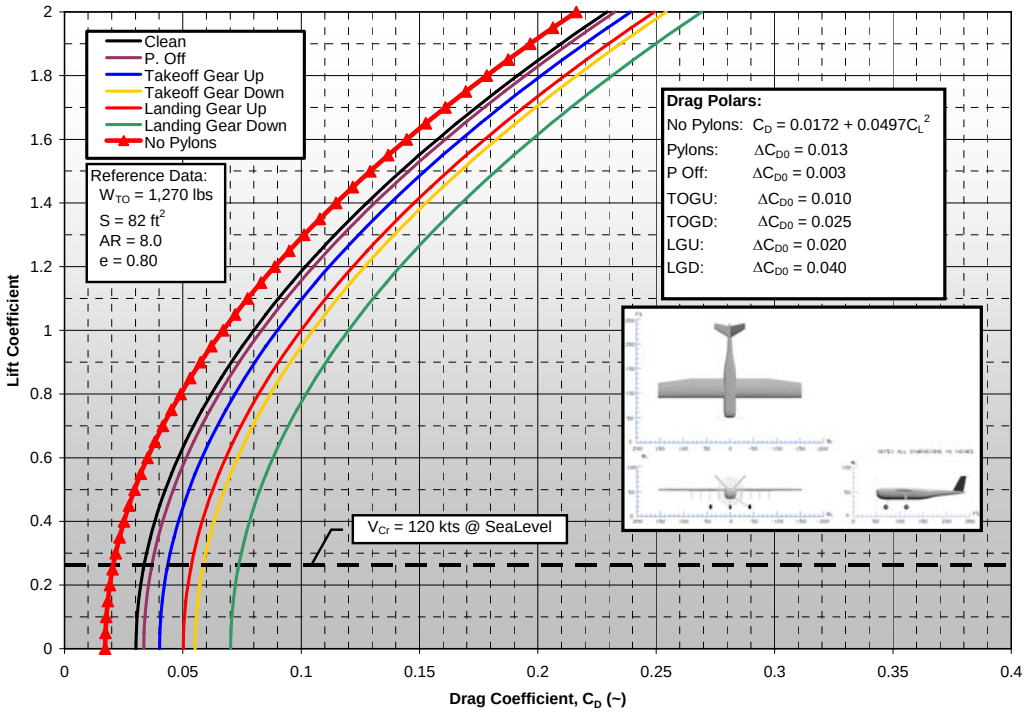

Figure 5.28: Drag Polars for the White Design

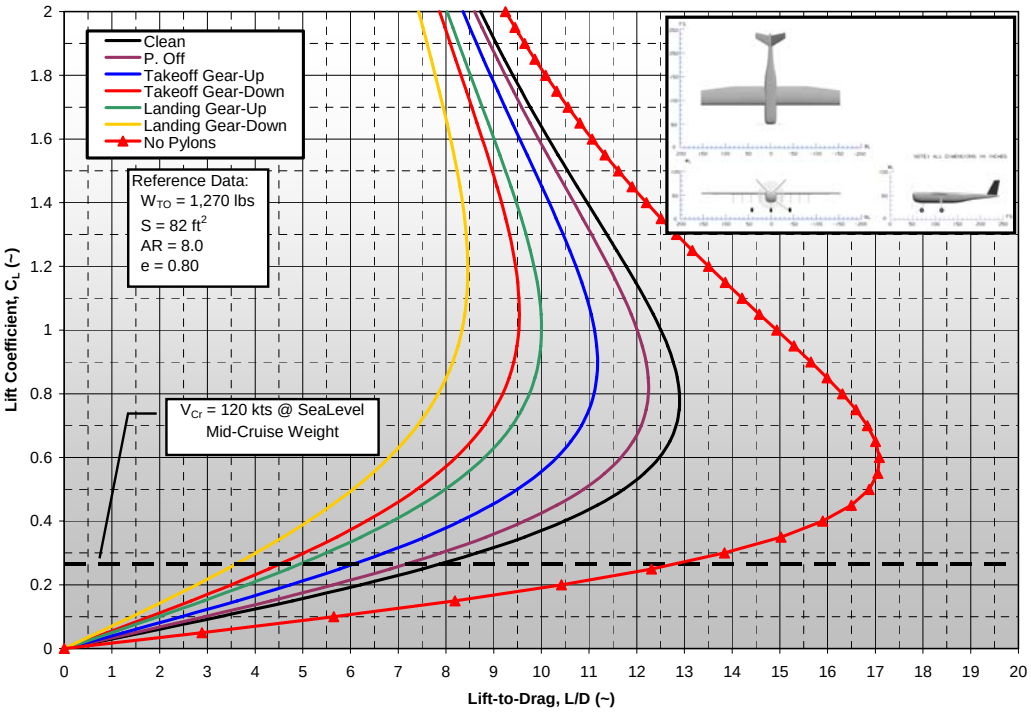

Figure 5.29: Lift-to-Drag for the White Design

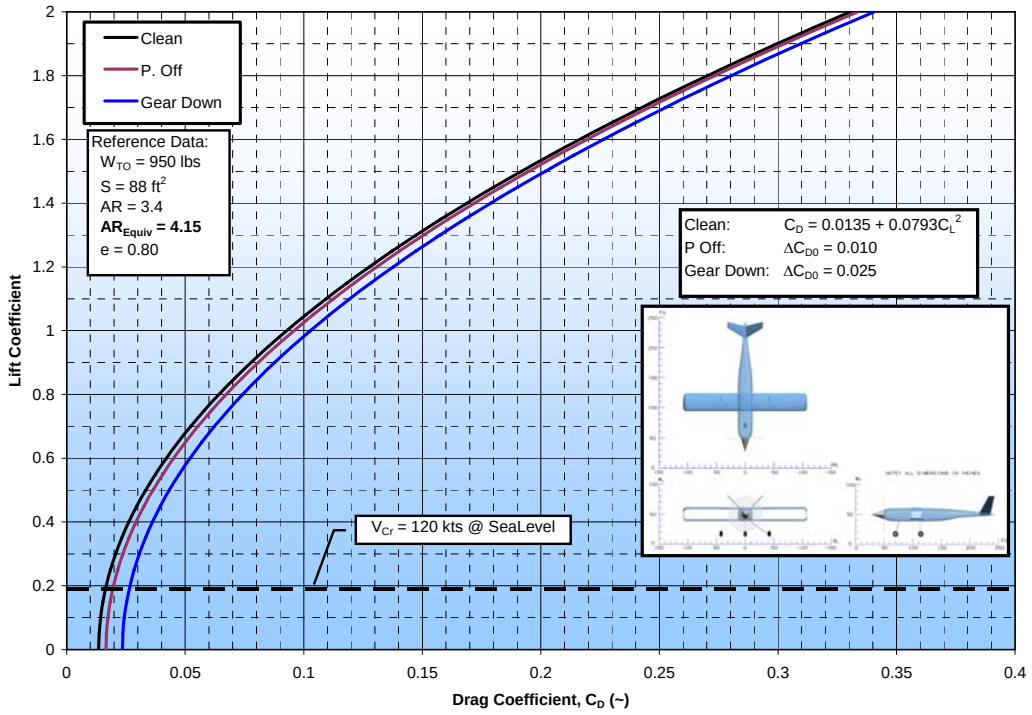

Figure 5.30: Drag Polars for the Blue Design

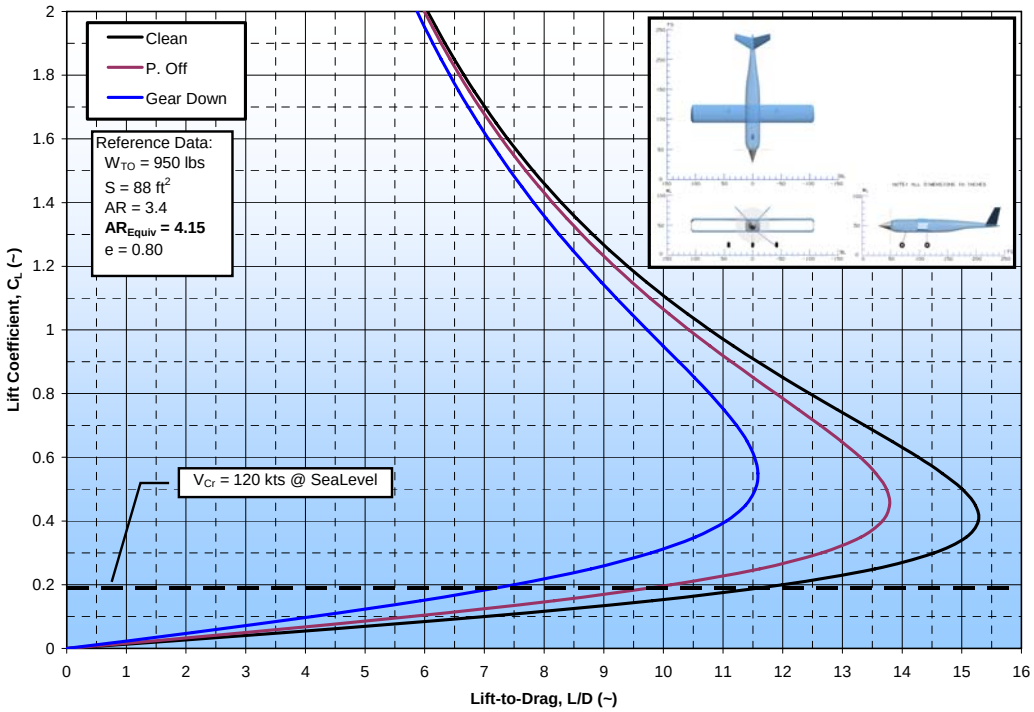

Figure 5.31: Lift-to-Drag for the Blue Design

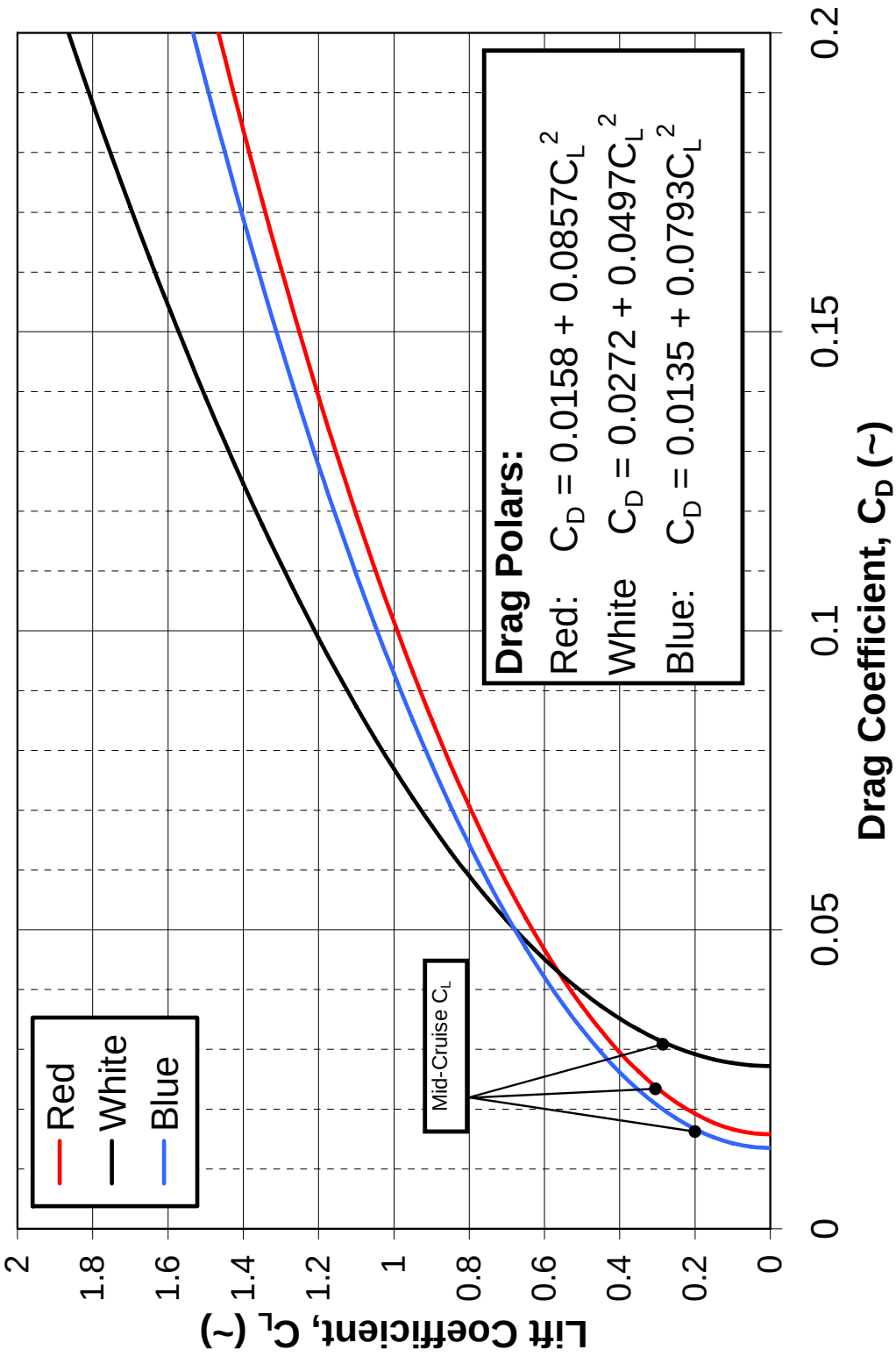

Figure 5.32: Combined Drag Polars

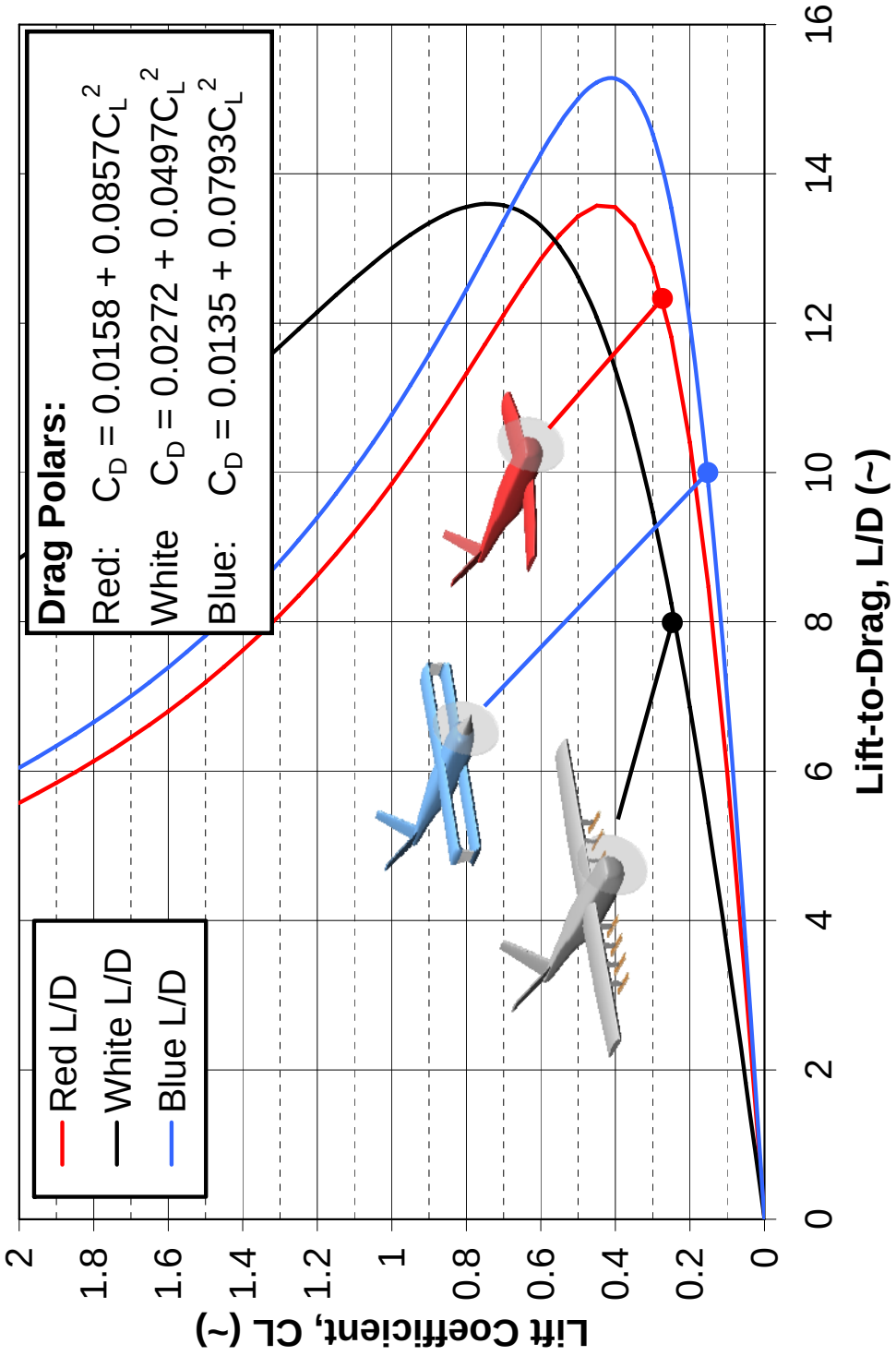

Figure 5.33: Combined Lift-to-Drag Ratios

5.9 Preliminary Concept Summary

Three preliminary concepts have been developed including:

- A low-wing monoplane with antennas integrated into the wing structure.
- A high-wing monoplane with antennas hanging from the wing.
- A biplane with antennas integrated into the structure of a dielectric lower wing.

5.9.1 Red Design Summary

The Red Design is a monoplane with flush-mounted antennas. This integration of the antennas into the wing allowed for a moderate L/D for the Red Design. However, the antennas drove the wing chord to be large with respect to the wing area, hence the very low aspect ratio. Aerodynamic efficiency depends primarily on wing span and wetted area. As the antennas have constrained the wing chord, the only way to gain wingspan is to add wing area, thereby decreasing the wing loading and increasing wetted area. While this results in an aerodynamically inefficient design in terms of span-loading, the lift-to-drag ratio of the Red design is higher than the others due to the integration of the antennas into the wing structure. The Red design is summarized in Figure 5.34.

While the Red Design is feasible, it is suboptimal for several reasons:

- The center antenna will interfere with ski retraction.
- A higher L/D ratio could be achieved if the antennas are reduced in size.
- The feasibility of integrating the antennas into the wing is questionable [22].

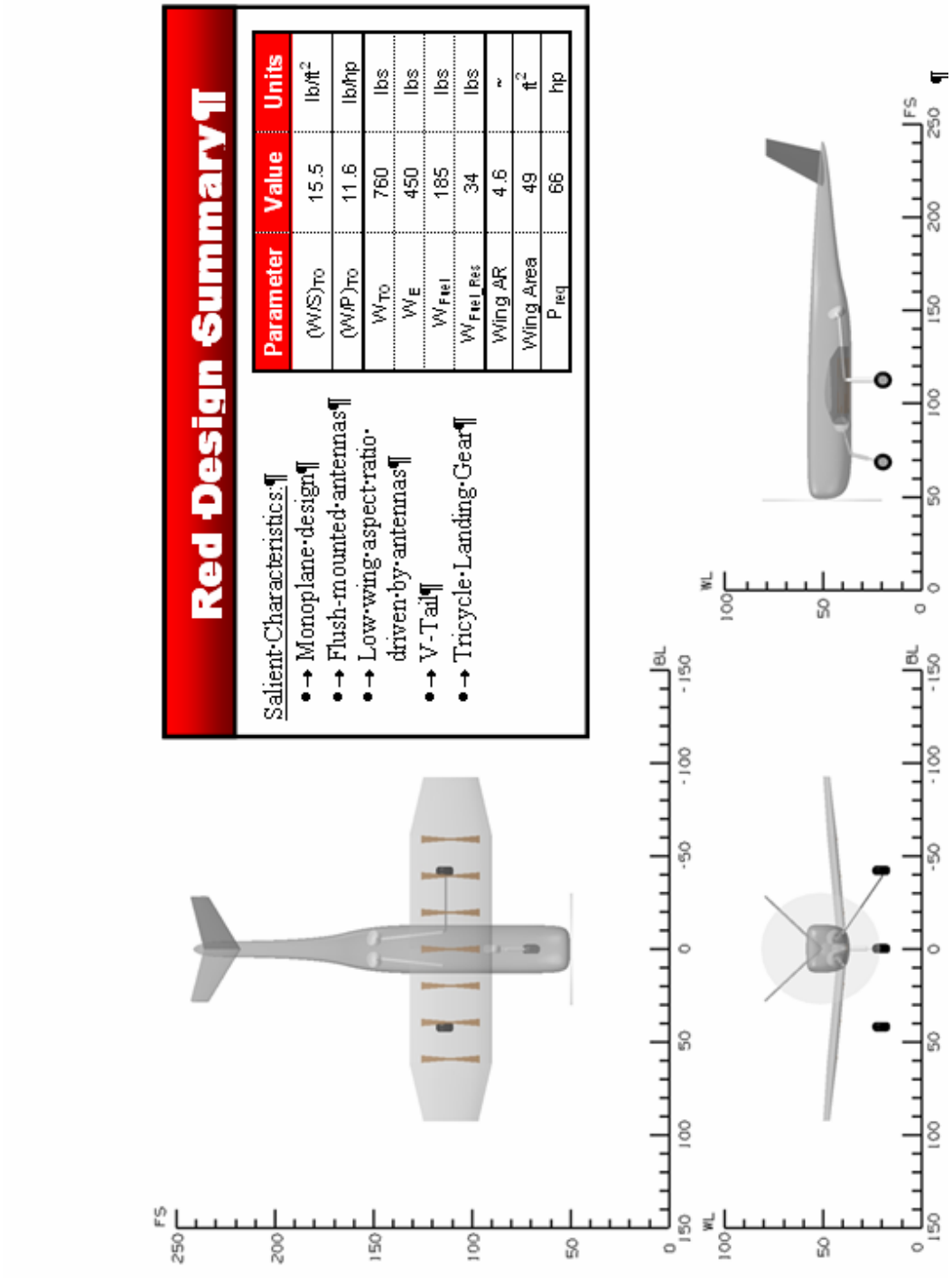

Figure 5.34: Summary of the Red Design

5.9.2 White Design Summary

The results of the Class I design of the White aircraft are shown in Figure 5.35. The pylon mounted antennas created a decrease in the L/D of the aircraft from 12.75 to 8.0 despite the fact that a higher aspect ratio wing was used. This reduction in aerodynamic efficiency resulted in a much higher takeoff weight than the other designs (1,270 lbs). This larger weight resulted in a larger wing, which allowed for a more reasonable aspect ratio. As with the other designs, the wing chord near the root was driven by the antenna requirements. The additional wing area was added by increasing the wingspan such that the aircraft aspect ratio is maximized.

The White design is the least efficient design in terms of aerodynamics, which resulted in a higher gross weight. However, this design is the most robust in terms of the antenna integration as a wide variety of antennas operating at a wide range of frequencies could be used with this design.

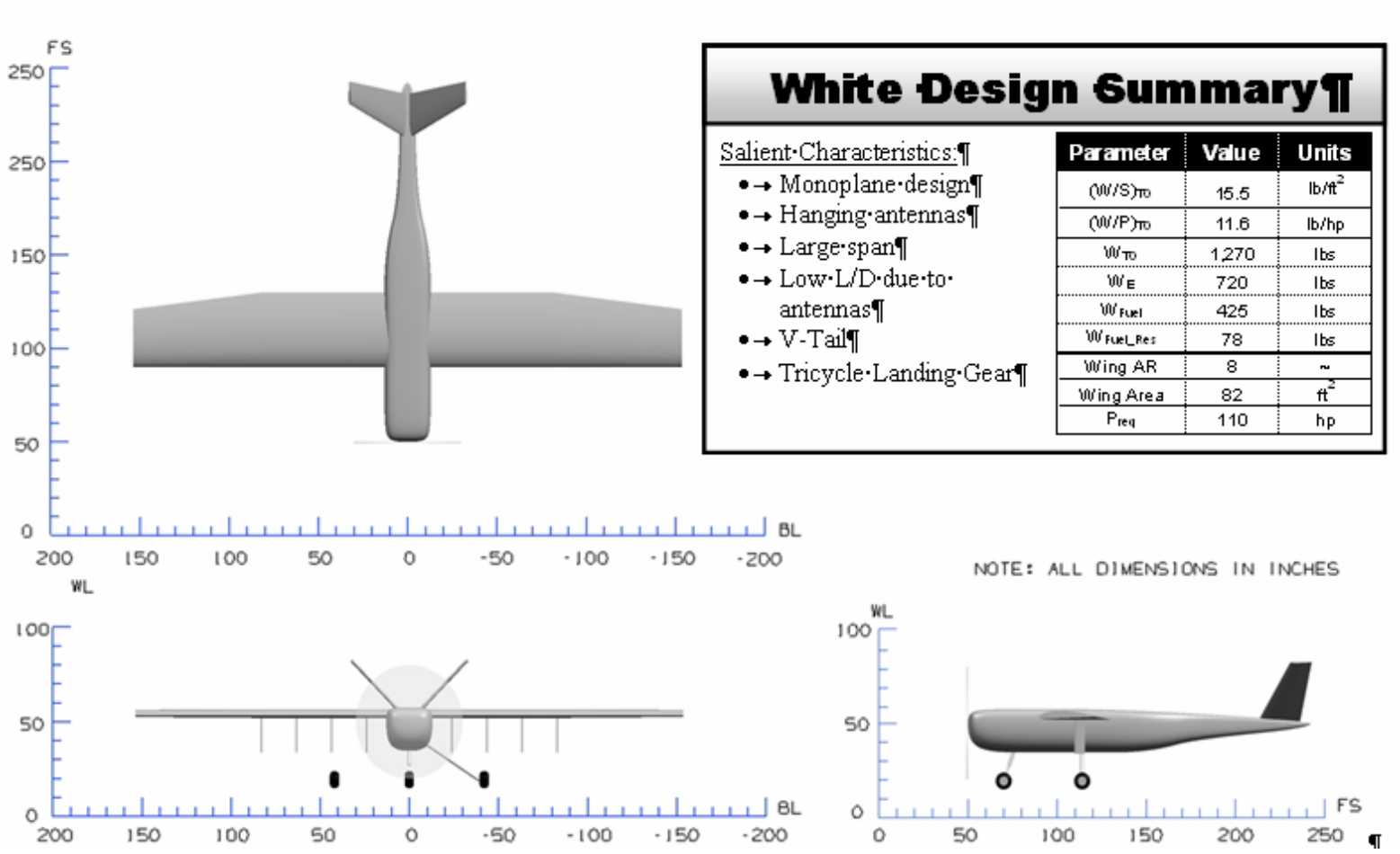

Figure 5.35: Summary of the White Design

5.9.3 Blue Design Summary

The Blue aircraft is a novel approach to this design problem in that it invokes a seldom used configuration – the biplane. The biplane – or box-wing – concept fits very well with the requirements for this aircraft, namely the low cruise speed and large, wing-mounted antennas. The Blue design helped to resolve the following problems found in the Red and White designs:

- Integrating the antennas into the structure of the wing would either require some radar-absorbing material to be developed or the wing structure would have to be made of some dielectric material such as fiberglass.
- Hanging the antennas from the wing allows for the use of non-dielectric materials in the wing structure, but greatly increases drag.

The Blue design allowed for the upper wing to be made of reflective materials, while the lower wing provided an aerodynamically efficient method of integrating the antennas.

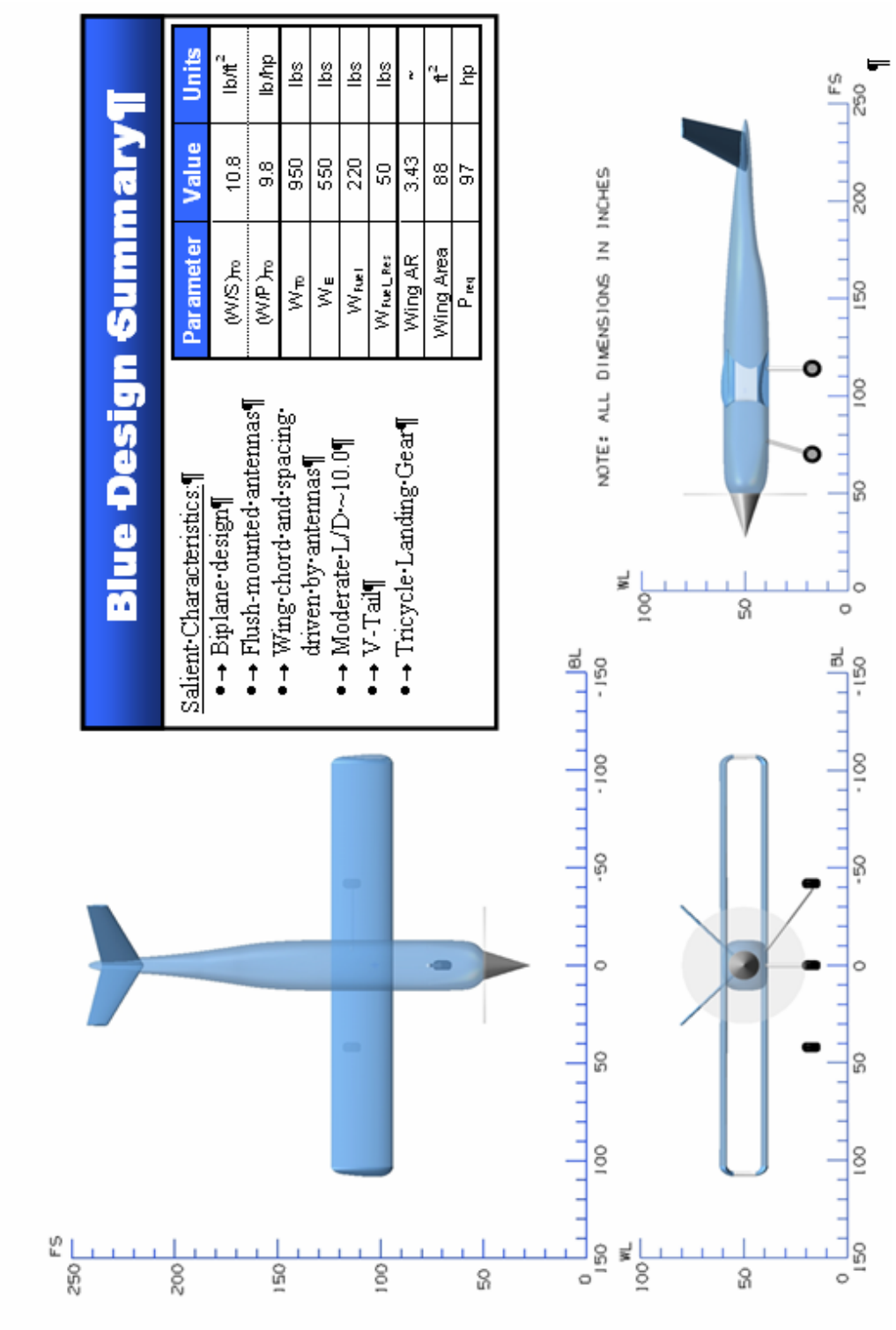

Figure 5.36: Summary of the Blue Design

5.10 Selection of the Preliminary Design

The three designs are summarized in Table 5.17. Figure 5.37 shows the aircraft plotted on the takeoff weight regression chart. In aircraft preliminary design, the primary objective is often to minimize aircraft takeoff weight for a given mission as this will also minimize the acquisition and operational costs of the aircraft. With this in mind, the Red design appears to be the most desirable. However, the Red design relies on the successful integration of the antennas into the electrically reflective structure of the wing. This is a high-risk assumption and was deemed unacceptable. The Blue design represents a lower risk approach as the antennas are integrated into structure composed only of dielectric materials. However, the Blue concept would limit the bandwidth and frequency range of the antennas as the spacing of the wings would not be adjustable. This was also deemed unacceptable. The White design was selected as the prime candidate for this design based almost entirely on the antenna integration. The White design is the most robust in terms of accepting various types of antennas operating at various frequencies. While it is not the most efficient in terms of aerodynamics, the White design offers the best solution with regard to the whole system. In addition, comparison of the fuel required to fly 3 fine scale missions between the three concepts and the aircraft currently used for these missions shows that significant savings can be made by using uninhabited aircraft. While, the White design is the least efficient of the three concepts, it still uses an order of magnitude less fuel than the aircraft currently in use.

The fuel required to complete 3 fine-scale mission is shown in Figure 5.38 for the three designs as well as the Lockheed P-3 and the De Havilland Twin Otter. The fuel consumption of the P-3 was estimated at 590 gal/hr [24] and the Twin Otter was estimated at 85 gal/hr [24].

Table 5.17: Summary of Preliminary Design Concepts

Parameter	Units	Red Design	White Design	Blue Design
Geometry				
Wing				
Area	ft^2	49	82	88
Span	ft	15.33	25.6	17.2
Aspect Ratio	ft	4.8	8.0	3.4
Taper Ratio	~	0.49	0.59	1
Sweep (c/4)	deg	0	0	0
Airfoil	~	Clark Y	Clark Y	Clark Y (Both)
Thickness-to-chord	%	11.8	11.8	11.8
Dihedral	deg	5	0	0
V-Tail				
Area	ft^2	5.5	7.0	6.0
Span	ft	4.7	5.3	4.9
Aspect Ratio	ft	4	4	4
Taper Ratio	~	0.5	0.5	0.5
Sweep (c/4)	deg	26.3	26.3	26.3
Airfoil	~	NACA 0012	NACA 0012	NACA 0012
Thickness-to-chord	~	12	12	12
Dihedral	deg	45	45	45
Length Overall	ft	16	17.5	16.5
Height Overall	ft	5.5	5.6	5.6
Weights				
Takeoff Weight	lbs	760	1,270	950
Empty Weight	lbs	450	720	550
Payload Weight	lbs	121	121	121
Fuel Weight	lbs	185	425	270
Performance				
Range	nm	945	945	945
L/D_{Cr}	~	12.5	8.0	10.0
Powerplant				
Engine	~	Rotax 912-A	Rotax 914-F	Rotax 914-F
Power	hp	81	115	115

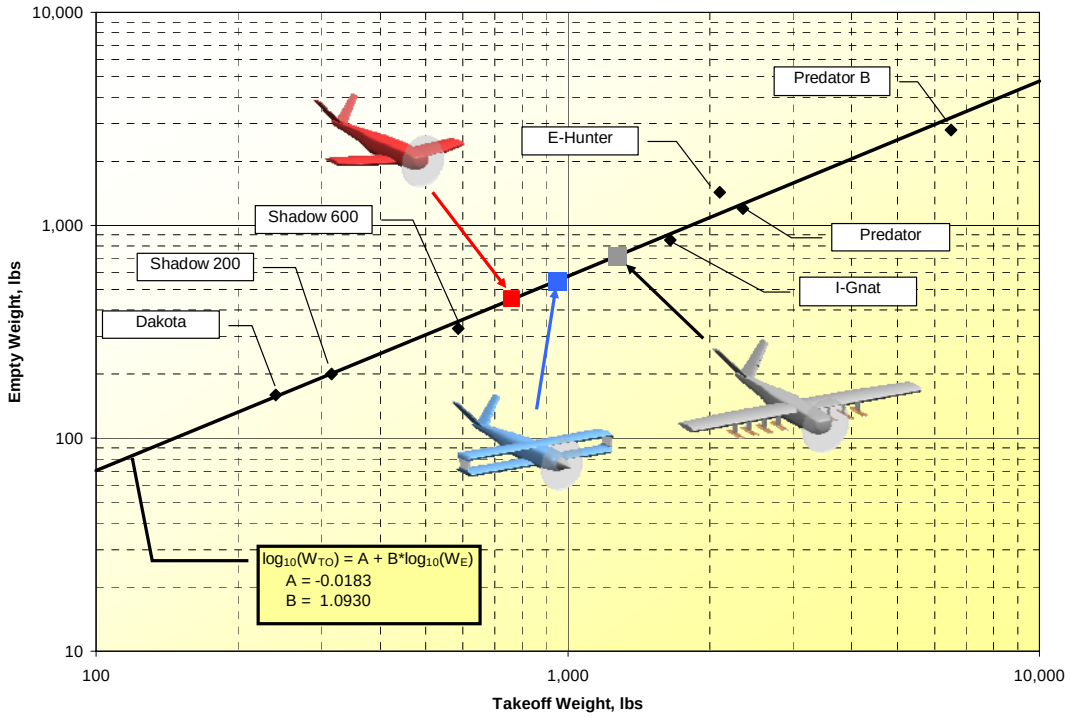

Figure 5.37: Combined Takeoff Weight Regression Chart

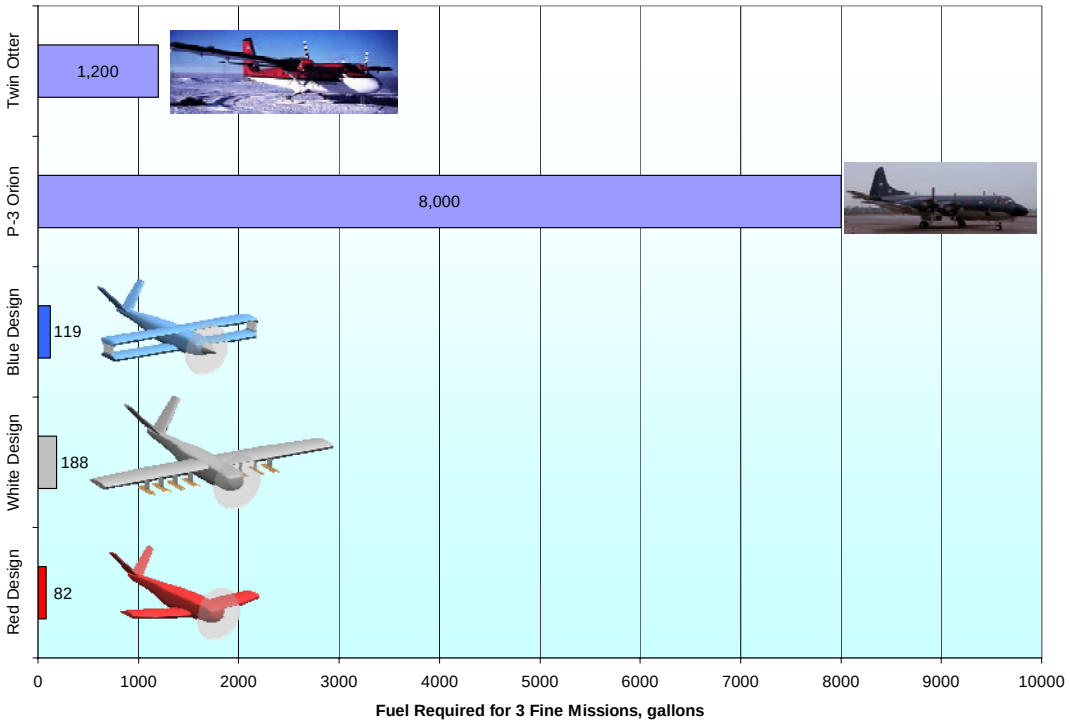

Figure 5.38: Comparison of Fuel Usage for 3 Fine Scale Missions

6 Configuration and Requirement Changes Applied to the Class I Design

The White concept was selected as the primary configuration for further design refinement based on a preliminary design review involving several members of the CReSIS team as well as outside reviewers. Several changes to the design requirements were suggested based on the findings of the Class I analyses. These changes are:

- The primary antennas have changed from bow-tie antennas to Vivaldi antennas (Figure 6.1)
- The antenna integration requirement has changed such that the aircraft should be designed with up to 10 hard points for antenna mounting along the wing span.
- The payload weight was changed from 55kg (120 lbs) to 75kg (165lbs)

L = 0.5 m
H = 0.5 m
T = 0.125 m

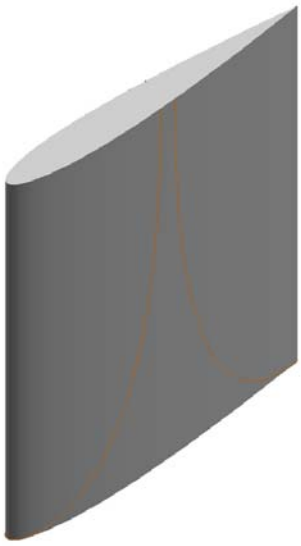

Figure 6.1: Vivaldi Antenna

Several configuration changes were made to the White Design as is evident when Figure 5.35 and Figure 6.2 are compared. The major changes are:

- High wing → Low wing
- Tricycle Landing Gear → Taildragger
- Fuselage Mounted Landing Gear → Wing Mounted Landing Gear
- Rotax Piston Engine → Innodyn Turbopropeller Engine
- $t/c_w = 0.119$ → $t/c_w = 0.18$ (Still uses Clark Y airfoil)

These changes were made as the result of several design iterations and are discussed throughout the remainder of this document. The Meridian (Figure 6.2) is summarized in Table 6.1.

Table 6.1: Summary of the Meridian UAV

Parameter	Units	Meridian
Geometry		
Wing		
Area	ft^2	69.6
Span	ft	26.4
Aspect Ratio	ft	10.0
Taper Ratio	~	1.0
Sweep (c/4)	deg	0
Airfoil	~	Clark Y
t/c	%	18
Dihedral	deg	5
V-Tail		
Area	ft^2	7.5
Span	ft	5.5
Aspect Ratio	ft	4
Taper Ratio	~	0.5
Sweep (c/4)	deg	26.3
Airfoil	~	NACA 0012
t/c	~	12
Dihedral	deg	37
Length Overall	ft	16.7
Height Overall	ft	6.6
Weights		
Takeoff Weight	lbs	1,083
Empty Weight	lbs	618
Payload Weight	lbs	165
Fuel Weight	lbs	295
Performance		
Range	nm	950
L/D_{Cr}	~	13.9
Powerplant		
Engine	~	Innodyn 165TE
Power	hp	165

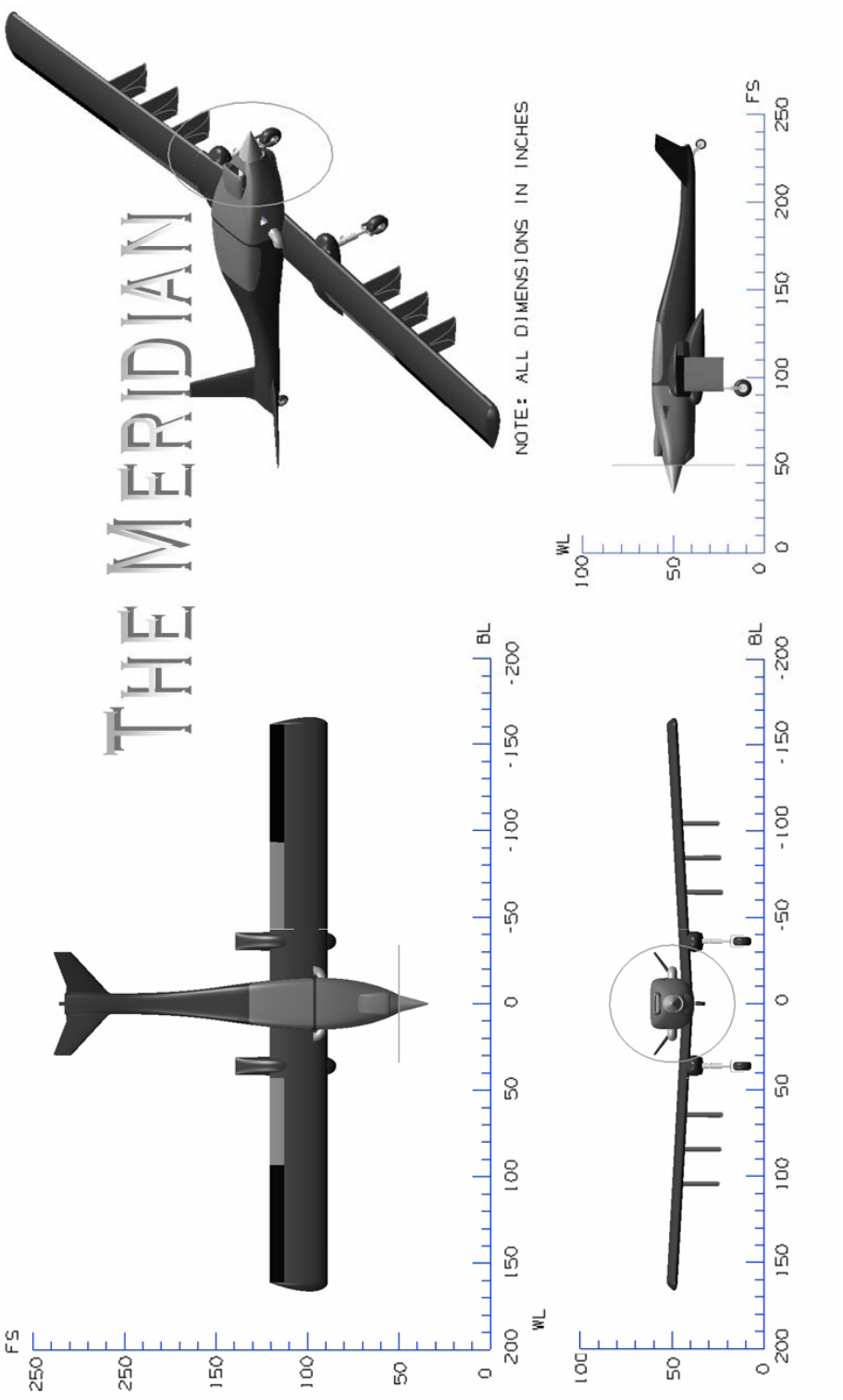

Figure 6.2: The Meridian UAV

7 Class II Design

The purpose of this section is to expand upon the White aircraft configuration (Monoplane with antennas hanging from the wing) through Class II design. Class II aircraft design consists of:

- Listing all systems needed in the aircraft
- Performing more detailed landing gear sizing and retraction design
- Generating initial structural layout
- Constructing a V-n diagram
- Performing a Class II weight and balance analysis
- Performing a Class II stability and control analysis
- Performing a Class II aerodynamic analysis
- Computing the installed power
- Computing critical performance capabilities of the aircraft
- Preparing a preliminary manufacturing breakdown
- Performing a preliminary cost analysis

The new Meridian design shown in Figure 6.2 is the result of several design iterations focused on manufacturability and operational constraints.

7.1 Class II Weight and Balance

The purpose of this section is to describe the Class II weight and balance performed for the Meridian UAV. This consisted of first calculating and plotting a V-n diagram to determine the limit and ultimate loading for the Meridian. The results of the V-n

diagram were then used to create weight estimates for each vehicle component. Finally, a weight and balance analysis is presented to show the aircraft center of gravity travel.

7.1.1 The Aircraft V-n Diagram

A V-n diagram was constructed for the Meridian UAV to help determine the maximum load factors and design speeds that will be used for structural sizing. The V-n diagram was created based on FAR 23 requirements for Normal class aircraft as there are currently no certification requirements for UAVs. The inputs used for the V-n diagram creation are shown in Table 7.1.

Table 7.1: V-n Diagram Parameters

Parameter	Value	Units
Altitude	0	ft
W_{gross}	1,083	lbs
S	69.6	ft^2
W/S	16.2	psf
m.g.c.	2.64	ft
$C_{L\alpha}$	3.98	rad^{-1}
C_{Lmax} (+)	1.42	~
C_{Lmax} (-)	-0.97	~
C_D @ C_{Lmax} (+)	0.085	~
C_D @ C_{Lmax} (-)	0.064	~

The V-n diagram for the Meridian is shown in Figure 7.1. The design speeds and limit load factors are shown in Table 7.2. The positive load factor was set to 3.8g based on FAR 23 requirements [46]. The negative load factor was set to 40 percent of the positive load factor according to FAR 23 requirements [46].

Table 7.2: Design Speeds and Load Factors for the Meridian

Parameter	Value	Units
V_s	58	kts
V_C	133	kts
V_D	186	kts
V_A	113	kts
$V_{S,neg}$	66	kts
n_{limit} (+)	3.8	~
n_{limit} (-)	-1.5	~

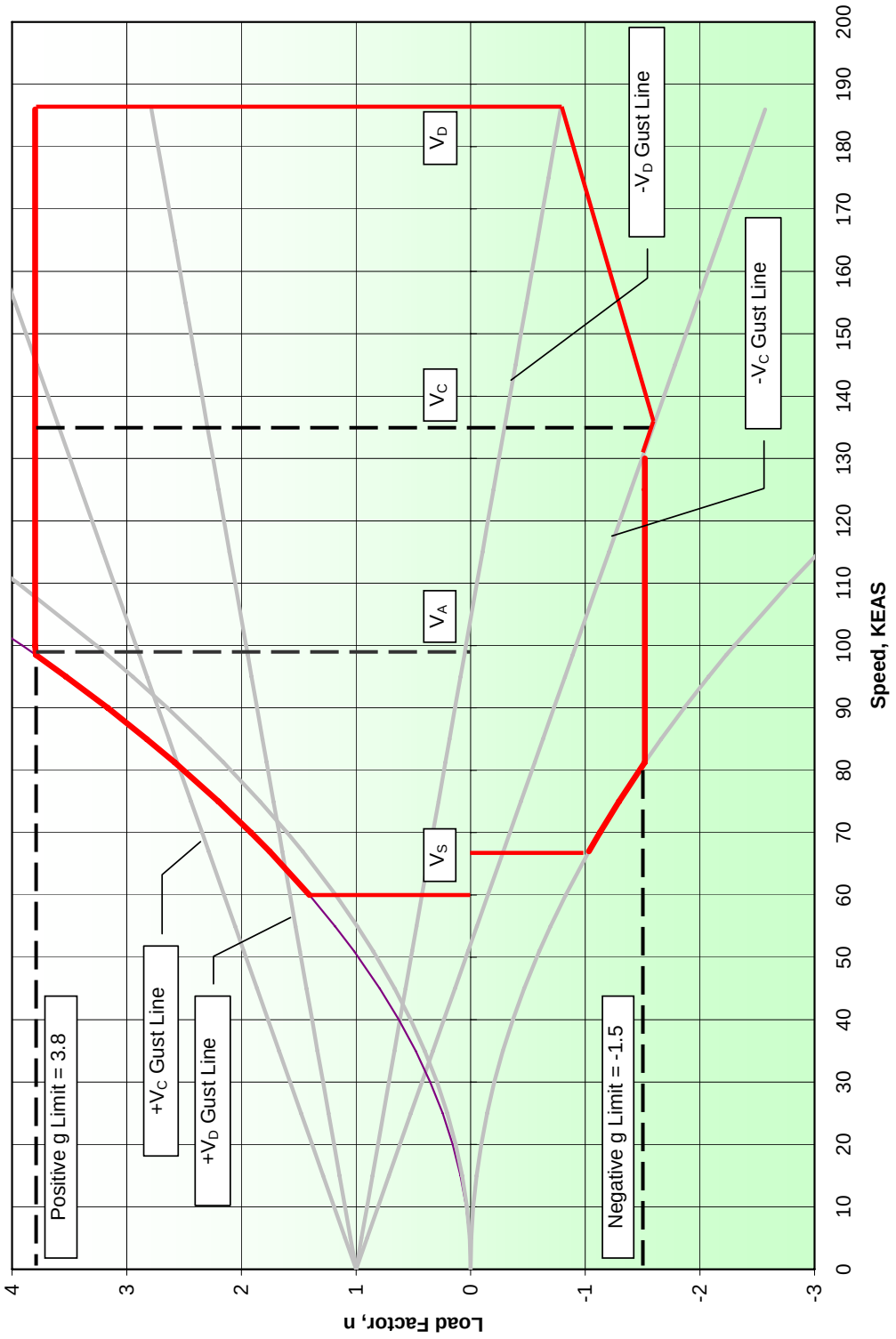

Figure 7.1: V-n Diagram for the Meridian

7.2 Component Weight Estimations

Four methods were used for estimating aircraft component weights: the Cessna, Torenbeek, General Dynamics, and USAF methods. These methods are integrated into the AAA software, which was used for the weight estimations [2].

These methods are designed for conventional, inhabited aircraft, which the Meridian is not. For this reason a certain amount of designer intuition was employed to select the most applicable methods for each component. For example, the Cessna method produced a wing weight of approximately 300 lbs, while the USAF and Torenbeek methods resulted in weights of approximately 100 lbs. The latter results were deemed to be reasonable, while the Cessna method was not used for the wing weight estimation. Table 7.4 shows the component weights as well as the methods used. The data shown in Table 7.4 are the result of several iterations. The values produced by the different methods were averaged to determine the final weight estimates.

Table 7.3: Weight and Balance Summary for the Meridian

Parameter	Inches	% mgc
Most Forward c.g.	94.86	0.18
Most Aft c.g.	99.89	0.34
Total Excursion	5.03	0.16
Fuel Excursion	2.76	0.09

Table 7.4: Class II Weight and Balance for the Meridian

	Method	Class II Weight lbs	X_{CG}	Y_{CG}	Z_{CG}
Structure					
Wing	USAF, Torenbeek	100.0	101.6	0.0	40.0
Empennage	Cessna, USAF	22.5	224.0	0.0	50.0
Fuselage	Cessna, USAF	59.3	121.2	0.0	50.0
Landing Gear					
Main Gear	Cessna	51.5	96.0	0.0	38.0
Tail Wheel	Cessna	9.0	220.0	0.0	48.0
Main Gear - Retracted	Cessna	51.5	101.0	0.0	42.0
Tail Wheel - Retracted	Cessna	9.0	225.0	0.0	48.0
Propulsion					
Propeller	Torenbeek/GD	34.8	50	0	50
Engine	Manufacturer	188.0	64.0	-0.8	48.0
Fuel System	USAF, Torenbeek	31.7	102.0	0.0	40.0
Engine Systems	Torenbeek/GD	43.6	70.0	0.0	0.0
Fixed Equipment					
Flight Control System	Cessna, Torenbeek	22.4	120.0	0.0	50.0
Avionics/Electronics	Class I/Manufacturer	11.2	120.0	0.0	50.0
Electrical System	Cessna, Torenbeek	24.4	118.0	0.0	50.0
Icing System	USAF, Torenbeek	15.6	120.0	0.0	50.0
Paint	Torenbeek	3.6	120.0	0.0	50.0
Fuel and Payload					
Mission Fuel		239.9	107.0	0.0	50.0
Fuel Reserves		54.0	107.0	0.0	50.0
Trapped Fuel and Oil		5.4	107.0	0.0	50.0
Payload					
Radar System		105.0	104.0	0.0	50.0
Antenna 1		6.0	104.0	-120.0	50.0
Antenna 2		6.0	104.0	-100.0	50.0
Antenna 3		6.0	104.0	-80.0	50.0
Antenna 4		6.0	104.0	-60.0	50.0
Antenna 5		6.0	104.0	-20.0	50.0
Antenna 6		6.0	104.0	20.0	50.0
Antenna 7		6.0	104.0	60.0	50.0
Antenna 8		6.0	104.0	80.0	50.0
Antenna 9		6.0	104.0	100.0	50.0
Antenna 10		6.0	104.0	120.0	50.0
Totals					
Structure - Gear Extended		242	121.0	0.0	43.2
Structure - Gear Retracted		242	122.2	0.0	44.1
Powerplant		298	67.3	-0.5	40.4
Fixed Equipment		77	119.4	0.0	50.0
Empty Weight		618	94.9	-0.1	42.3
Useful Load		464	105.9	0.0	50.0
Total - Gear Extended		1082	97.9	-0.1	44.6
Total - Gear Retracted		1082	98.1	-0.1	44.7

The c.g. locations of each component are shown in Figure 7.3. The c.g. travel due to fuel and payload loading is shown in Table 7.3 and Figure 7.2.

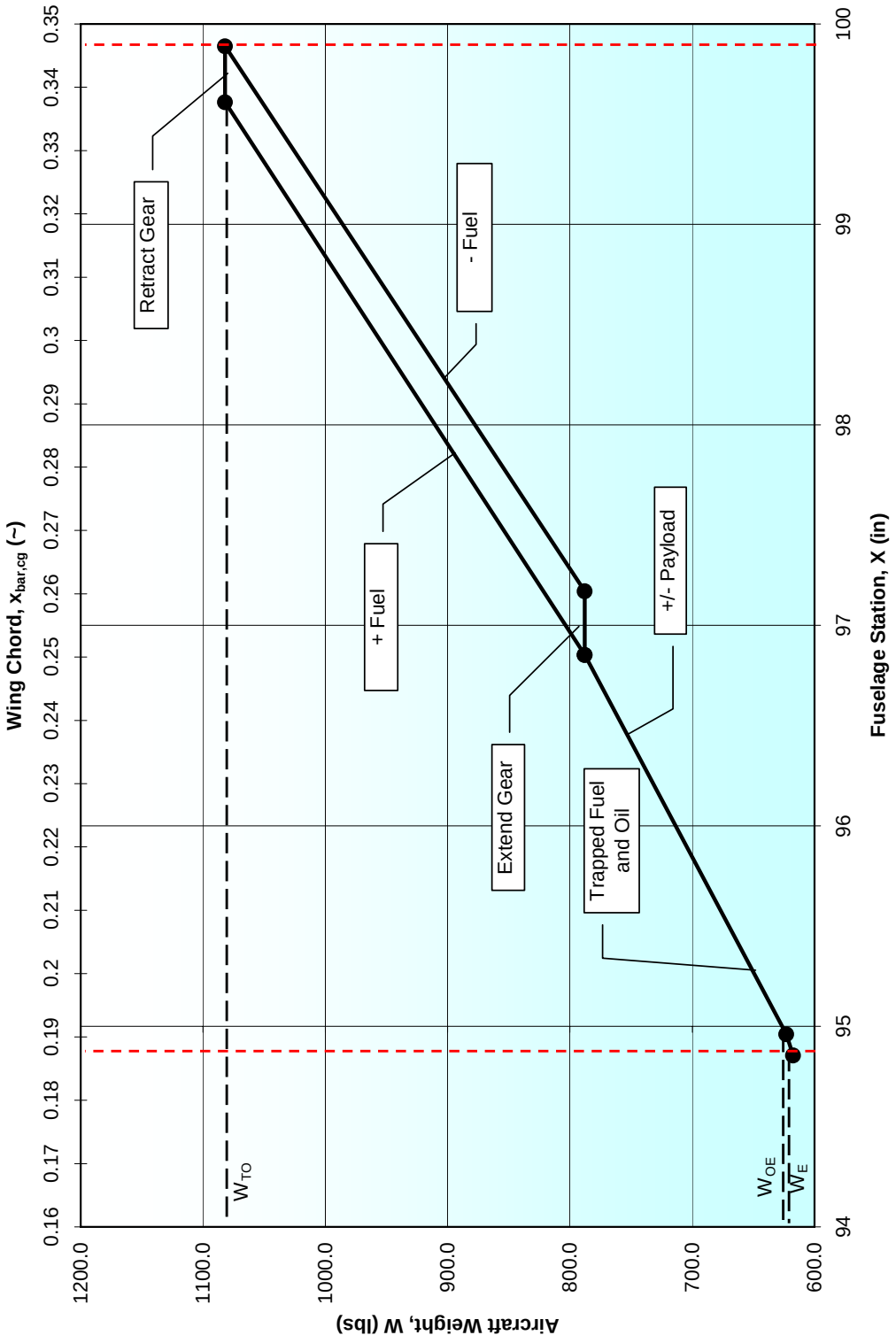

Figure 7.2: Center of Gravity Excursion for the Meridian

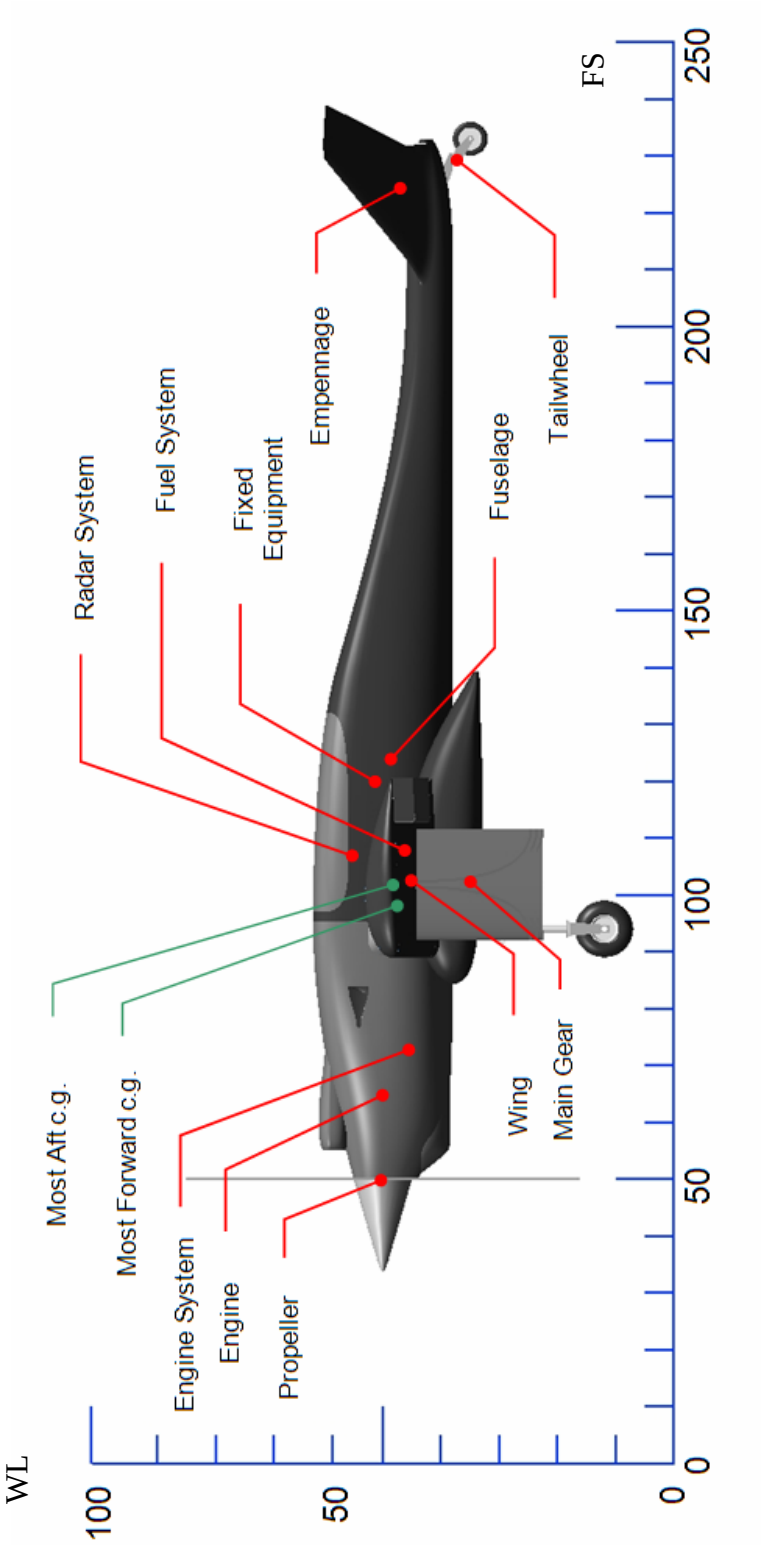

Figure 7.3: Component C.G. Locations

7.2.1 Moment of Inertia Estimates

The aircraft moments of inertia were estimated for the Meridian using the radii of gyration method from [2]. This method uses Equation 7.1 through Equation 7.3 to find the aircraft moments of inertia. The variable R represents an average value of the non-dimensional radius of gyration of aircraft with similar configurations. The aircraft used are shown in Table 7.5.

$$I_{xx_B} = \frac{b_w^2 W_{gross} \overline{R}_x^2}{4g} \qquad \text{Equation 7.1}$$

$$I_{yy_B} = \frac{L^2 W_{gross} \overline{R}_y^2}{4g} \qquad \text{Equation 7.2}$$

$$I_{zz_B} = \frac{\left(\frac{b_w + L}{2}\right)^2 W_{gross} \overline{R}_z^2}{4g} \qquad \text{Equation 7.3}$$

Table 7.5: Radius of Gyration of Similar Aircraft [19]

Aircraft	W_{gross} lbs	b_w ft	L ft	R_x ~	R_y ~	R_z ~	Engines
Beech N-35	3125	32.8	25.1	0.248	0.338	0.393	1 in fuselage
Cessna 150M	1127	33.5	21.5	0.254	0.405	0.418	1 in fuselage
Cessna 172M	1477	36.2	26.5	0.242	0.386	0.403	1 in fuselage
Cessna 177A	1761	35.6	27	0.212	0.362	0.394	1 in fuselage
Cessna R182	1885	36.2	28	0.342	0.397	0.393	1 in fuselage
Average:				**0.260**	**0.378**	**0.400**	

The resultant moments of inertia are:

- I_{xx} = 394 slug-ft^2
- I_{yy} = 307 slug-ft^2
- I_{zz} = 604 slug-ft^2

The values of Ixx and Izz are augmented by the inclusion of the wing mounted antennas according to Equations 7.4 and 7.5.

$$I_{xx_{w/Ant.}} = I_{xx_{w/o\,Ant}} + \sum m_{Ant} y_{Ant}^2 \qquad \text{Equation 7.4}$$

$$I_{zz_{w/Ant.}} = I_{zz_{w/o\,Ant}} + \sum m_{Ant} y_{Ant}^2 \qquad \text{Equation 7.5}$$

The weight of each antenna is estimated at 6 lbs (0.19 slugs). The antennas are located at buttock lines 20", 60", 80", 100", and 120". The moments of inertia with antennas are:

- I_{xx} = 440 slug-ft^2
- I_{yy} = 307 slug-ft^2
- I_{zz} = 650 slug-ft^2

7.3 Class II Stability and Control

The purpose of this section is to describe the Class II stability and control analyses performed for the Meridian UAV. These include:

- Trim Diagram (Power on and power off)
- Roll Performance
- Open Loop Dynamic Handling
- Actuator Size and Rate Requirements

7.3.1 Control Surface Geometry

The finalized control surface geometries for the flaps, ailerons, and ruddervators are shown in Figure 7.4 and Figure 7.5.

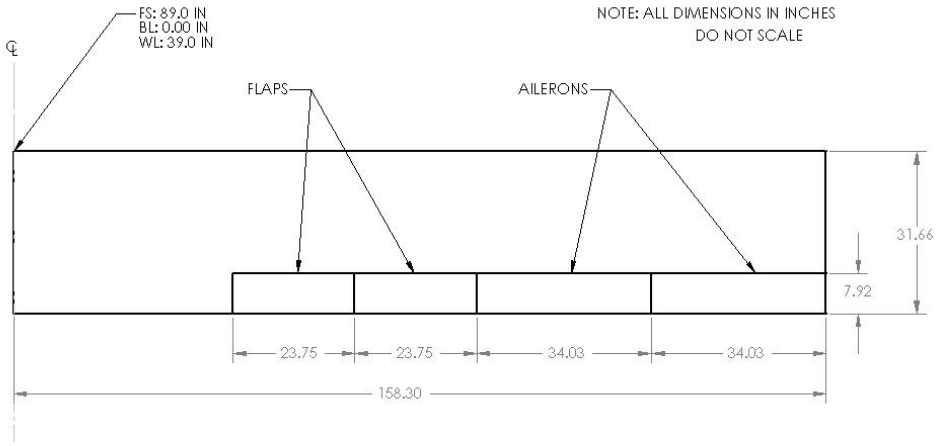

Figure 7.4: Meridian Wing Geometry (Top View)

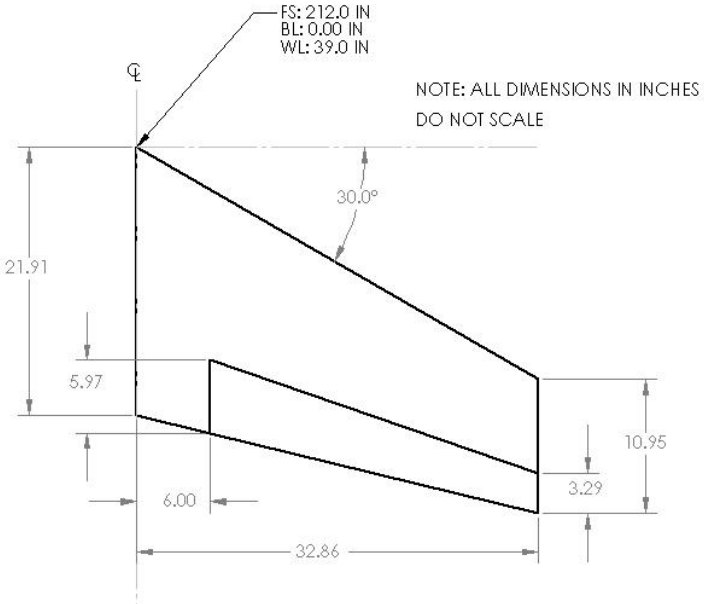

Figure 7.5: Meridian V-Tail Geometry (Top View)

7.3.2 Trim Diagrams

Trim diagrams were created for the flight conditions listed in Table 7.6. The trim diagram for the cruise condition is shown in Figure 7.6. The trim diagrams were created using the AAA software [2]. Only the cruise condition is shown for brevity. The V-tail incidence was adjusted to i_{vee} = -3.5 deg so that the aircraft could be

trimmed at the stall speed with the most forward center of gravity. This was the result of several iterations of the trim calculations.

Table 7.6: Meridian Flight Conditions

Flight Condition	Altitude ft	Speed kts	Weight lbs	Flaps deg	Gear ~
Clean	5,000	120	963	0	Up
Takeoff Gear Down	0	60	1,082	0	Down
Takeoff Gear Up	0	60	1,082	0	Up
Landing Heavy, Gear Down	0	65	1,082	30	Down
Landing Heavy, Gear Up	0	65	1,082	30	Up
Landing Light, Gear Down	0	65	843	30	Down
Landing Light, Gear Up	0	65	843	30	Up
OEI	5,000	80	963	0	Up

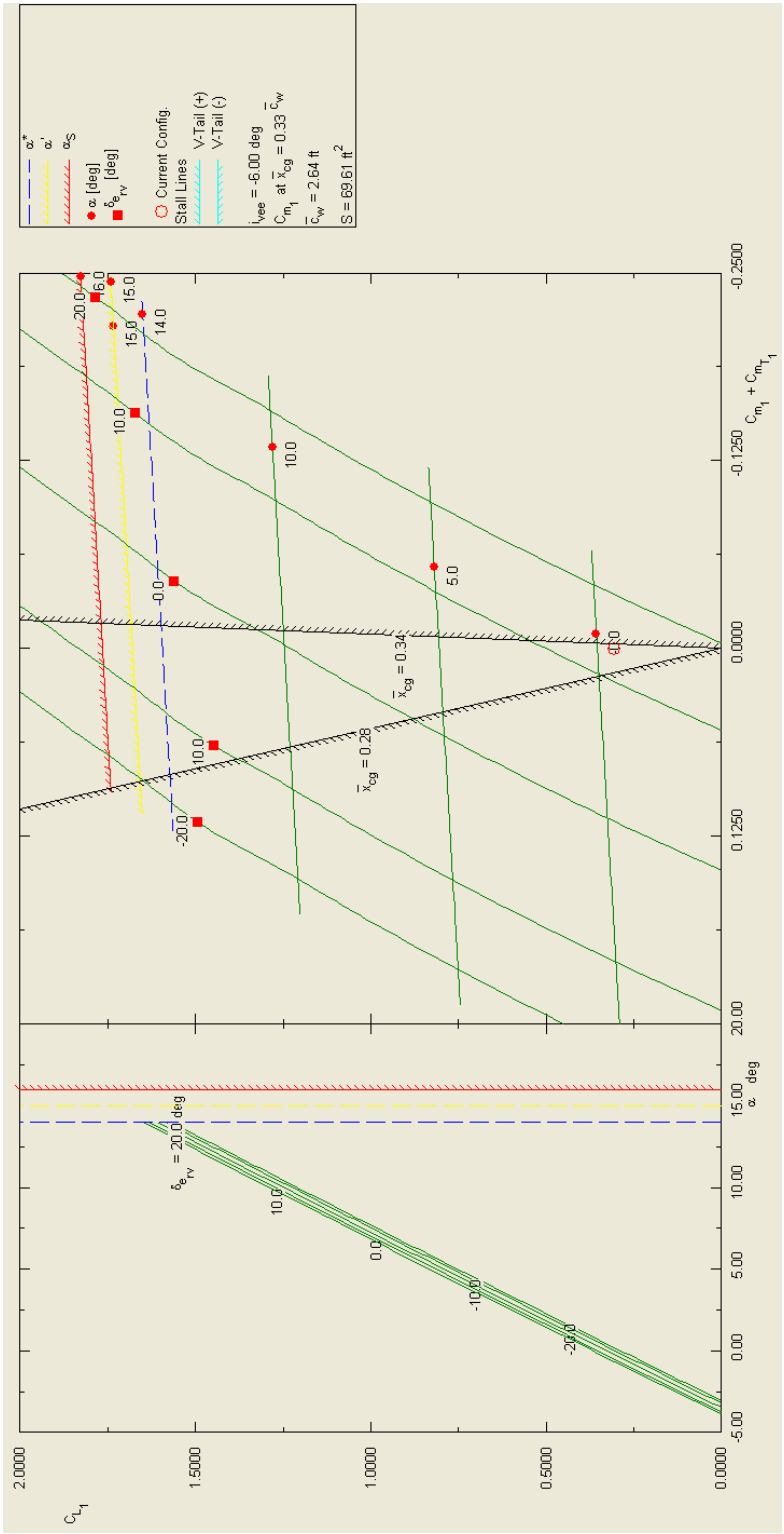

Figure 7.6: Trim Diagram - Cruise

The trim diagram shown in Figure 7.6 shows that the aircraft can be trimmed throughout the entire flight envelope requiring no more than 20 degrees of control surface deflection.

7.3.3 Open Loop Dynamics

The open loop dynamics were calculated for the Meridian using the AAA program [2]. The longitudinal and lateral-directional dynamics and flying qualities were calculated for the takeoff, cruise, and approach flight conditions as specified in Table 7.7. These were compared to the flying quality requirements specified in MIL-F-8785C [2] and MIL-STD-1797A [2] for a Class I aircraft. While it is not necessary for a UAV to meet the military specifications, it is common design practice to use the military flying quality requirements as a basis for the dynamic analysis.

Table 7.7: Dynamic Analysis Flight Conditions

Parameter	Units	Flight Condition		
		Takeoff	Cruise	Approach
Altitude	ft	0.00	5000.00	0.00
ΔT	deg F	0.00	-40.00	0.00
U_1	kts	60.00	120.00	65.00
W	lbs	1083.4	962.9	843.2
α	deg	13.28	0.63	6.82
C_{L1}	~	1.15	0.30	0.84
n	g	1.00	1.00	1.00
δ_F	deg	0.00	0.00	40.00
X_{cg}	in	99.97	99.21	98.25
Z_{cg}	in	45.66	45.12	44.42
ε_{vee}	deg	0.96	0.41	1.28
$\eta_{vee,\ p.\ off}$	~	1.00	1.00	1.00
η_{vee}	~	1.96	1.15	1.00

Table 7.8: Stability Derivatives for the Meridian

Parameter	Units	Flight Condition		
		Takeoff	Cruise	Approach
C_{Tx}	~	0.54	0.08	0.05
C_{MT}	~	-0.072	-0.011	-0.007
C_{Du}	~	0	0	0
C_{Lu}	~	0.010	0.012	0.008
C_{Mu}	~	0.002	0.003	0.002
C_{TXu}	~	-1.61	-0.23	-0.135027
C_{MTu}	~	0.22	0.03	0.0237792
$C_{D\alpha}$	rad^{-1}	0.39	0.10	0.29
$C_{L\alpha}$	rad^{-1}	4.01	4.06	4.01
$C_{M\alpha}$	rad^{-1}	-0.42	-0.52	-0.64
$C_{MT\alpha}$	rad^{-1}	-0.46	-0.31	-0.07
$C_{D\alpha}$	rad^{-1}	0	0	0
$C_{L\alpha,dot}$	rad^{-1}	0.53	0.55	0.54
$C_{M\alpha}$	rad^{-1}	-2.09	-2.17	-2.16
C_{Dq}	rad^{-1}	0	0	0
C_{Lq}	rad^{-1}	3.58	3.82	4.03
C_{Mq}	rad^{-1}	-9.63	-9.85	-9.94
$C_{Y\beta}$	rad^{-1}	-0.42	-0.42	-0.42
$C_{l\beta}$	rad^{-1}	-0.13	-0.09	-0.12
$C_{n\beta}$	rad^{-1}	0.11	0.11	0.11
$C_{nT\beta}$	rad^{-1}	-0.001	-0.001	-0.001
$C_{Y\beta}$	rad^{-1}	0.0125	0.0003	0.0107
$C_{l\beta dot}$	rad^{-1}	-0.0005	0.0000	0.0000
$C_{n\beta}$	rad^{-1}	0.0051	0.0001	0.0044
C_{YP}	rad^{-1}	-0.06	-0.12	-0.09
C_{lP}	rad^{-1}	-0.46	-0.46	-0.46
C_{nP}	rad^{-1}	-0.16	-0.04	-0.10
C_{Yr}	rad^{-1}	0.27	0.27	0.27
C_{lr}	rad^{-1}	0.31	0.10	0.20
C_{nr}	rad^{-1}	-0.13	-0.11	-0.12
C_{Divee}	rad^{-1}	0.01	0.01	0.01
C_{Livee}	rad^{-1}	0.30	0.30	0.30
C_{mivee}	rad^{-1}	-1.17	-1.19	-1.19

The stability and control derivatives for Meridian are shown in Table 7.8 and Table 7.9, respectively. These values represent the result of several iterations of control surface sizing.

Table 7.9: Control Derivatives for the Meridian

Parameter	Units	Flight Condition		
		Takeoff	Cruise	Approach
$C_{D\delta rv}$	rad^{-1}	0.003	0.004	0.006
$C_{L\delta rv0}$	rad^{-1}	0.14	0.14	0.14
$C_{L\delta rv}$	rad^{-1}	0.05	0.14	0.14
$C_{M\delta rv0}$	rad^{-1}	-0.56	-0.56	-0.56
$C_{M\delta rv}$	rad^{-1}	-0.18	-0.56	-0.56
$C_{h\beta rv}$	rad^{-1}	-0.03	-0.07	-0.03
$C_{h\delta rv}$	rad^{-1}	-0.28	-0.35	-0.29
$C_{Y\delta a}$	rad^{-1}	0	0	0
$C_{l\delta a}$	rad^{-1}	0.12	0.13	0.12
$C_{n\delta a}$	rad^{-1}	-0.03	-0.01	-0.02
$C_{h\alpha a}$	rad^{-1}	0.21	0.18	0.21
$C_{h\delta a}$	rad^{-1}	0.04	-0.03	0.03
C_{L0}	~	0.26	0.26	0.26
C_{L0}	~	0.26	0.26	0.39
C_{M0}	~	0.002	-0.003	-0.021
C_{m0wf}	~	-0.05	-0.05	-0.08

The stability and control derivatives shown in Table 7.8 and Table 7.9 were used to calculate the open loop transfer functions for the Meridian. This was done with the AAA software [2]. The transfer functions for the Cruise condition are shown in Table 7.10 through Table 7.12. The dynamic stability parameters related to the aircraft flying qualities are shown in Table 7.13. The Meridian met Level I flying quality requirements for all flight conditions.

Table 7.10: Longitudinal Transfer Functions for Cruise

Longitudinal
$\frac{u(S)}{\delta_{rv}(S)} = \frac{-38.0191\ (S - 20.2157)(S + 22.6302)(S + 5.5353)}{202.9655\ (S^2 + 4.0510\ S + 19.6006)(S^2 + 0.0476\ S + 0.0587)}$ $K_{gain} = 412.618905$
$\frac{\alpha(S)}{\delta_{rv}(S)} = \frac{-6.9804\ (S + 229.0171)(S^2 + 0.0522\ S + 0.0519)}{202.9655\ (S^2 + 4.0510\ S + 19.6006)(S^2 + 0.0476\ S + 0.0587)}$ $K_{gain} = -0.355340$
$\frac{\theta(S)}{\delta_{rv}(S)} = \frac{-1605.4055\ (S + 1.8161)(S + 0.0751)}{202.9655\ (S^2 + 4.0510\ S + 19.6006)(S^2 + 0.0476\ S + 0.0587)}$ $K_{gain} = -0.938342$

Table 7.11: Lateral Transfer Functions for Cruise

Lateral
$\frac{\beta(S)}{\delta_a(S)} = \frac{178.6824\ S(S + 18.6567)(S + 0.1615)}{202.5290\ S(S - 0.0021)(S + 6.4155)(S^2 + 0.8757\ S + 11.6128)}$ $K_{gain} = -16.697350$
$\frac{\phi(S)}{\delta_a(S)} = \frac{4398.0604\ S(S^2 + 0.9386\ S + 9.5883)}{202.5290\ S(S - 0.0021)(S + 6.4155)(S^2 + 0.8757\ S + 11.6128)}$ $K_{gain} = -1307.596036$
$\frac{\psi(S)}{\delta_a(S)} = \frac{-195.2256\ (S - 1.3932)(S + 13.5544)(S + 1.8043)}{202.5290\ S(S - 0.0021)(S + 6.4155)(S^2 + 0.8757\ S + 11.6128)}$ $K_{gain} = -206.262151$

Table 7.12: Directional Transfer Functions for Cruise

Directional

$$\frac{\beta(S)}{\delta_{rv}(S)} = \frac{67.2362\ \ S(S - 0.0296)(S + 136.6612)(S + 6.5583)}{202.5290\ \ S(S - 0.0021)(S + 6.4155)(S^2 + 0.8757\ S + 11.6128)}$$

$K_{gain} = 55.355101$

$$\frac{\psi(S)}{\delta_{rv}(S)} = \frac{4089.8354\ \ S(S - 7.2192)(S + 4.3370)}{202.5290\ \ S(S - 0.0021)(S + 6.4155)(S^2 + 0.8757\ S + 11.6128)}$$

$K_{gain} = 3970.613462$

$$\frac{\Psi(S)}{\delta_{rv}(S)} = \frac{-9224.4949\ \ (S + 6.4930)(S^2 + 0.0271\ S + 0.3370)}{202.5290\ \ S(S - 0.0021)(S + 6.4155)(S^2 + 0.8757\ S + 11.6128)}$$

$K_{gain} = 625.878993$

Table 7.13: Meridian Dynamic Stability Parameters

Parameter	Units	Flight Condition		
		Takeoff	Cruise	Approach
Longitudinal				
ω_{sp}	rad/s	2.9	4.63	2.31
ζ_{sp}	~	0.57	0.45	0.59
ω_p	rad/s	0.34	0.25	0.2
ζ_p	~	0.23	0.1	0.09
n/α	g/rad	3.2	12.1	5.8
CAP	1/gsec^2	2.63	1.77	0.92
Lateral-Directional				
TC_{Spiral}	sec	-25.6	106.5	-650.7
TC_{roll}	sec	0.3	0.16	0.27
ω_D	rad/s	2.2	2.9	2.1
ζ_D	~	0.12	0.1	0.09
Note: Level I flying qualities met for all flight conditions.				

Roll Control Effectiveness

The roll control effectiveness is a vital parameter for aircraft controllability, especially during approach and landing. The roll control requirements for a Class I

aircraft are specified in Table 7.14. The requirement states that the aircraft must be able to achieve the specified bank angle in the specified amount of time.

Table 7.14: Roll Control Requirements - Time to Achieve Bank Angle (Seconds)

Level	Cat A ϕ_t = 60 deg	Cat B ϕ_t = 60 deg	Cat C ϕ_t = 30 deg
I	1.3	1.7	1.3
II	1.7	2.5	1.8
III	2.6	3.4	2.6

The roll control analysis results are shown in Table 7.15. These values were calculated using AAA [2]. As can be seen, the Meridian meets Level I flying qualities for all flight conditions.

Table 7.15: Roll Control Results

	Takeoff	Cruise	Approach
Cat.	C	B	C
ϕ_t	30	60	30
t_r	1.25	1.1	1.2

7.3.4 Actuator Sizing

The actuators were sized using the control surface hingemoments calculated with the AAA program. The actuators were then sized for a factor of safety of 2.0 at maximum deflection. The most critical actuator size was determined to be the flaps, which required a servo with a maximum torque of at least 100 in-lbs. Two candidate servos were selected. The Model 820 servo manufactured by Moog Components Group (www.polysci.com) has a peak torque of 150 in-lbs and accepts a PWM signal, which is compatible with the selected autopilot. The second servo option is the K2000 servo produced by Kearfott Guidance and Navigation Corporation (www.kearfott.com).

7.4 Class II Aerodynamics

The Class II aerodynamics analysis consists of performing a spanwise lift distribution and a detailed drag analysis.

7.4.1 Spanwise Lift Distribution

The spanwise lift distribution for the Meridian was created using the AAA software as well as using the Shrenk's approximation from [47] as shown in Figure 7.7. The use of a wing taper ratio of 1.0 results in no need for geometric wing twist. The lift distribution is for an angle of attack of 3 degrees.

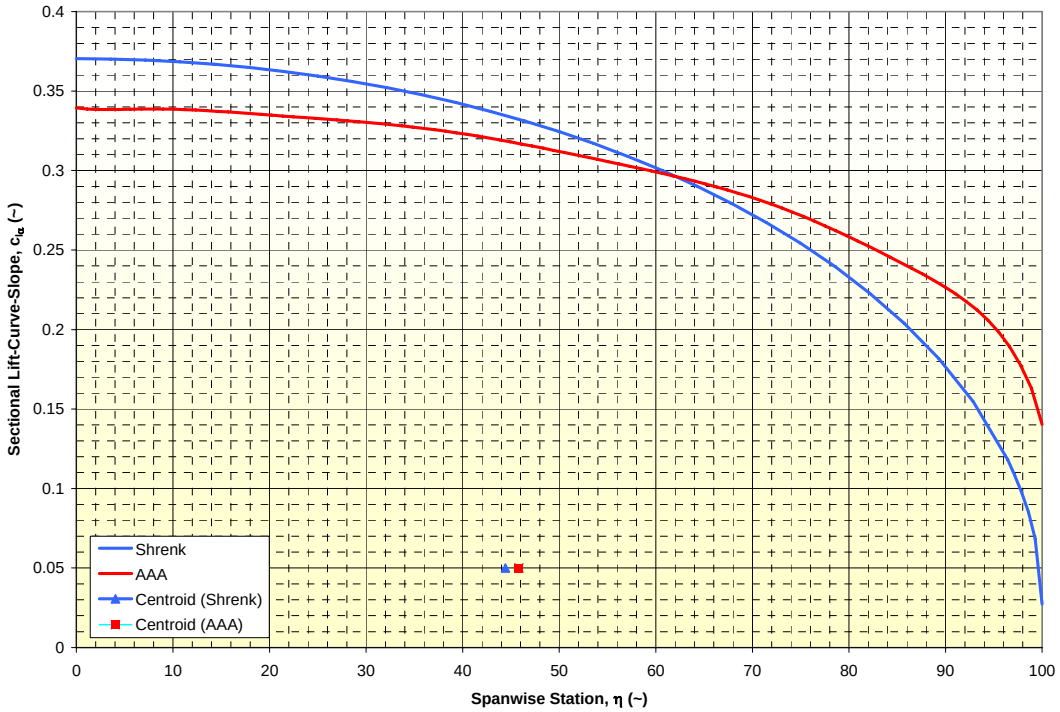

Figure 7.7: Spanwise Lift Distribution for the Meridian

7.4.2 Class II Drag

The Class II drag analysis was performed for the Meridian with the AAA software [2]. The geometries used in the drag calculations are shown in Table 7.16 through

Table 7.19. The drag analysis was performed for the takeoff, cruise, approach, and OEI flight conditions with and without antennas. These flight conditions are described in Table 7.6.

Table 7.16: Wing Geometry for Drag Calculations

Parameter	Units	Value
S	ft^2	69.6
AR	~	10
λ	~	1
$\Lambda_{c/4}$	deg	0
$(t/c)_r$	%	18
$(t/c)_t$	%	18
LER/c	%	1.1
L'	~	1.2
x_{lam}/c	%	25
Cl_α	rad^{-1}	6.1
f_{gap}	~	0.97
k_{sand}	$10^{-3}ft$	0.00167

Table 7.17: V-Tail Geometry for Drag Calculations

Parameter	Units	Value
S	ft^2	6.1
AR	~	4
λ	~	0.5
$\Lambda_{c/4}$	deg	26.3
$(t/c)_r$	%	12
$(t/c)_t$	%	12
LER/c	%	1.58
L'	~	2
x_{lam}/c	%	20
Cl_α	rad^{-1}	6.25
f_{gap}	~	0.96
k_{sand}	$10^{-3}ft$	0.00167

Table 7.18: Fuselage Geometry for Drag Calculations

Parameter	Units	Value
S_b	ft^2	0.01
S_{wet}	ft^2	75.1
L	ft	14.8
$S_{frontal}$	ft^2	3
x_{lam}/L	%	0
$S_{wet-lam}$	ft^2	0
S_{plf}	ft^2	23.9
$D_{f\ max}$	ft	24
k_{sand}	10^{-5}ft	0.00167

Table 7.19: Flap and Landing Gear Geometry for Landing Gear Calculations

Parameter	Units	Value
Flaps		
Flap Type	~	Plain
$\eta_{i\ f}$	%	27
$\eta_{o\ f}$	%	57
c_f/c_w	%	25
Main Gear		
S_{ft}	ft^2	0.25
L_{strut}	ft	2.5
Tailwheel		
C_{Dref}	~	0.5
S_{ref}	ft^2	0.02
F_D	~	0

Table 7.20: Drag Analysis Results

Component	Takeoff	Cruise	Approach	P. Off
Zero-Lift Drag Coefficient				
Wing	0.0124	0.0096	0.0122	0.0117
Vee Tail	0.0021	0.0018	0.0021	0.002
Fuselage	0.0018	0.0034	0.0018	0.0041
Flap	0	0	0.0188	0
Retract	0.0108	0	0.0108	0
Fixed Gear	0.0001	0.0001	0.0001	0.0001
Trim	0.0018	0.0005	0.0015	0.0004
Propeller	0	0	0	0.0267
Inlet	0.0001	0.0001	0.0001	0.0001
Nozzle	0.0015	0.0015	0.0021	0.0015
Power	0.0064	0.0004	0.0013	0
Gear Pod	0.0014	0.0012	0.0014	0.0013
Total Zero-Lift	**0.0384**	**0.0186**	**0.0522**	**0.0479**
Drag Coefficient Due to Lift				
Wing	0.0548	0.0034	0.0254	0.0142
Vee Tail	0.0009	0	0	0
Fuselage	0.0051	0	0.0006	0
Total Due to Lift	**0.0608**	**0.0034**	**0.026**	**0.0142**
Total, C_D (No Ant.)	**0.0992**	**0.022**	**0.0782**	**0.0621**

The drag results are shown in Table 7.20. The drag analysis results were used to create drag polar trend lines based on Equation 7.6. The values of the parameters in Equation 7.6 are shown in Table 7.21. These are shown in Figure 7.8 through Figure 7.11. The mid-cruise lift-to-drag ratio for the aircraft with no antennas was found to be 13.9 as indicated on Figure 7.9. This is higher than the value estimated in the Class I design. This is due to the higher aspect ratio and removal of excessive conservatism used in the Class I design.

$$C_D = C_{D_0} + B_{C_{D_1}} C_L + B_{C_{D2}} C_L^2 + B_{C_{D_3}} C_L^3 + B_{C_{D_4}} C_L^4 + B_{C_{D_5}} C_L^5 \qquad \text{Equation 7.6}$$

Table 7.21: Drag Polar Summary

Component	Takeoff	Cruise	Approach	P. Off
C_{D0}	0.0384	0.0186	0.0522	0.0479
B_1	0	0.0006	0	0.0002
B_2	0.03	0.033	0.0343	0.0329
B_3	0.0026	0.0028	0.0003	0.0026
B_4	0.0027	0.001	0.002	0.0011
B_5	-0.0007	-0.0002	0.0004	-0.0002

The antenna drag coefficient per antenna was determined using Equation 7.7 for pylon drag from [2]. The inputs and result of the pylon drag calculations are shown in Table 7.22. Note that laminar flow is assumed for the first 25 percent of the pylons. Also, note that the drag coefficient shown in Table 7.22 is for one antenna.

$$C_{D_{0_{py}}} = R_{w,py} R_{l.s.} \left[1 + L_w^{'} \left(\frac{t}{c} \right) + 100 \left(\frac{t}{c} \right)^4 \right] \left[\frac{\left(C_{f_{PY_{lam}}} - C_{f_{PY_{turb}}} \right) \bar{x}_{lam} S_{wet_{py}} + C_{f_{PY_{turb}}} S_{wet_{py}}}{S_w} \right] \qquad \text{Equation 7.7}$$

Table 7.22: Pylon Drag Coefficient Summary

Parameter	Units	Value
$R_{w,py}$	~	1.2
$R_{l.s.}$	~	1
S_{py}	ft^2	2.78
$S_{wet,py}$	ft^2	5.7
λ	~	1
$\Lambda_{c/4}$	deg	0
$(t/c)_r$	~	0.2
$(t/c)_t$	~	0.2
Arpy	~	1
L'	~	1.2
x_{lam}/c	~	0.25
$C_{f,lam}$	~	0.002
$C_{f,turb}$	~	0.0055
k_{sand}	10^{-3}ft	0.00167
$C_{D0,py}$	~	0.000636

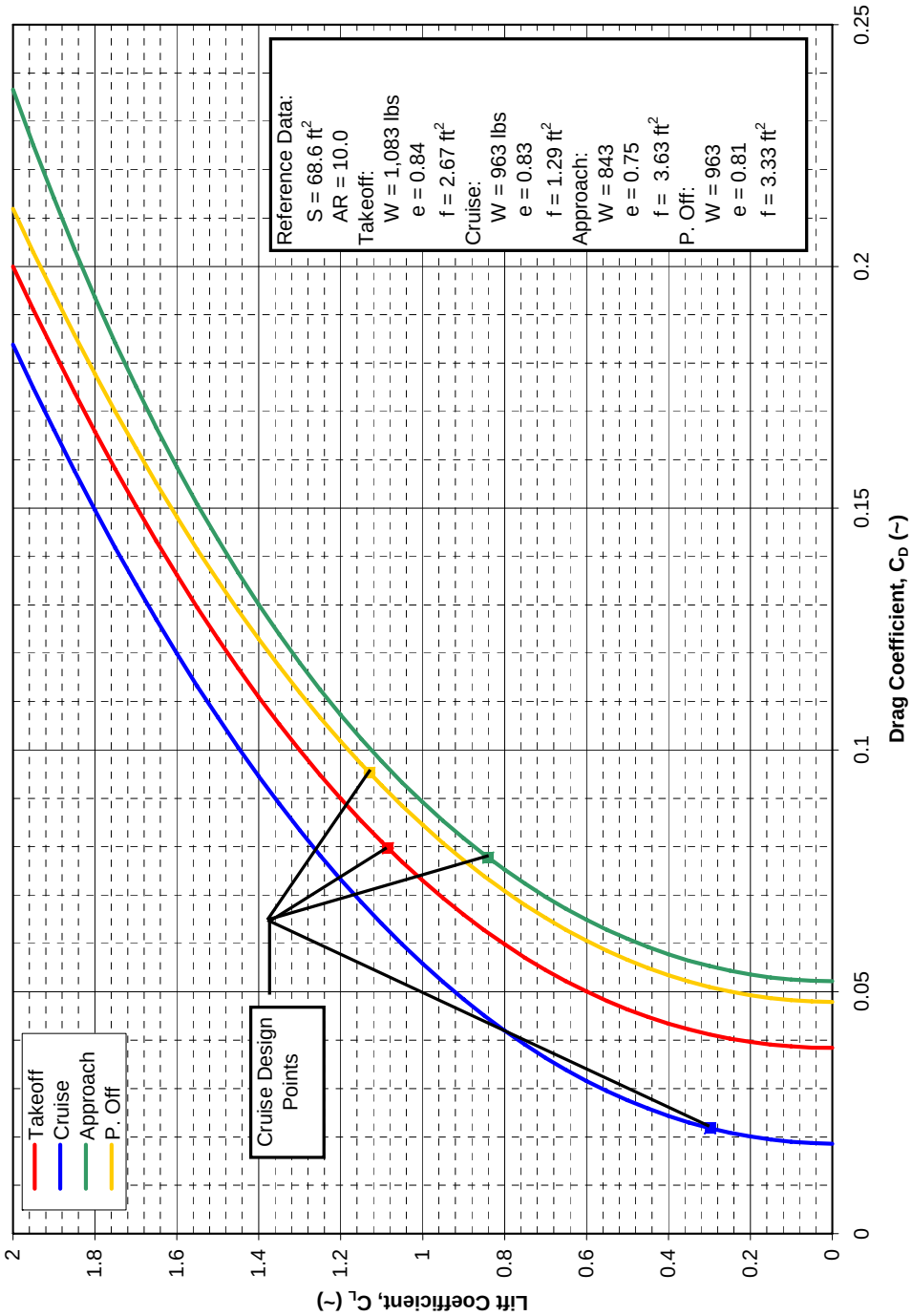

Figure 7.8: Drag Polars for the Meridian without Antennas

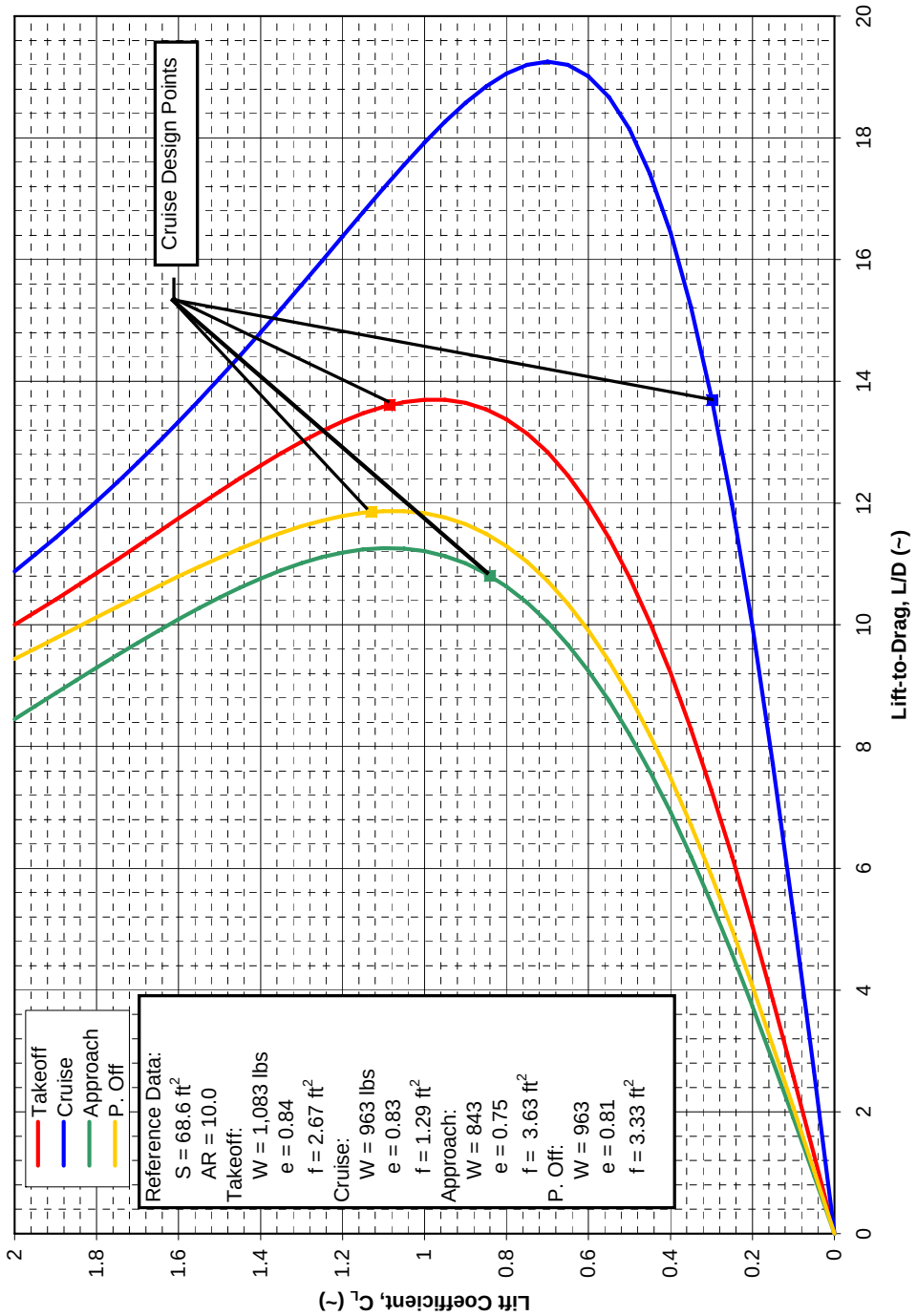

Figure 7.9: Lift-to-Drag for the Meridian without Antennas

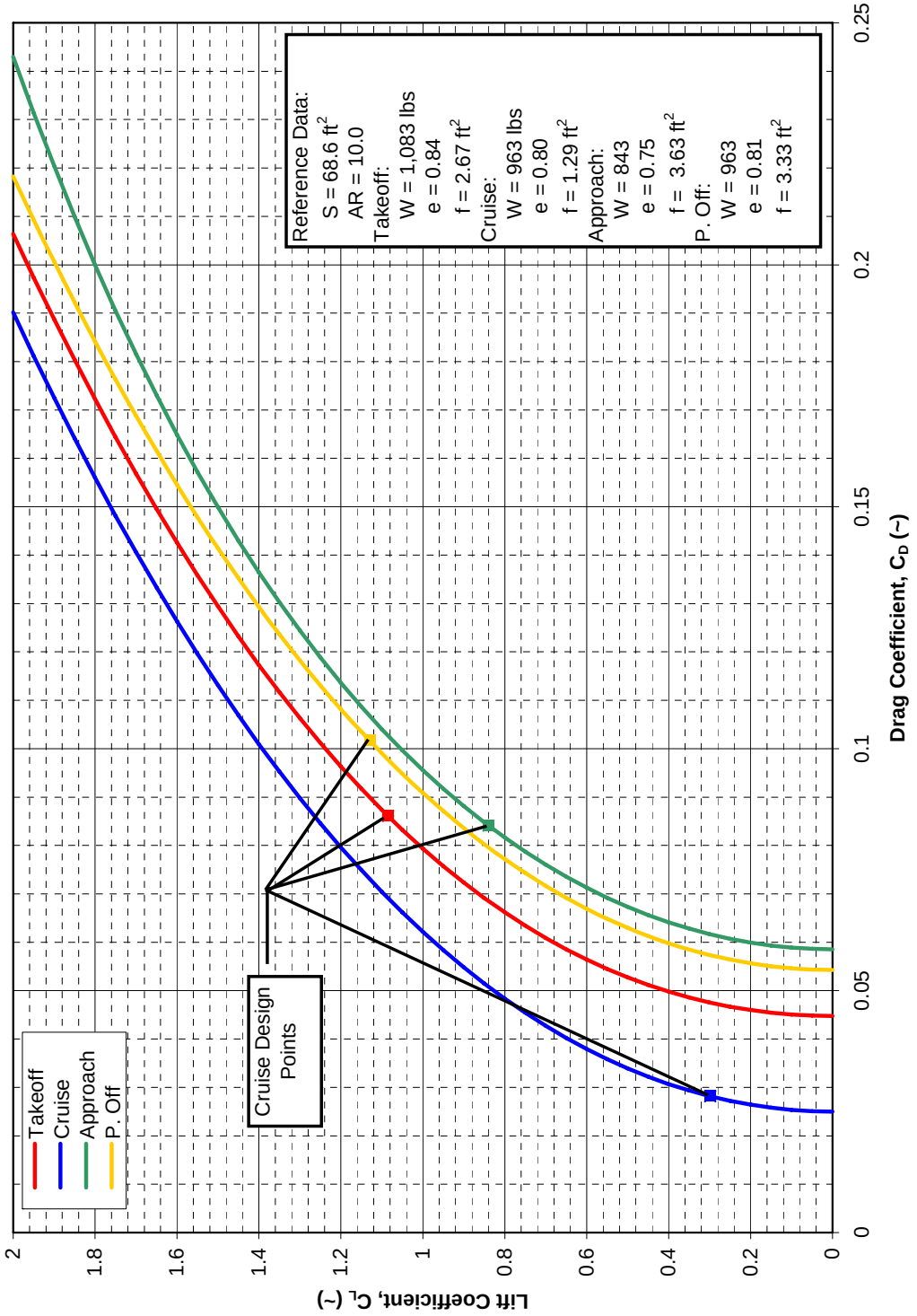

Figure 7.10: Drag Polars for the Meridian with 10 Antennas

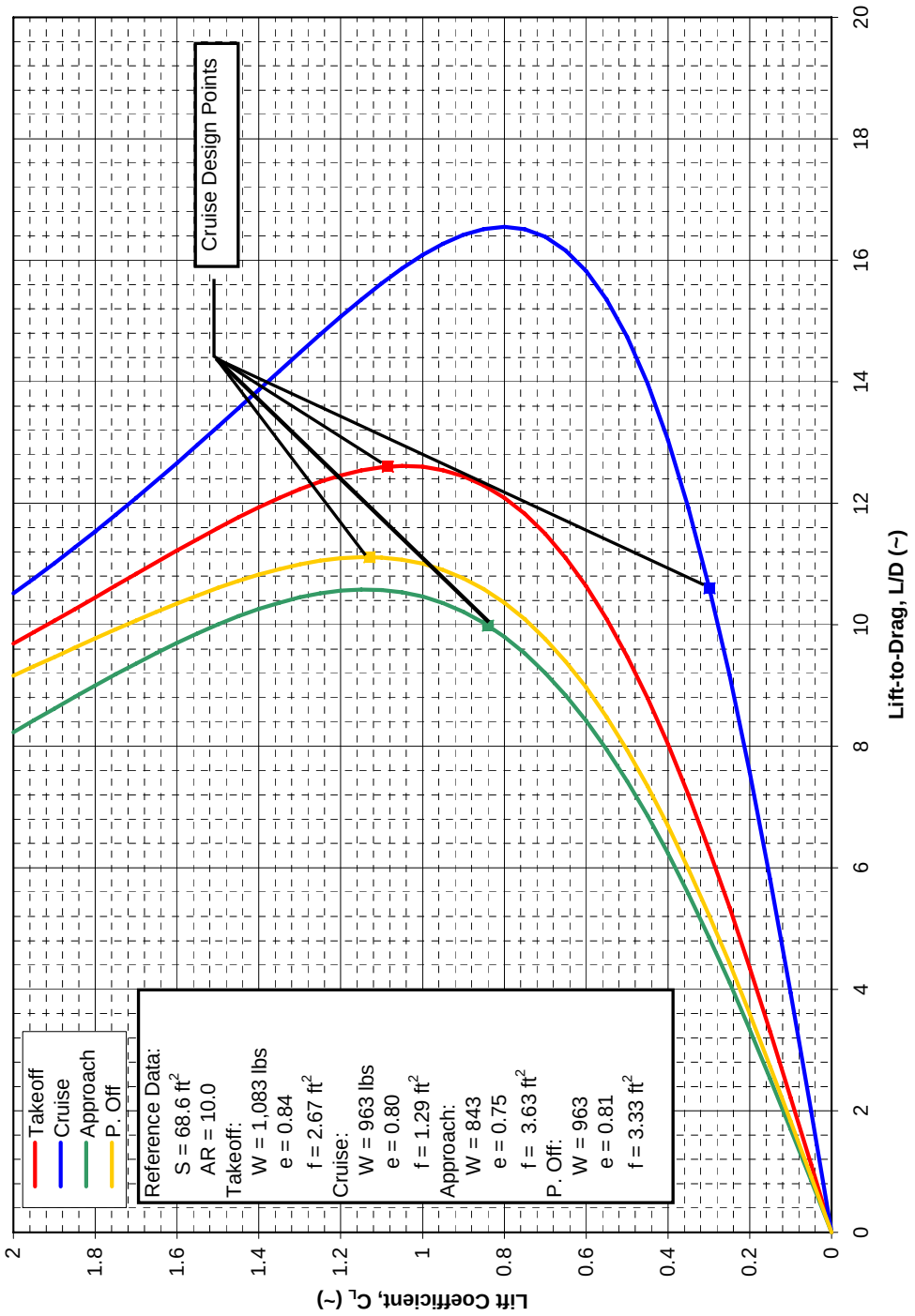

Figure 7.11: Lift-to-Drag for the Meridian with 10 Antennas

To verify the validity of the drag analysis the Oswald's efficiency and parasite area were calculated for each flight condition using Equation 7.8 and Equation 7.9 respectively. These values are shown on the drag polar plots in Figure 7.8 through Figure 7.11 and Table 7.23. The cruise values of the parasite area with and without the antennas were plotted against known aircraft in Figure 7.12 from [2] for further verification. As can be seen, Meridian falls somewhere between the lines for overall skin friction coefficient values of C_f = 0.005 to 0.006 depending on whether the antennas are installed or not. This is a good indication that the Class II drag results are reasonable.

$$e = \frac{1}{\delta C_D \Big/ \delta C_L^2 \pi A}$$ Equation 7.8

$$f = C_{D_0} S_w$$ Equation 7.9

Table 7.23: Resultant Oswald's Efficiency and Parasite Area for the Meridian

		No Antennas S_{wet} = 240 ft^2	10 Antennas S_{wet} = 297 ft^2
Flight Condition	**e ~**	**f ft^2**	**f ft^2**
Takeoff	0.84	2.67	3.12
Cruise	0.80	1.29	1.74
Approach	0.75	3.63	4.08
OEI	0.81	3.33	3.78

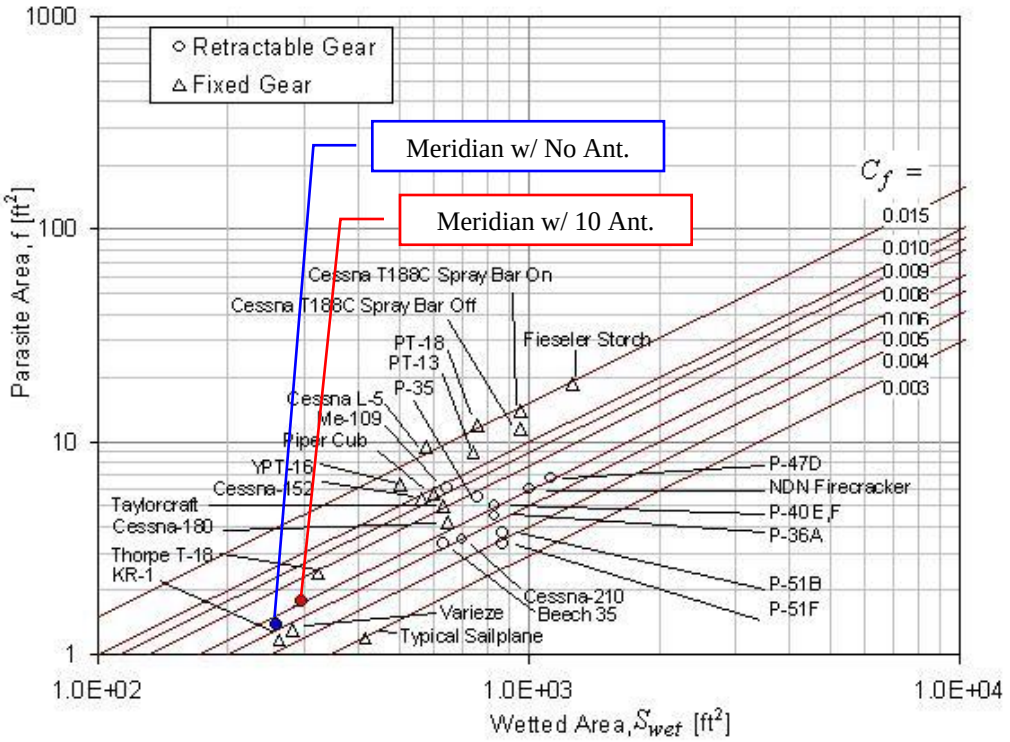

Figure 7.12: Relationship of Parasite Area and Wetted Area for Various Single Engine Aircraft [2]

7.5 Propulsion

The installed thrust of the Innodyn engine was calculated using the AAA program. The Innodyn is rated at 165 SHP. The extracted power is estimated at 5 hp based on the electrical power generation required. The total installed power was calculated to be 125 hp, which is above what is required for takeoff and climb performance.

The AAA program was also used to calculate an estimate for the inlet area. This resulted in an inlet with an area of 0.2 ft^2.

7.6 Performance Analysis

The purpose of this section is to describe the performance requirements imposed on this aircraft design and to verify that these requirements have been met by the Meridian. This includes:

- Stall speed
- Takeoff Distance
- Cruise Performance
- Landing Distance

7.6.1 Stall Speed

The stall speed of the Meridian was calculated for heavy and light flight conditions with zero and full flaps as shown in Table 7.24. The maximum trimmed lift coefficients determined in Section 7.3.2 were used for the clean and full flap configurations. Power effects were ignored for the stall speed calculations.

Table 7.24: Stall Speed Summary

		Clean		Full Flaps	
Parameter	**Units**	**Light**	**Heavy**	**Light**	**Heavy**
Weight	lbs	843	1,082	843	1,082
Flaps	deg	0	0	30	30
C_{Lmax}	~	1.42	1.42	1.70	1.70
Altitude	ft	0	0	0	0
V_s	**kts**	**50**	**57**	**46**	**52**

7.6.2 Takeoff Distance

The takeoff distance for the Meridian was calculated for conventional tires as well as ski operations using the AAA program. This process uses methods found in [2] to

calculate the takeoff distance to clear an obstacle of a specified height. The following assumptions were used in the takeoff distance calculations:

- Ground Friction Coefficient ($\mu_G = 0.02$ for Tires, $\mu_G = 0.15$ for skis)
- The obstacle height is 50 ft
- Weight = 1,082 lbs
- Standard sea level conditions
- Drag is based on Class II drag analysis for Takeoff condition:
  - $C_{D0} = 0.041$
- $V_3/V_{TO} = 1.3$ (Based on FAR 23)

The takeoff analysis resulted in the following takeoff distances:

- Standard Tires on Asphalt: $S_{TO} = 415$ ft
- Skis on Snow: $S_{TO} = 635$ ft

The takeoff distances with and without skis both exceed the required distance of 1,500 ft by a large amount. This is due to the fact that the selected engine has more power than required by performance matching.

7.6.3 Cruise Performance

The cruise performance calculations for the Meridian were performed with the AAA program. This consisted of estimating the range and endurance assuming constant speed cruise.

7.6.3.1 Range

The range of the Meridian was calculated using the constant speed range equation found in [2]. The lift-to-drag value was calculated using the mid-cruise Class II drag polar (Section 7.4). The following assumptions were used for the range calculation:

- W_{begin} = 1,050 lbs
- W_{fuel} = 220 lbs, $W_{fuel, res}$ = 40 lbs
- η_p = 0.80
- c_p = 0.90 lbs/hp-hr

The range of the Meridian was determined to be:

- Without Antennas
  - 950 nm (1,760 km) without reserves
  - 1,150 nm (2,130 km) with fuel reserves
- With 10 Antennas
  - 730 nm (1,350 km) without fuel reserves
  - 886 nm (1,640 km) with fuel reserves

The range for the Meridian without antennas is above the required range of 945nm (1,750 km). The effect the antennas have on the vehicle range is shown in Figure 7.13.

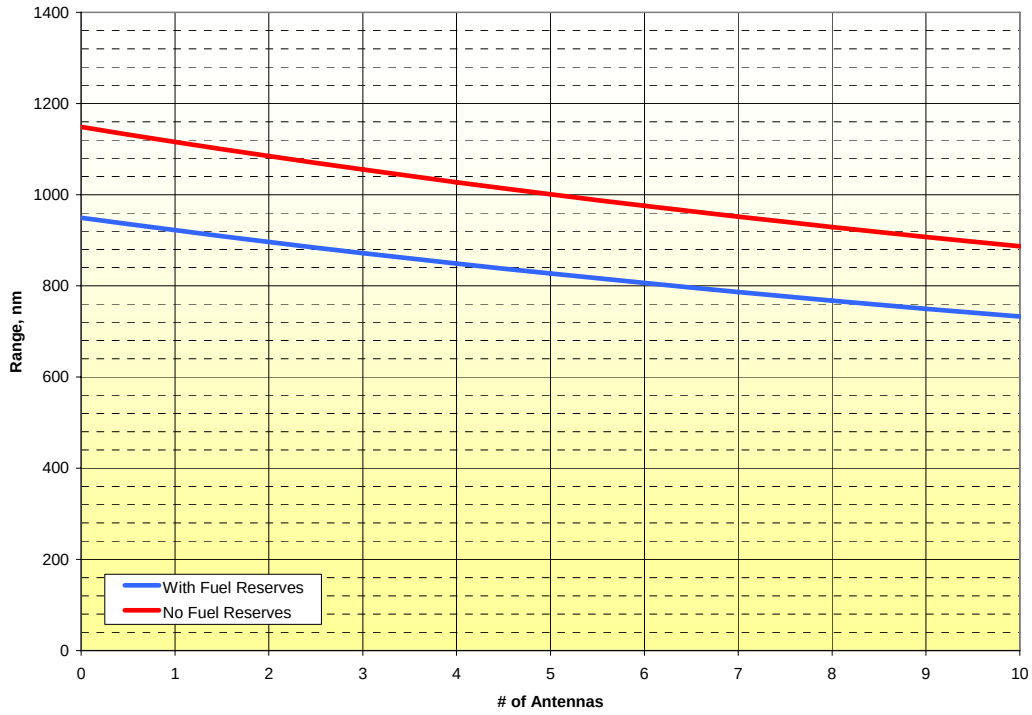

Figure 7.13: Effect of Antennas on Meridian Range

7.6.3.2 Endurance

The endurance of the Meridian was calculated using Equation 7.10. The following assumptions were made for the endurance calculation:

- Constant speed cruise
- W_{begin} = 1,050 lbs
- W_{fuel} = 220 lbs, $W_{fuel,\ res}$ = 40 lbs
- η_p = 0.80
- c_p = 1.2 lbs/hp-hr (From manufacturer data)
- U_1 = 80 kts
- Drag based on mid cruise Class II drag polar

$$E = 60\,\text{min/sec}\left(\frac{550\text{ft-lbs/hp-s}}{1.688\text{fps/kts}}\right)\left[\frac{\eta_p}{c_p U_1}\left(\frac{L}{D}\right)\ln\left(\frac{W_{begin}}{W_{begin}-W_{fuel}}\right)\right] \qquad \text{Equation 7.10}$$

The loiter speed was set at 80 kts as this is the speed for maximum L/D. The results from the endurance calculations are:

- Without Antennas
  - 12.4 hours without reserves
  - 15.0 hours with fuel reserves
- With 10 Antennas
  - 11.5 hours without fuel reserves
  - 14.8 hours with fuel reserves

The Meridian exceeds the specified endurance requirements with and without the antennas and fuel reserves. The effect of the antennas is shown in Figure 7.14.

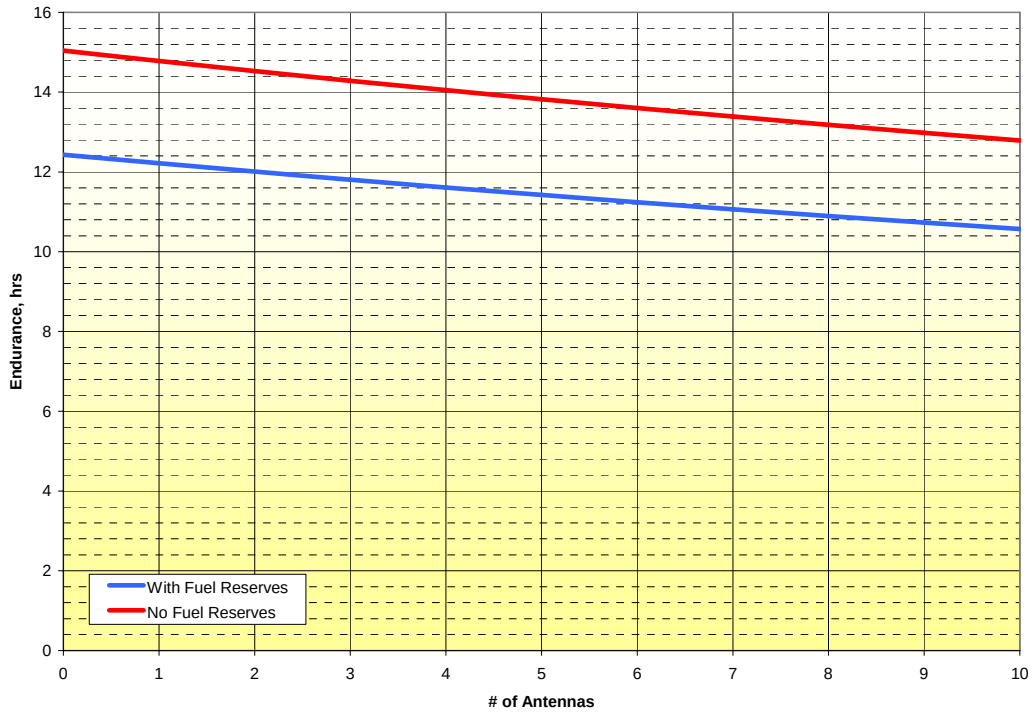

Figure 7.14: Effect of Antennas on Meridian Endurance

7.6.4 Landing Distance

The landing distance for the Meridian was calculated with the AAA program. The landing distance includes the distance from a 50 ft obstacle to the ground and the distance from touchdown to a full stop. The following assumptions were used for the landing gear calculation:

- Weight = 1,082 lbs
- C_{Lmax} = 1.7 (Based on maximum trimmed lift coefficient)
- Drag based on Class II drag polar for the Approach flight condition
- Average ground deceleration = 0.25 g
- Δn = 0.10 (Correction factor due to pilot technique)

The results of the landing distance calculation are:

- S_{air} = 754 ft (Distance in air from obstacle to ground)
- S_{LG} = 747 ft (Ground run distance)
- S_L = 1,501 ft (Total distance)

The total landing distance is acceptably close to the required landing distance of 1,500 ft. This distance depends heavily on the average deceleration during the landing ground run, which was assumed to be 0.25g. This value is conservative for small aircraft with brakes on asphalt, and should be reasonable for skis on snow.

7.7 Systems

The purpose of this section is to describe the systems both on and off the Meridian that are required for operation. These include:

- Payload System
- Flight Controls
- Electrical System
- Communications
- Fuel
- Anti-Icing

7.7.1 Payload System

The Meridian is designed to carry a primary system consisting of a Synthetic Aperture Radar (SAR) system with wing mounted antennas. In addition, the vehicle is designed to carry a variety of secondary payloads such as laser altimeters,

magnetometer, and gravity meters. The dimensions and weights of these systems are currently unknown.

The payload arrangement shown in Figure 7.15 includes a volume for the primary SAR system as well as a location for some secondary payload that would require a Nadir port.

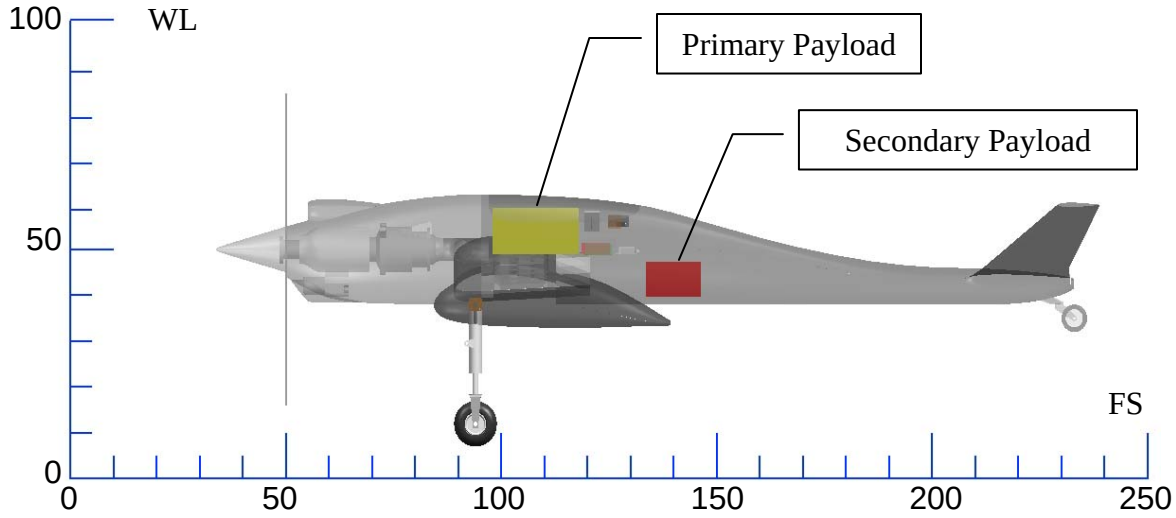

Figure 7.15: Payload System Integration (Not to Scale)

The payload system is under development and will be completely separate from the other systems on board the aircraft other than the power connection.

7.7.2 Flight Control System

The Meridian will utilize a fly-by-wire control system based around the Piccolo autopilot, which is produced by Cloud Cap Technologies [48]. The Piccolo requires dynamic and static pressure inputs and electrical power. The Piccolo interfaces with the servo actuators using a Pulse Width Modulated (PWM) signal, which is standard for remote control aircraft. The architecture for the Piccolo is shown in Figure 7.17.

Figure 7.16: Cloud Cap Tech. Piccolo II Autopilot [48]

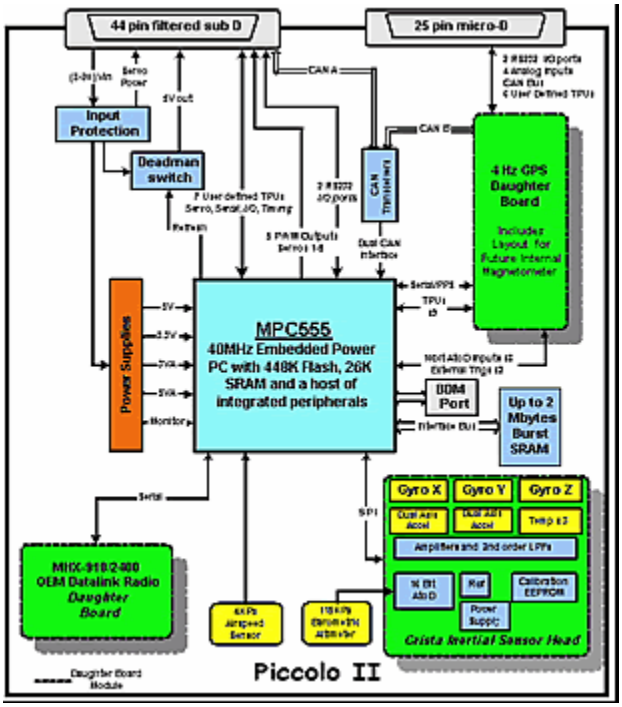

Figure 7.17: Piccolo II Architecture [48]

The ground equipment associated with the Piccolo autopilot consists of a ground station, operator interface (PC), and a pilot control unit (Futaba Controller) as shown in Figure 7.18.

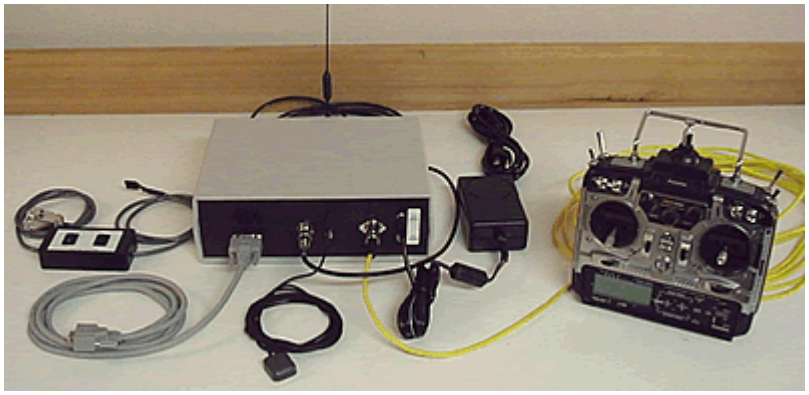

Figure 7.18: Piccolo Ground Station and Pilot Controller (Operator Interface Not Shown) [48]

7.7.3 Electrical System

The Meridian will require both 12 and 24VDC power busses. The power system consists of:

- Electrical Generator
- Battery
- Electrical Bus
- Electrical Wiring

The first step in developing the electrical system layout was to generate an electrical load profile for the Meridian. This was done by listing all necessary systems required during each phase of a given flight as shown in Table 7.25 for the takeoff flight phase.

The results of the load profile are shown in Figure 7.19. The total load was estimated assuming the radar system is turned on at takeoff, while the essential load assumes the radar system only requires power during the on-station flight phase. The most critical flight phases are the takeoff and landing segments as the landing gear

and flap actuators will be operated in addition to the other systems. The emergency flight phase is representative of an engine flame-out situation. The battery was sized such that all necessary systems could remain operating will the aircraft descends and attempts tot restart the engine. This however, will require the ability to turn some systems off autonomously.

The current configuration of the Innodyn engine is with one 600W, 12 V generator and a starter. The current generator is a standard off-the-shelf automotive alternator, and can be replaced with a larger generator for the Meridian. The electrical load profile indicates that a 1,000 W generator would be sufficient.

The electrical system layout is shown in Figure 7.20. The wiring is not shown in Figure 7.20 for clarity. The aileron and flap servo and landing gear actuator wiring will be located just aft of the aft spar. The antenna wiring will be located just behind the forward spar. A more detailed view of the systems located in the fuselage is shown in Figure 7.21.

Table 7.25: Electrical Power Requirements for Takeoff

Item	Power W
Engine	3.5
Fuel Pumps	4.5
Fuel Flow Meters	5.5
Line-of-Site Communications	7.5
Telemetry	5
Air Data Probe	5
Onboard Processer	5
Systems Communications	5
Transponder	6.875
Autopilot	18
Control Surface Actuators (6)	72
Throttle Servo (1)	12
Nose Gear Servo (1)	12
Fuselage Environmental Control	15
Anti/De-Icing System	240
SAR	300
Landing Gear Actuators	200
Flap Actuators	48
Total	**965**

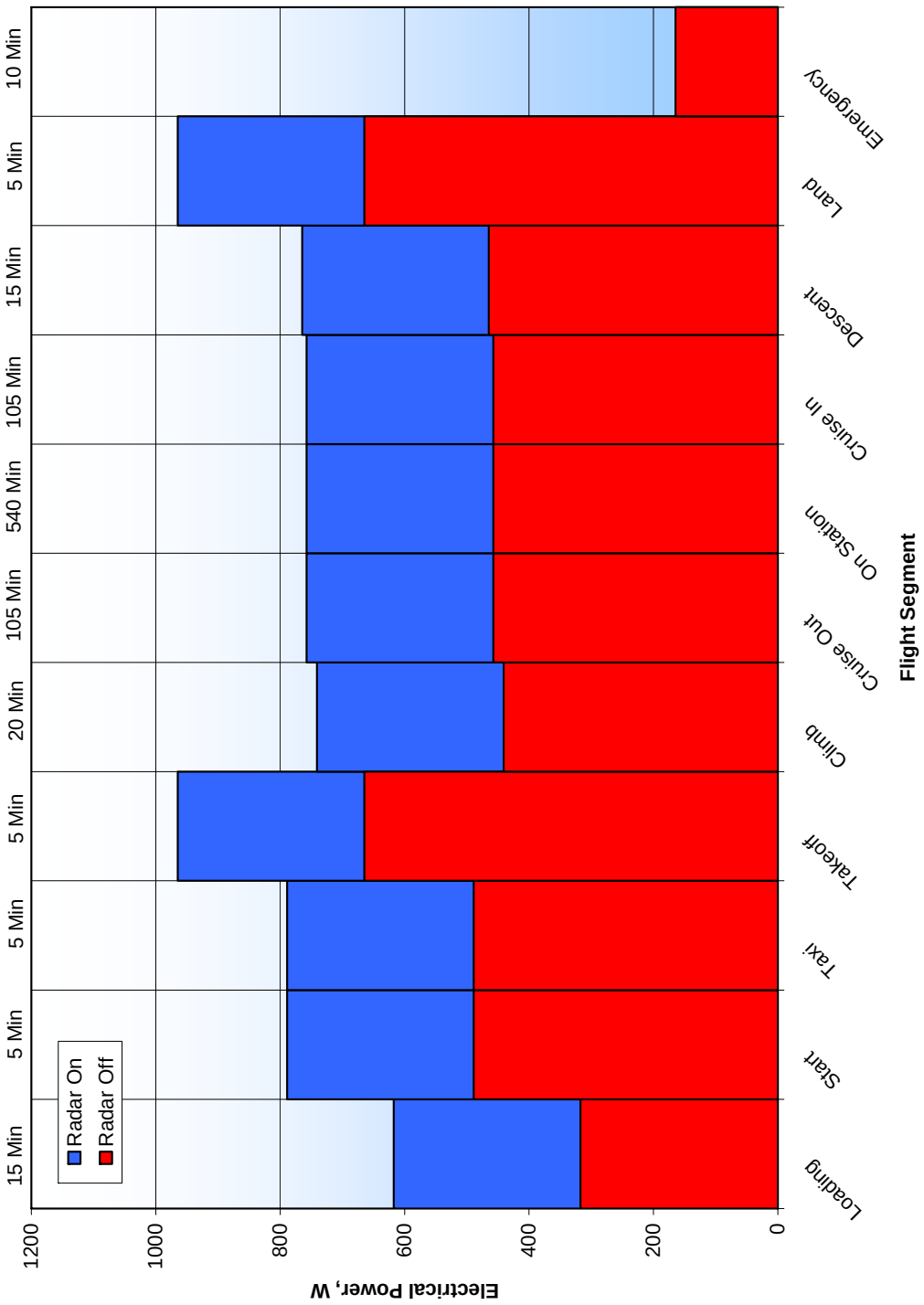

Figure 7.19: Electrical Load Profile for the Meridian UAV

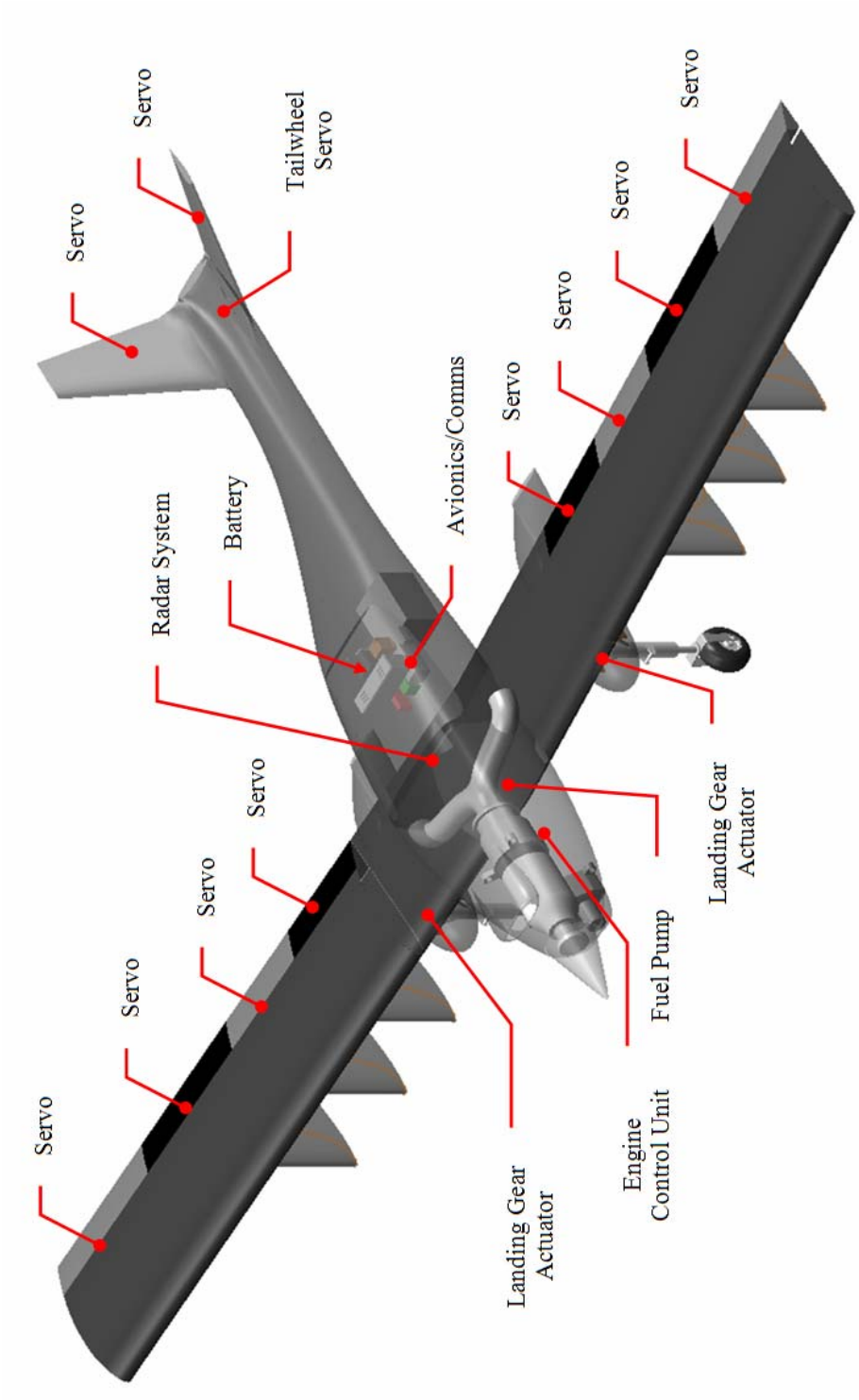

Figure 7.20: Electrical System Layout

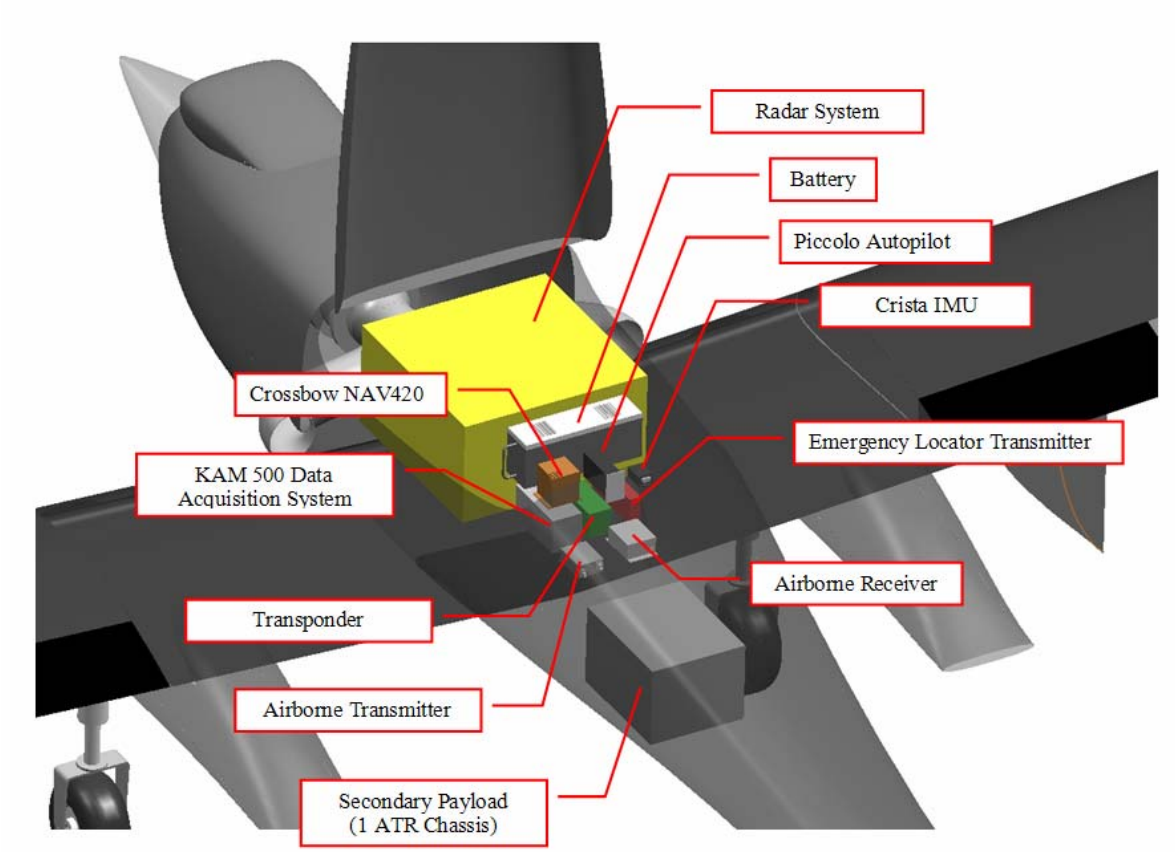

Figure 7.21: Fuselage Systems Layout

7.7.4 Communications/Telemetry System

The Meridian will utilize dual line-of-site communication links: the piccolo communications will be used for command and control and a secondary communications link will be used for vehicle health monitoring/telemetry. For beyond line-of-site (BLOS) communications, an Iridium satellite communication link will be utilized. The Piccolo autopilot is configured to transmit and receive data over an Iridium link. This communications link will be used for low-bandwidth health monitoring and limited control.

7.7.5 Fuel System

The fuel tank integration was difficult for the Meridian due to the removable wing design. Several options were investigated including a hinged wing joint such that the wing pivots rearward but is not removed. This would theoretically allow for fuel to be placed in the outboard wing section, but this type of fuel system would have an extremely high probability of leaking. Another option is to use quick fuel line connectors at the wing split. Again, this type of integration poses serious leaking problems. The design was iterated such that the fuel could be stored inboard of the wing split. This involved increasing the wing thickness to an 18 percent thick airfoil and adding a tank in the fuselage. The latter decision required the fuselage height to grow.

The required fuel volume is 43.7 gallons or 5.84 ft^3. Approximately 45 gallons of fuel fits in the fuel tanks in the inboard wing and fuselage sections as shown in Figure 7.22. Fuel bladders will be utilized for the wing and fuselage tanks. These bladders are commercially available and include all of the pickups, lines, and baffling as required. The fuel tank will be split into 3 separate bladders in the wing (1 center, and two outboard of the inboard rib), and 1 bladder in the fuselage. The center wing bladder will serve as the fuel collection point.

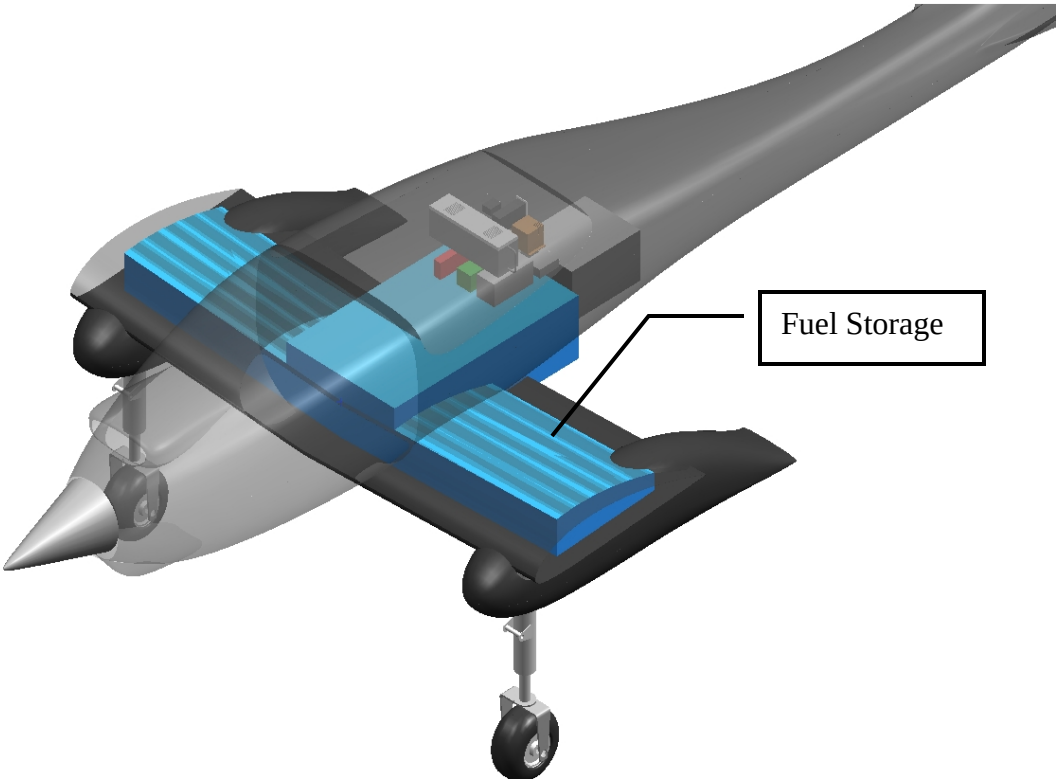

Figure 7.22: Fuel Tank Integration

7.7.6 Anti-Icing System

A combination of muffed engine exhaust and electrically heated elements will be utilized for the anti-icing system. The location of the wing is such that the leading edge of the wing is forward of the firewall. Similar engine installations have been performed (www.innodyn.com) utilizing NACA inlets to pressurize the engine cowl volume. This air will be pushed through a valve into the leading edge of the wing. The temperature of the muffed exhaust air has been measured at 180^{o}F. Much attention should be given to the thermal effects on material properties and stress states in the detail design and analysis phases.

7.8 Class II Landing Gear

This section discusses the design of landing gear in terms of the general arrangement as well as calculations of stroke length, tire diameter, and strut diameter.

7.8.1 Landing Gear Arrangment

The landing gear must be retractable so as not to interfere with the radar. More importantly, the landing gear must be retractable with skis or conventional wheels as the Meridian will be operated from snow and paved runways. The Red, White, and Blue designs all incorporated tricycle type landing gear that retracted on a tilted pivot into the fuselage. While this is feasible for conventional tires, this retraction scheme does not work with skis. The tricycle gear had several other design problems:

- The nose gear had to be mounted far enough from the propeller to leave room for the nose ski. This required a very wide gear to meet lateral tipover.
- The Meridian should be able to be shipped in a 20 foot container, which is approximately 90 inches wide. Lateral tipover requirements called for a wider gear than this, so the gear would have to be removed for shipping.
- There is no commercially available landing gear similar to the previous design.

All of these problems lead to the development of a new landing gear integration scheme. The gear disposition was changed to a tail dragger to solve the nose ski

integration and lateral tip-over problems. The man landing gear was then moved to pods mounted to the wing. This had two benefits:

- The landing gear could be purchased commercially
- The landing gear retract directly aft, which allows for ski retraction

Utilizing a wing-mounted landing gear has implications in terms of the antennas. However, the problems associated with the Vivaldi antennas are much less severe than with the bow-tie antennas used in the Class I designs.

The critical tipover parameters are shown in Figure 7.23. The aircraft meets all of the tipover requirements.

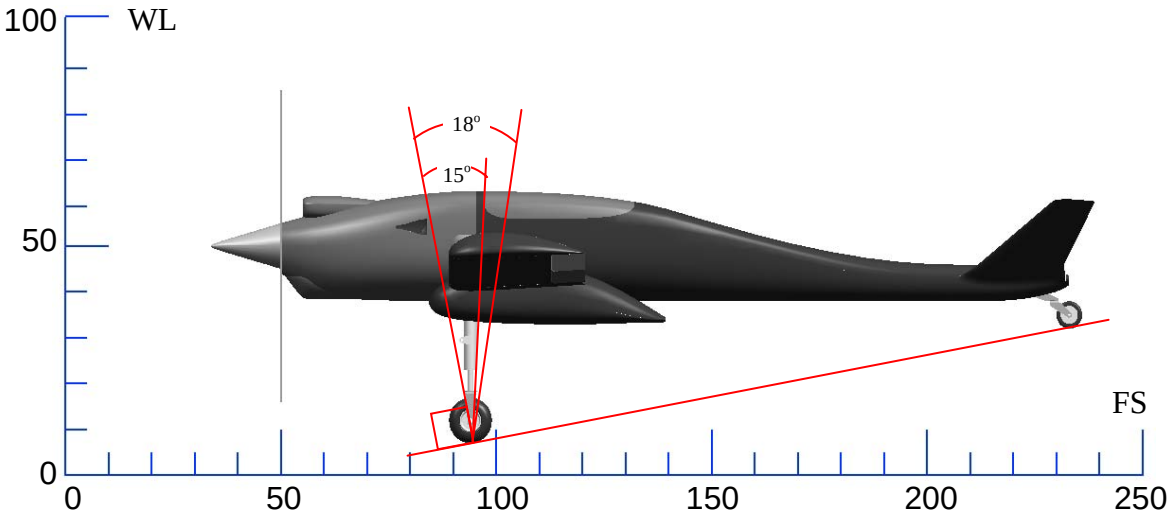

Figure 7.23: Landing Gear Longitudinal Tipover

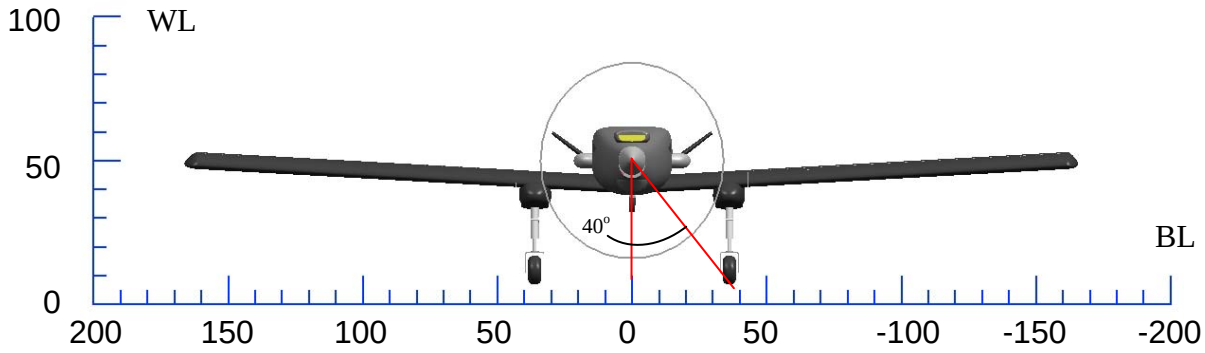

Figure 7.24: Lateral Tipover Plot

The decision to put the landing gear on the wing calls for the use of either an oleo, pneumatic, or rubber damped type strut. The oleo gear was chosen as this type of gear is commercially available.

The following assumptions were made for the landing gear design:

- The main gear shall be able to sustain 100% of the static load. (This is due to the tail dragger configuration.)
- The gear will be sized for a maximum touchdown rate of 10 ft/s.
- The stroke length will be sized such that a 10 ft/s decent rate imparts 1g on the airframe.
- The strut will have an energy absorption efficiency of 80%.
- The strut will be sized for skis, thereby setting the energy absorption due to tire deflection to zero.

7.8.2 Tire Selection

The main gear tires will be 3.00 x 4 tires. These tires have an outer diameter of 10.0 inches, a width of 3.2 inches, a maximum pressure of 50 psi, and weigh 3.5 lbs each.

The tail wheel tire will be a 6.0 inch diameter solid rubber tire, which weighs 4.75 lbs. The main and tail gears are commercially available parts currently used on homebuilt aircraft.

7.8.3 Strut Sizing

The strut stroke length and diameter sizing were performed using the methods described in [2]. The stroke length is calculated by determining the touchdown energy using Equation 7.11. The gear absorption energy equation is then used to determine the appropriate stroke length using Equation 7.12. The results are shown in Table 7.26.

$$E_T = \frac{1}{2} W_L \frac{w_t^2}{g}$$ Equation 7.11

$$S_s = \frac{\frac{E_T}{n_s P_m N_g} - \eta_t s_t}{\eta_s}$$ Equation 7.12

Where:

- S_s = Strut stroke length
- E_t = Touchdown energy
- n_s = Number of struts
- P_m = Max static load per gear
- N_g = Ratio of max load to static load
- η_t = Tire energy absorption efficiency
- s_t = Tire deflection

- η_s = Strut energy absorption efficiency

Table 7.26: Landing Gear Strut Sizing

Parameter	Units	Value
W_L	lbs	1082
w_t	fps	10
n_s	~	2
P_m	lbs	541
N_g	g	1
η_t	~	0
s_t	in	0
η_s	~	0.6
Diameter	in	0.1
Stroke	in	2.6

7.8.4 Landing Gear Integration

The landing gear placement, integration, and sizing were iterated such that a commercially available landing gear could be integrated with the Meridian. This greatly increases the feasibility of manufacturing the Meridian in the time allotted as landing gear development is a fairly complicated process. The landing gear strut produced for the Lancair Legacy homebuilt aircraft [49] will be used for the main gear (Figure 7.25 and Figure 7.26).

Figure 7.25: Lancair Legacy Landing Gear Strut [49]

Figure 7.26: Lancair Legacy Landing Gear Installation [50]

The tail wheel will also be purchased commercially. The tail wheel assembly is manufactured by Matco [51] and is commonly used on homebuilt aircraft.

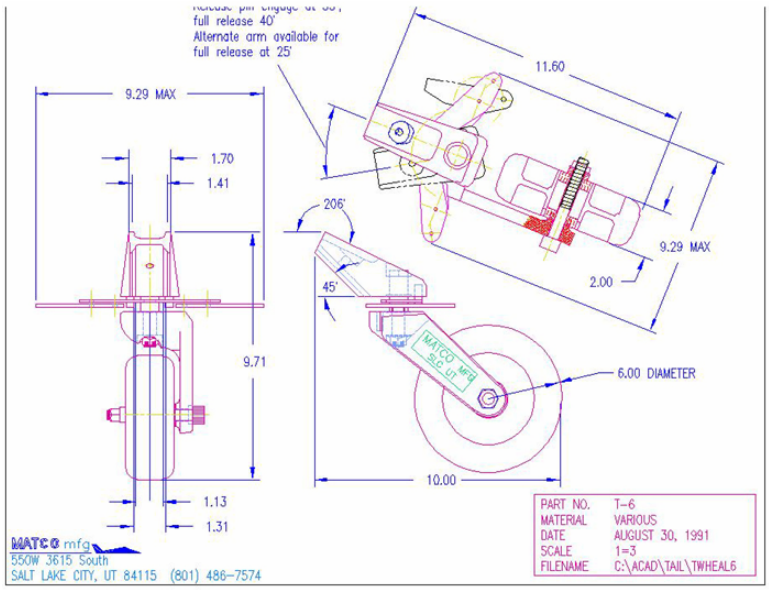

Figure 7.27: Matco Tailwheel Assembly [51]

7.9 Structural Arrangement

The purpose of this section is to discuss the proposed structural arrangement for the Meridian UAV. This includes material selection, structural layouts for the wing, v-tail, and fuselage, as well as preliminary structural sizing.

The mission of the Meridian is considered to be extreme in that the locations of operation, Greenland and Antarctica, are known for extremely cold weather. While this must be considered during the structural arrangement and material selection, it must be noted that the temperatures the Meridian will experience are not much different from High Altitude Long Endurance (HALE) UAVs. In fact, the Meridian mission may be less extreme than a HALE UAV because it will not experience large changes in temperature throughout a flight. This is mentioned only to emphasize the fact that the material selections should not be arbitrarily limited due to cold weather operations. Rather, the changes in material properties due to temperature should be acknowledged and accounted for in the design process such that the final product is an optimized solution in terms of weight, manufacturability, and service life.

One of the primary drivers of the material selection and structural layout is the advanced development time requirement. For the Meridian to be a successful project, manufacturability has to play a big role in the structural design process. In addition, many of the structures will be manufactured and assembled by graduate students with limited manufacturing experience. Therefore, the aircraft should be designed in such a way that limits the manufacturing skills and facilities required as is often done with homebuilt aircraft. These two concerns warrant the need for a limited part count as

well as a high level of automated processes such as computer numerically controlled machining.

7.9.1 Wing Structure

The structural arrangement of the wing for the Meridian was driven by the following concerns and requirements:

- Shipping requirement
- Hard point mounting requirement for antennas
- Fuel system integration
- Cost
- Manufacturability
- Weight
- On site storage facility limitations

The shipping, storage, and hard point requirements were determined to be the most critical and therefore had the biggest effect on the wing structural arrangement. In terms of structural optimization, the best solution would be to make the wing in two pieces. This however, does not consider the other system requirements and limitations such as landing gear and fuel tank integration nor does it consider manufacturability. The systems, shipping, and storage limitations [1] were such that the wing had to be designed in at least three pieces.

The structural layout of the wing was determined by integrating the landing gear placement, fuel tank sizing, control surface sizing, shipping requirements, and manufacturing limitations. The final solution is a three-piece wing: the inboard

section contains the fuel tanks and landing gear and the outboard sections contain all of the control surfaces. The outboard sections are removable for shipping and storage in small field hangars. In addition the length of the longest part in the wing is less than that of the current composite curing facilities at the University of Kansas (~10 ft).

Several possible arrangements were investigated for the wing structure including:

- Single spar
- Two Spar
- Three Spar
- Tube Spar

The two spar concept was selected as the primary configuration with the tube spar as a secondary. This decision was made based on investigation of the structural arrangements of aircraft with similar size. The wing is designed with a rectangular forward spar and a C-channel rear spar. The spar of the outboard wing slides into the inboard spar and is held by fasteners on top and bottom. This allows the outer portion of the wing to be removable without adding a great deal of complexity or weight. This, however, does require the spar to carry all of the wing loads. The effects of this should be investigated with a detailed structural analysis.

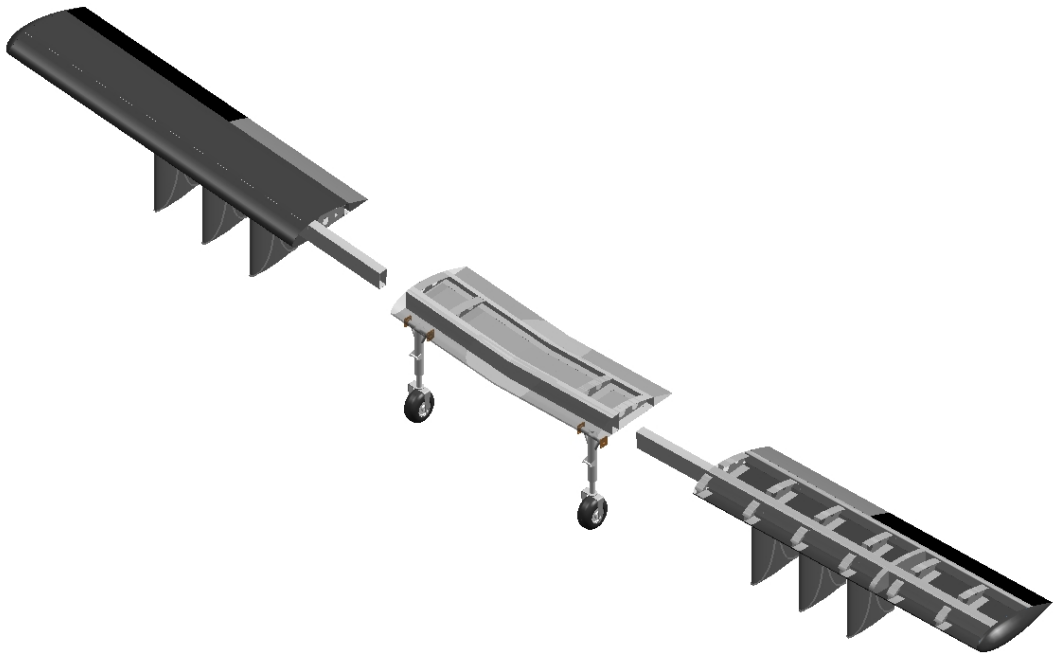

Figure 7.28: Wing Structural Layout (Not to Scale)

The material selection for the wing was influenced primary by manufacturability, load types, and thermal considerations. In terms of manufacturability, composite skins allow for a high level of automation in the tooling manufacturing and provide excellent surface finish. In terms of the substructure, there are several locations where loaded fasteners are required such as the landing gear attachment, the wing joint, and the antenna hard points. This warrants the use of aluminum in several of the structural components such as the forward and aft spar as well as several of the ribs. The combination of different materials in the wing has implications in terms of thermal expansion. These will be investigated further in the detailed design and analysis of the structure.

7.9.2 Fuselage Structural Layout

The structural layout of the fuselage was driven by the following:

- Wing-Fuselage Integration
- Manufacturability
- Weight
- Engine Installation
- Payload Integration
- Accessibility Requirements

The structural layout of the fuselage was integrated with the configuration design in terms of wing and payload placement. The wing placement, which is driven by the aircraft center of gravity was iterated until the main spar of the wing was collocated with the firewall. To produce structurally efficient aircraft designs, this type of synergy must be implemented between the design aspects such that the amount of structural members required is decreased. By locating the landing gear, wing main spar, and fuselage firewall at the same fuselage station, the amount of heavy structural members has been decreased, which provides weight savings and improves the manufacturability of the vehicle.

The primary frames in the fuselage were placed at the locations of the wing spars, payload hatch closure, payload rack mount, fuselage split, and v-tail spars. The remainder of the fuselage frames were spaced according to preliminary buckling calculations. The upper longerons were placed in line with the top engine mounting bracket as well as the payload hatch opening. The lower longerons were located at

the upper surface of the wing and coincide with the lower engine mounting brackets. Two frames were located at the forward and aft v-tail spar locations. These frames were also used to mount the tailwheel assembly.

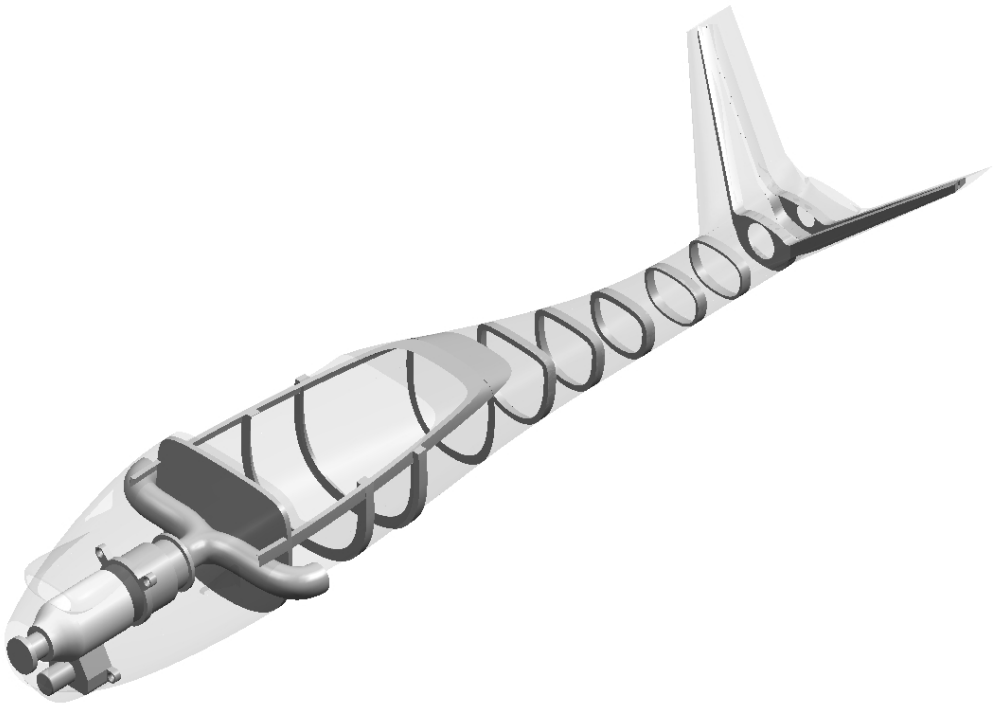

Figure 7.29: Fuselage Structural Layout

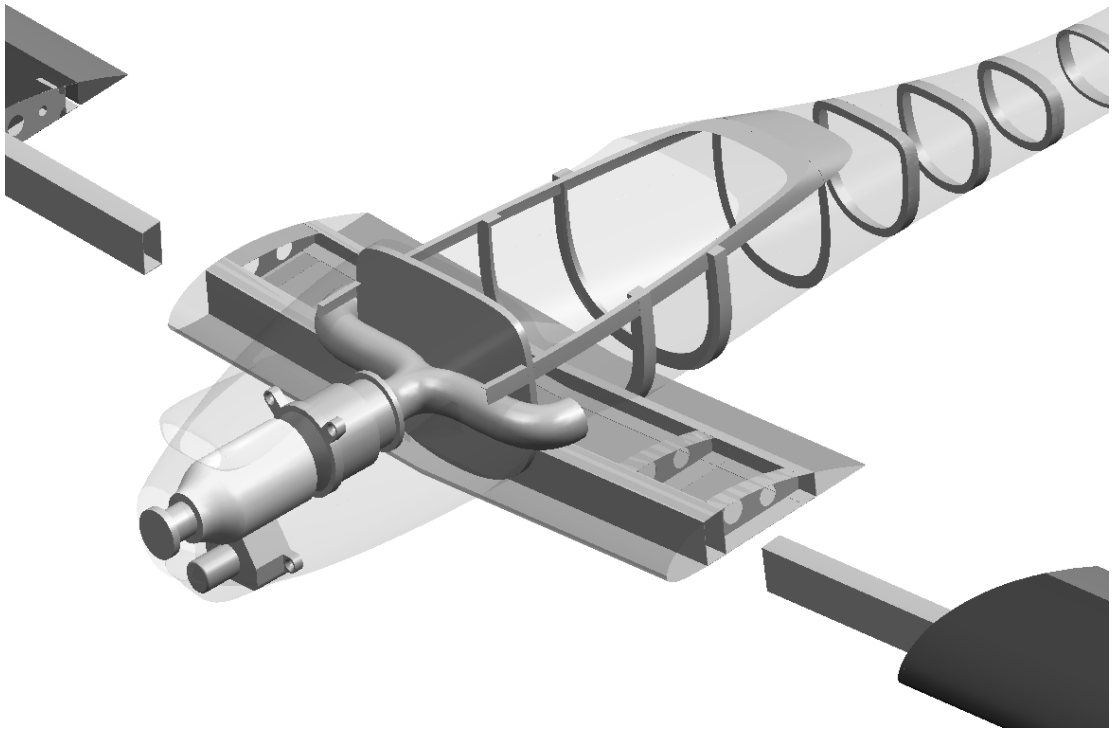

Figure 7.30: Wing-Fuselage Attachment

The aircraft structure was iterated several times such that the fuselage and center wing section would fit in a standard 20 foot container [22]. The goal was to minimize the amount assembly that would have to be performed on-site. This is important for shipping, but also for on-site storage. The projected hangar size is approximately 15 feet wide, which means the wings must be removed after every flight. The aircraft is shown in a 20 foot container in Figure 7.31.

Figure 7.31: Standard 20 Foot Shipping Container Door [22]

The engine mount will be procured from the engine manufacturer and will be very similar to the mount shown in Figure 7.32.

Figure 7.32: Typical Engine Mount for the Innodyn 165TE (Picture courtesy Innodyn, LLC)

7.10 Manufacturing Breakdown

The aircraft skin is divided into 6 pieces: 2 for the cowl, left and right sections for the forward fuselage, and top and bottom sections for the aft fuselage sections. Again, manufacturability was a primary driver in the fuselage design as the leading edge of the v-tail was placed such that it coincides with the mold line of the fuselage. This allows for the aft fuselage and v-tail skin to be continuous, which improves structural rigidity and reduces the parts count.

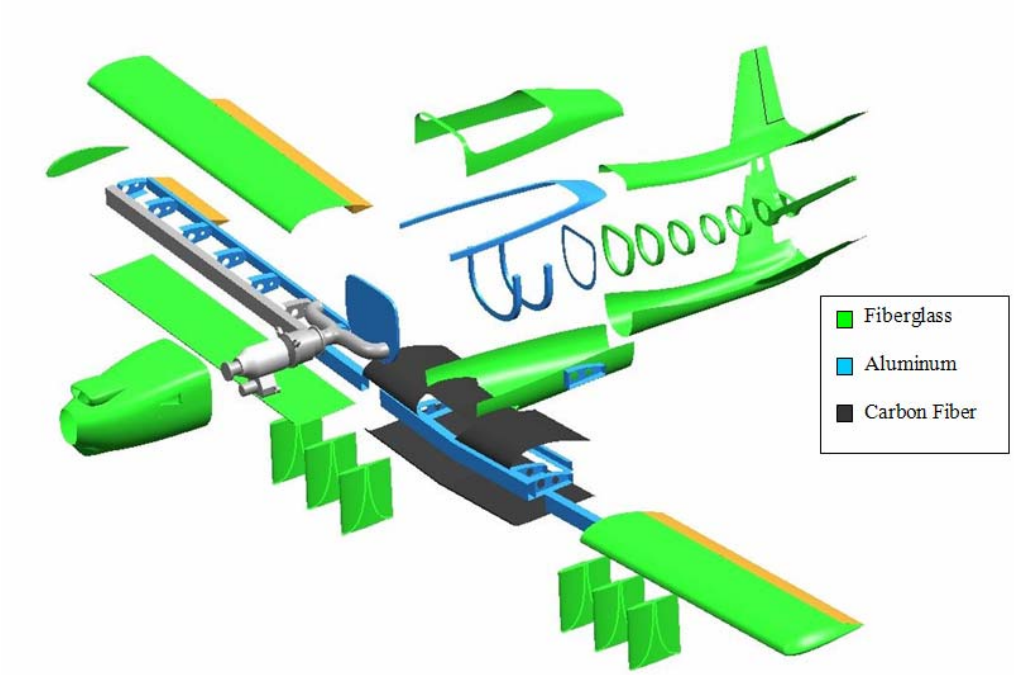

Figure 7.33: Manufacturing Breakdown

7.11 Cost Analysis

There are several methods for aircraft cost estimation. Roskam [2] and Raymer [52] have similar but slightly different methods, which are both based on reports generated by the RAND Corporation [53] and [54]. These reports used data from military aircraft programs to generate Cost Estimation Relationships (CERs). Methods for UAV cost estimation have also been developed [55]. These methods use trends of UAV cost versus empty weight, payload weight, and endurance to estimate the cost of a new aircraft.

To understand the differences in these methods, some terminology must be defined. The first is the difference between aircraft cost and price. Aircraft cost is defined as the total expenditure required to manufacture and aircraft. Aircraft price is defined as

the amount paid for an aircraft by a customer. The difference between cost and price is profit. Furthermore, the aircraft cost can be broken down into the following elements as is done in [2]:

- Research, Development, Testing, and Evaluation Cost
- Acquisition Cost
- Operating Cost
- Disposal Cost

Roskam's method calculates each of these costs separately, where Raymer's method combines the RDT&E and Acquisition Costs. The UAV cost estimation method [55] is only based on aircraft price data and is therefore less detailed than the other methods.

The goal of this cost analysis is to estimate the costs associated with the development of two vehicles for the CReSIS project. For a production run so small, the RDT&E cost methods are the most applicable. Roskam's methods were used for the RDT&E as the primary cost estimation. This was deemed the most reasonable method based on the nature of the Meridian program. The Raymer method was not used as it combines the RDT&E costs with production costs, which results in a much higher estimate. The UAV cost estimate was not used as it does not account for the number of aircraft produced, which is vital to cost estimations.

The first step in the cost estimation is to determine the Aeronautical Manufacturer's Planning Report (AMPR) weight. This is defined as the vehicle empty weight less all

of the items that will be purchased from vendors such as the engine, actuators, avionics, wheels, etc. The AMPR weight of the Meridian was estimated to be:

- W_{AMPR} = 310 lbs

The next step in the cost estimation was to develop the hourly rates to apply to each cost estimate. This project is different from a typical aircraft manufacturing process as much of the work will be performed by students, whom work at much lower rates than typical industry standards. Average rates for manufacturing and engineering time were developed based on the rates for undergraduate students, graduate students, professors, and industry labor as shown in Table 7.27. The expected breakdown of time is also shown in Table 7.27, which was used to create a time-weighted average. The industry rate was included in the wage calculations as some of the part manufacturing will be outsourced. The rates shown in Table 7.27 include typical overhead rates.

Table 7.27: Engineering and Manufacturing Rate Estimation

	Engineering Labor		Manufacturing Labor	
	% of Total Time %	Hourly Rate $/hr (2006)	% of Total Time %	Hourly Rate $/hr (2006)
Undergraduate	15	$16.00	30	$16.00
Graduate	60	$24.00	60	$24.00
Professor	15	$96.00	0	$96.00
Industry	10	$60.00	10	$60.00
Total (Averged)		**$37.20**		**$25.20**

The total RDT&E cost for an aircraft is defined as the sum of the following costs:

- Airframe engineering and design cost
- Development, support and testing cost
- Aircraft manufacturing cost
- Flight test operations cost

This cost is then adjusted by factors accounting for test facilities, profit, and financing. This was not done for the Meridian, however, as there will be no profit or financing, and the manufacturing facilities will be paid for by other university funding.

The following assumptions were made in the RDT&E cost estimation:

- The workforce is assumed to be relatively skilled in Computer Aided Design
- The engine cost was estimated at $30,000 per manufacturer data.
- The propeller cost was assumed to be $5,000 per manufacturer data.
- No profit or financing were included in the RDT&E phase.

The vehicle cost estimations are dependent on the number of aircraft produced. A learning curve effect causes the aircraft production cost to decrease as more aircraft are built. The primary production schedule is for two aircraft, however, there is a possibility of the procurement of up to eight more for similar science missions upon the successful completion of this project. For this reason the cost analysis was performed for production runs of up to ten total aircraft.

7.11.1 Engineering and Design Costs

The engineering and Design costs were created using Equation 7.13 from [2] to estimate the total number of engineering and design person-hours for this aircraft. This was then multiplied by the engineering pay rate.

$$MHR_{AED} = (0.0396) W_{AMPR}^{0.791} V_{cr}^{1.526} N^{0.183} F_{Diff} F_{CAD}$$ Equation 7.13

The results of this analysis for the first aircraft are:

- MHR_{AED} = 5,045 hours
- C_{AED} = $188,000

7.11.2 Development, Support, and Testing Costs

The development, support, and testing (DST) costs were estimated using Equation 7.14 from [2], which calculates cost directly using a cost escalation factor (CEF). Equation 7.14 was originally based on the 1970 dollar therefore the cost escalation factor is defined as the consumer price index of the current year divided by the consumer price index of 1970. The cost escalation factor used is CEF = 5.11.

$$C_{DST} = (0.008325) W_{AMPR}^{0.873} V_{cr}^{1.89} N^{0.346} F_{Diff} CEF$$ Equation 7.14

The development, support, and testing cost for the first aircraft is:

- C_{DST} = $64,000

7.11.3 Manufacturing Labor Costs

The manufacturing cost is estimated using Equation 7.15 from [2] to determine the manufacturing man-hours, MHR_{Man}, which is then multiplied by the manufacturing labor rate.

$$MHR_{Man} = (28.984) W_{AMPR}^{0.740} V_{cr}^{0.543} N^{0.524} F_{Diff} \quad \text{Equation 7.15}$$

The results of the manufacturing cost estimation for the first aircraft are:

- MHR_{Man} = 28,580 hours
- C_{Man} = $720,000

The number of man-hours calculated is equivalent to 14.3 man-years. This number is reasonable considering that the majority of the manufacturing will be completed by relatively unskilled workers.

7.11.4 Material/Equipment Costs

The material/equipment costs are defined as the costs of the aircraft structure in terms of raw materials and hardware as well as items such as motors, actuators, environmental systems, and fuel pumps. The material costs are estimated using Equation 7.16 from [2].

$$C_{Mat} = (37.632) W_{AMPR}^{0.689} V_{cr}^{0.624} N^{0.792} F_{Mat} CEF \quad \text{Equation 7.16}$$

The result of the material/equipment costs estimation for the first aircraft is:

- C_{Mat} = $210,000

7.11.5 Tooling Costs

The Meridian structure is primarily composite materials, which require a substantial amount of tooling. The low production rate allow for the use of low-cost tooling options, which are typically impractical for production aircraft. The tooling cost is based on a quote for resin-infusion molds produced using machined foam plugs. The cost of this tooling is:

- Foam Plugs: $\$140/ft^2$
- Resin Molds: $\$380/ft^2$

These general cost factors were used to estimate the total tooling costs:

- C_{Tool} = \$120,000

7.11.6 Quality Control Costs

The quality control costs were estimated using Equation 7.17 from [2]. The quality control costs are assumed to scale linearly with manufacturing costs.

$$C_{QC} = (0.13)C_{Mat}$$ Equation 7.17

7.11.7 Engine Costs

The engine and propeller costs for each aircraft are based on manufacturer information. These costs are:

- C_{Engine} = \$30,000
- C_{Prop} = \$5,000

7.11.8 Flight Test Operations Costs

The flight test operations costs were calculated using an estimated operating cost of $1,000/hr for a total of 100 flight-hours. This resulted in a total flight test cost of:

- C_{fto} = $100,000

7.11.9 Cost Estimate Summary

The summary of the cost estimations are shown in Table 7.28. The cost estimates are shown for production runs of one through ten aircraft. The acquisition cost shown represents the total cost for the number of aircraft shown.

Table 7.28: Cost Analysis Results

Item	Cost (10^6 $ 2006)									
	Number of Aircraft Produced									
	1	2	3	4	5	6	7	8	9	10
Engineering and Design	0.169	0.192	0.207	0.218	0.228	0.235	0.242	0.248	0.253	0.258
Development, Support, and Testing	0.064	0.081	0.094	0.103	0.112	0.119	0.125	0.131	0.137	0.142
Manufacturing Labor	0.651	0.936	1.158	1.346	1.513	1.665	1.805	1.936	2.059	2.176
Material/Equipment	0.210	0.364	0.501	0.630	0.751	0.868	0.981	1.090	1.197	1.301
Tooling	0.120	0.120	0.120	0.120	0.120	0.120	0.120	0.120	0.120	0.120
Quality Control	0.085	0.122	0.151	0.175	0.197	0.216	0.235	0.252	0.268	0.283
Engine	0.035	0.070	0.105	0.140	0.175	0.210	0.245	0.280	0.315	0.350
Flight Test Operations	0.100	0.100	0.100	0.100	0.100	0.100	0.100	0.100	0.100	0.100
Acquisition Cost	**1.434**	**1.985**	**2.436**	**2.833**	**3.195**	**3.534**	**3.853**	**4.157**	**4.449**	**4.730**

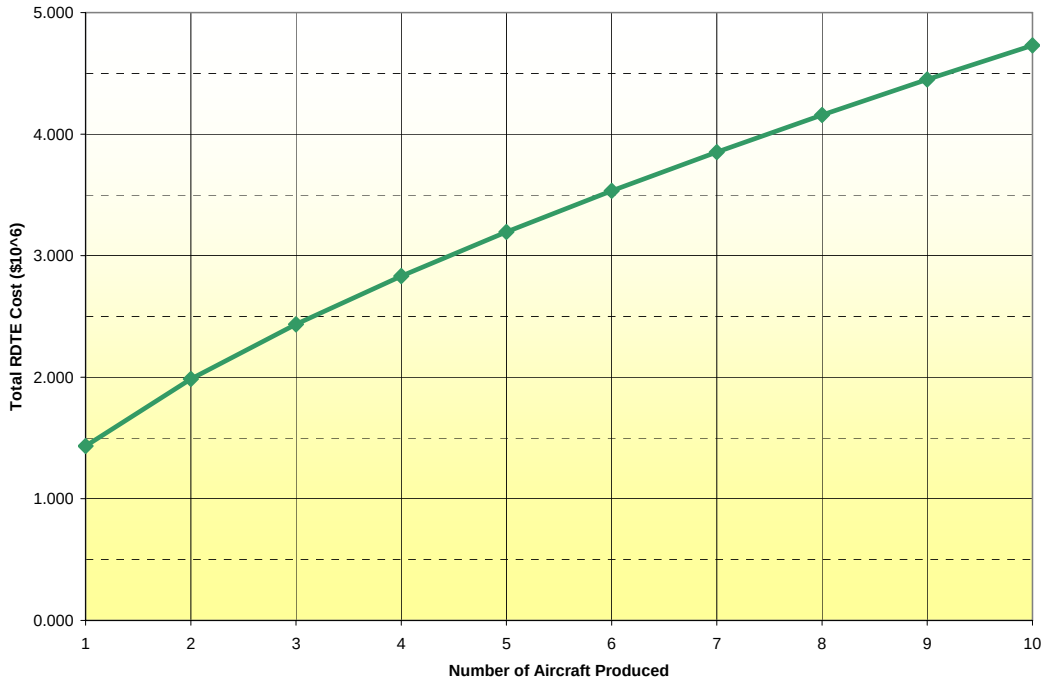

Figure 7.34: Cost Analysis Results

8 Conclusions

The primary focus of this work is to develop an aircraft that will support field campaigns conducted by the Center for Remote Sensing of Ice Sheets (CReSIS). This includes the development of a mission specification including a list of requirements. Much of the requirements development was related to translating the technical specifications for the desired missions into performance requirements that can be used in preliminary aircraft design such as range, endurance, and operating field length.

A large factor in the development of the vehicle requirements as well as the preliminary designs is the concurrent development of the radar system for the Meridian. One of the primary goals of CReSIS is to support multidisciplinary collaboration through integrated system development. The simultaneous development of two highly integrated systems requires the utilization of a robust design methodology. This was manifested in the development of three different design concepts based on different interpretations of what would become one of the most critical and dynamic requirements: the antenna integration.

This robust design philosophy was employed further along in the design process as the selection of the primary aircraft configuration was made based on this important feature. The White concept was selected almost entirely on the basis of adaptability as a means of risk mitigation. The simple fact is that there are still too many unknowns in the development of the radar system to support a highly optimized aircraft tailored for the radar system. While this concept may seem less than ideal, it

actually results in what may be a more useful product. For example, the Blue concept is a novel design in terms of the antenna integration, but it would not be very competitive for other missions with different types of payloads. The Meridian represents a vehicle that is specifically designed for Cryospheric remote sensing, but is capable of many more missions with a variety of payloads.

The decision to utilize a somewhat generic antenna integration scheme calls attention to the decision to design a new aircraft as opposed to modifying an existing platform. This decision can be supported by the key design features integrated into the Meridian. Firstly, the Meridian will be designed specifically for cold weather operations. This means that factors such as anti-icing as well as system heating and cooling requirements will be accounted for. In addition, the Meridian is designed to be shipped in a 20 foot container with minimal disassembly. This is a key factor as the Meridian will be used in remote locations with minimal facilities.

The final product is a vehicle that can be shipped in a standard 20 foot container and quickly assembled and disassembled with minimal tools. The Meridian will be one of the smallest turboprop powered UAVs in the world.

9 References

1 Anon., “Mission Concepts for Uninhabited Aerial Vehicles in Cryospheric Science Applications”. University of Kansas Remote Sensing Laboratory. KS, 2004.

2 Roskam, Jan. *Airplane Design: Parts I-VIII.* DARCorporation. Lawrence, KS. 1997.

3 Advanced Aircraft Analysis Software. DARCorporation. Lawrence, KS. 2005.

4 Raymer, D.P., “RDS-Professional User’s Manual,” Version 4.1, Conceptual Research Corporation, Sylmar, CA, December 1997.

5 Anon., “Adaptive Modeling Language Reference Manual, Version 4.17.” Technosoft Inc. Cincinnati, OH. 2006.

6 Anemmaat, William., Hale, Richard D, Ramabadran, Narayanan. “A Knowledge-Based Design Framework for Aircraft Conceptual and Preliminary Design.” SAE Paper 06GATC-75. 2006.

7 Dahl, Jorgen, Hill, Stephen, Chemaly, Adel. “AMRaven – An Integrated Air Vehicle Design and Analysis Environment.” SAE Paper 06GATC-78. 2006.

8 Sobieszczanski-Sobieski, J., “Multidisciplinary Design Optimization: An Emerging New Engineering Discipline,” *Advances in Structural Optimization* (483-496), Kluwer Academic Publishers, the Netherlands, 1995.

9 http://www.ggy.bris.ac.uk/research/antarctic_history/Project_summary.pdf. December 13, 2007.

10 Waite, AH, International Experiments in Glacier Sounding, 1963 and 1964, Canadian Journal of Earth Sciences, vol. 3 1966, p;. 887.

11 Raymer, Daniel P. *Enhancing Aircraft Conceptual Design using Multidisciplinary Optimization.* Ph. D. Thesis, Swedish Royal Institute of Technology, Stockholm, Sweden, 2002.

12 Krabill, W, et al., “Greenland Ice Sheet: High-Elevation Balance and Peripheral Thinning.” *Science*, pp. 289, July 21, 2000.

13 Lawrence, Roland W, “Autonomous Aerial Observation System Concepts for Microwave Remote Sensing,” AIAA2005-7055, Infotech@Aerospace, Arlington, VA, September 2005.

14 Hilliard, Lawrence M, et al., “Microwave Instrumentation for UAV Platforms Enabling Thin Ice Measurement.” AIAA 2005-7019, Infotech@Aerospace, Arlington, VA, September 2005.

15 Bland, Geoff, et al., “’Sensors with Wings’ – Small UAVs for Earth Science.” AIAA 2004-6418, 3rd Unmanned Unlimited Technical Conference, Chicago, Illinois, September 2004.

16 Wegener, Steven S, et al., “UAV Autonomous Operations for Airborne Science Missions.” AIAA 2004-6416, 3rd Unmanned Unlimited Technical Conference, Chicago, Illinois, September 2004.

17 “Science Requirements for Field Work in CReSIS. The University of Kansas. September 15, 2005.

18 Anandakrishnan, Sridhar. "Science Requirements for Field Work in CReSIS," Penn State University, 2005.
19 www.nsf.gov. May 19, 2006.
20 Donovan, William. "CReSiS Airborne Platform Summary". The University of Kansas. 2006.
21 Palais, July, et al. "Meeting with NSF Representatives." February, 2006.
22 Allen, Christopher. "Discussion Regarding Antenna Design." The University of Kansas. April 2006.
23 www.oceanairlogistics.com.
24 Lambert, Mark ed. *Jane's All the World's Aircraft 1993-94.* Jane's Information Group. Alexandria, VA. 1993.
25 http://www.scoop.co.nz/stories/PO0601/S00042.htm. May 19, 2006.
26 www.uavforum.com. 6/19/06.
27 *Worldwide UAV Roundup.* www.aiaa.org/images/PDF/WilsonChart.pdf. 2003.
28 Munson, Kenneth. *Jane's Unmanned Aerial Vehicles and Targets Issue 11.* 1999.
29 www.uav.com. May 19, 2006.
30 www.is.northropgrumman.com
31 www.aaicorp.com. May 19, 2006.
32 www.genaero.com. May 19, 2006.
33 www.diamondair.com. May 19, 2006.
34 http://www.diamond-air.at/en/press/pressarchive/40820.htm. May 19, 2006.
35 www.rotax-aircraft-engines.com. May 19, 2006.
36 www.centurion-engines.com. October 31, 2006.
37 www.deltahawkengine.com. October 31, 2006.
38 www.dieselair.com. October 31, 2006.
39 www.uavenginesltd.co.uk. October 31, 2006.
40 www.zoche.de. October 31, 2006.
41 www.smaengines.com. October 31, 2006.
42 www.innodyn.com. October 31, 2006.
43 Munk, Max M. "General Biplane Theory." NACA Report No. 151. 1923.
44 Von Mises, Richard. *Theory of Flight.* Dover Publications. New York, 1959.
45 Drela, Mark, "XFOIL: An Analysis and Design System for Low Reynolds Number Airfoils" Low Reynolds Number Aerodynamics, T. J. Mueller (ed.), Lecture Notes in Engineering, Vol. 54, Springer-Verlag Berlin, 1989, pp. 1–12.
46 Anon., "Federal Aviation Regulations – Part 23, Airworthiness Standards: Normal, Utility, and Aerobatic Category Airplanes", Department of Transportation, Federal Aviation Administration, Washington, DC, 2006.
47 Kuethe, Arnold M, and Chow, Chuen-Yen, *Foundations of Aerodynamcis: Bases of Aerodynamic Design, 3rd ed.*, John Wiley and Sons, New York, 1976.
48 www.cloudcaptech.com, October 31, 2006.
49 www.lancair.com, December 1, 2006.
50 www.lancairlegacy.com/05-04.html, December 3, 2006.
51 www.aircraftspruce.com, December 3, 2006.

52 Raymer, D.P., *Aircraft Design: A Conceptual Approach*, 3rd ed., AIAA, Reston, VA, 1999.
53 Levenson, G.S., et al, "Cost-Estimating Relationships for Aircraft Airframes," Rand Corporation, R-761-PR, Santa Monica, CA, February 1972.
54 Hess, R.W., and Romanoff, H.P., "Aircraft Airframe Cost Estimating Relationships," Rand Corporation, Rept. N-1882-AF, Santa Monica, CA, 1982.
55 Anon., "Unmanned Aerial Vehicle System Acquisition Cost Estimating Methodology," 37th DoD Cost Analysis Symposium, 2004.